Cyclostationary Methods for Communication and Signal Detection Under Interference

Matthew Carrick

Dissertation submitted to the Faculty of the

Virginia Polytechnic Institute and State University

in partial fulfillment of the requirements for the degree of

Doctor of Philosophy

in

Electrical Engineering

Jeffrey H. Reed, Chair

R. Michael Buehrer

A. A. (Louis) Beex

Patrick C. Koelling

fredric j. harris

August 24, 2018

Blacksburg, Virginia

Keywords: cyclostationarity, interference mitigation, FRESH filters, spectral redundancy

Cyclostationary Methods for Communication and Signal Detection Under Interference

Matthew Carrick

ABSTRACT

In this dissertation novel methods are proposed for communicating in interference limited environments as well as detecting such interference. The methods include introducing redundancies into multicarrier signals to make them more robust, applying a novel filtering structure for mitigating radar interference to orthogonal frequency division multiplexing (OFDM) signals and for exploiting the cyclostationary nature of signals to whiten the spectrum in blind signal detection.

Data symbols are repeated in both time and frequency across orthogonal frequency division multiplexing (OFDM) symbols, creating a cyclostationary nature in the signal. A Frequency Shift (FRESH) filter can then be applied to the cyclostationary signal, which is the optimal filter and is able to reject interference much better than a time-invariant filter such as the Wiener filter. A novel time-varying FRESH filter (TV-FRESH) filter is developed and its Minimum Mean Squared Error (MMSE) filter weights are found.

The repetition of data symbols and their optimal combining with the TV-FRESH filter creates an effect of improving the Bit Error Rate (BER) at the receiver, similar to an error correcting code. The important distinction for the paramorphic method is that it is designed to operate within cyclostationary interference, and simulation results show that the symbol repetition can outperform other error correcting codes. Simulated annealing is used to optimize the signaling parameters, and results show that a balance between the symbol repetition and error correcting codes produces a better BER for the same spectral efficiency than what either method could have achieved alone.

The TV-FRESH filter is applied to a pulsed chirp radar signal, demonstrating a new tool to use in radar and OFDM co-existence. The TV-FRESH filter applies a set of filter weights in a periodically time-varying fashion. The traditional FRESH filter is periodically time-varying due to the periodicities of the frequency shifters, but applies time-invariant filters after optimally combine any spectral redundancies in the signal. The time segmentation of the TV-FRESH filter allows

spectral redundancies of the radar signal to be exploited across time due to its deterministic nature.

The TV-FRESH filter improves the rejection of the radar signal as compared to the traditional FRESH filter under the simulation scenarios, improving the SINR and BER at the output of the filter. The improvement in performance comes at the cost of additional filtering complexity.

A time-varying whitening filter is applied to blindly detect interference which overlaps with the desired signal in frequency. Where a time-invariant whitening filter shapes the output spectrum based on the power levels, the proposed time-varying whitener whitens the output spectrum based on the spectral redundancy in the desired signal. This allows signals which do not share the same cyclostationary properties to pass through the filter, improving the sensitivity of the algorithm and producing higher detection rates for the same probability of false alarm as compared to the time-invariant whitener.

Cyclostationary Methods for Communication and Signal Detection Under Interference

Matthew Carrick

GENERAL AUDIENCE ABSTRACT

This dissertation proposes novel methods for building robust wireless communication links which can be used to improve their reliability and resilience while under interference. Wireless interference comes from many sources, including other wireless transmitters in the area or devices which emit electromagnetic waves such as microwaves. Interference reduces the quality of a wireless link and depending on the type and severity may make it impossible to reliably receive information.

The contributions are both for communicating under interference and being able to detect interference. A novel method for increasing the redundancy in a wireless link is proposed which improves the resiliency of a wireless link. By transmitting additional copies of the desired information the wireless receiver is able to better estimate the original transmitted signal. The digital receiver structure is proposed to optimally combine the redundant information, and simulation results are used to show its improvement over other analogous methods.

The second contribution applies a novel digital filter for mitigating interference from a radar signal to an Orthogonal Frequency Division Multiplexing (OFDM) signal, similar to the one which is being used in Long Term Evolution (LTE) mobile phones. Simulation results show that the proposed method out performs other digital filters at the most of additional complexity.

The third contribution applies a digital filter and trains it such that the output of the filter can be used to detect the presence of interference. An algorithm which detects interference can tip off an appropriate response, and as such is important to reliable wireless communications. Simulation results are used to show that the proposed method produces a higher probability of detection while reducing the false alarm rate as compared to a similar digital filter trained to produce the same effect.

Contents

List of Abbreviations

- ACS: Almost Cyclostationary

- AWGN: Additive White Gaussian Noise

- BER: Bit Error Rate

- BPSK: Binary Phase Shift Keying

- CAF: Cyclic Autocorrelation Function

- CBRS: Citizen Broadband Radio Service

- CDMA: Code-Division Multiple Access

- CF: Cycle Frequency

- CS: Cyclostationary Signals

- DFT: Discrete Fourier Transform

- DSSS: Direct Sequence Spread Spectrum

- DVB-S2: Digital Video Broadcasting Second Generation

- ECC: Error Correcting Code

- FCC: Federal Communications Commission

- FFT: Fast Fourier Transform

- FIR: Finite Impulse Response

- FRESH: Frequency Shift (within context of the filtering structure)

- FS: Frequency Shift (within context of the operation)

- GACS: Generalized Almost Cyclostationary

- IDFT: Inverse Discrete Fourier Transform

- IFFT: Inverse Fast Fourier Transform

- ISM: Industrial, Scientific and Medical

- LAA: Licensed-Assisted Access

- LAPTV: Linearly Almost Periodically Time-Varying

- LCL: Linear Conjugate-Linear

- LDPC: Low Density Parity Check

- LPTV: Linear Periodically Time-Varying

- LTE: Long Term Evolution

- LTE-U: Long Term Evolution Unlicensed

- LTI: Linear Time-Invariant

- MMSE: Minimum Mean Squared Error

- MRC: Maximal Ratio Combining

- MSE: Mean Squared Error

- NMDFB: Non-Maximally Decimated Filter-bank

- OFDM: Orthogonal Frequency Division Multiplexing

- PFD: Paramorphic FRESH Demodulator

- PMW: Paramorphic Multicarrier Waveform

- PRI: Pulse Repetition Interval

- PSK: Phase-Shift Keying

- QAM: Quadrature Amplitude Modulation

- SAS: Spectrum Access System

- SCORE: Self-Coherence Restoral

- SFDR: Spurious Free Dynamic Range

- SINR: Signal to Interference and Noise Ratio

- SIR: Signal to Interference Ratio

- SNR: Signal to Noise Ratio

- SRRC: Square-Root Raised Cosine

- TD-LTE: Time-Division LTE

- TIW: Time-Invariant Whitener

- TTI: Transmission Time-Interval

- TV-FRESH: Time-Varying FRESH

- TVW: Time-Varying Whitener

- U-NII: Unlicensed National Information Infrastructure

- WLAPTV: Widely-Linearly Almost Periodically Time-Varying

List of Figures

List of Tables

Chapter 1

Introduction

Filtering is foundational in wireless communication. Signals can be modified based on the design and implementation of a filter, transforming an undesired signal into something that is usable. While a static filter can be useful, adaptive filters are much more powerful as they can alter their operation on the fly as the environment changes.

Wiener developed the first statistically designed filter, a time-invariant filter best suited to stationary time series [3]. The filter operates by shaping the frequency response of a signal to minimize the error at the output of the filter. The distortion of the underlying signal is balanced with the rejection of any interference or channel effects.

Many communications signals are not stationary but are instead cyclostationary. A stationary signal is one whose distribution does not vary with time, whereas a cyclostationary signal's distribution varies periodically with time. Consider a Binary Phase Shift Keying (BPSK) signal which is modeled to transmit a $+1$ or -1 with equal probability, which forms a stationary signal. When these symbols are upsampled prior to pulse shaping the signal becomes cyclostationary. The upsampling process transforms the original spectrum by creating additional mirror images of it, forming spectral redundancy.

The initial attempts at developing an optimal filter for cyclostationary signals provide some insight into the development of what is now referred to as a Frequency Shift (FRESH) filter [4]. The two

filtering methods partitioned the signal separately in time and frequency, called the translation series representation and the harmonic series representation. The harmonic series representation focuses on the spectral redundancy by implementing a series of mixers and band-pass filters which translate each part of the spectral redundancy to baseband, optimally combine them, and then mix them back to band-pass. The translation series representation transforms the cyclostationary signal into a discrete set of stationary signals through decimation, which are then filtered in parallel, and then upsampled and summed.

Gardner proposed a time-varying FRESH filter structure which can exploit spectrally redundant information within a cyclostationary signal [1]. This improves upon the time-invariant filter as it can combine redundant information within the desired signal, and exploit redundant information in the interference to mitigate it. The frequency shifts corresponding to the spectrally redundant information are included in the branches of the FRESH filter, which are each followed by a set of weights, and then all of the branches are summed. The sets of parallel filter weights are set such that the mean-squared error at the output of the filter is minimized, the condition for optimality.

FRESH filters are known for their ability to mitigate cyclostationary interference. The amount of cyclostationary interference that can be removed is dependent on the spectral redundancy within both the desired signal and the interference. Spectral redundancy is a property of cyclostationary signals and is a form of excess bandwidth. Redundant spectra within the received signal can be optimally combined which is the basis for the FRESH filter. This is in direct contrast to the Wiener filter which can only shape the spectrum. The performance of the FRESH filter directly relates to the amount of spectral redundancy within the received signal.

This dissertation focuses on the development and analysis of a Time-Varying Frequency Shift (TV-FRESH) filter and its applications to robust wireless communications, mitigating radar interference to orthogonal frequency division multiplexing (OFDM) signals, and the use of a spectral whitening FRESH filter for blind signal detection. The contributions are further detailed in Section 1.2. The applications of such techniques are discussed in Section 1.1.

1.1 Applications

The dramatic increase in wireless traffic has transformed communication channels which would normally be considered noise-limited or interference-limited. Many of the foundations of wireless communication assume a Additive White Gaussian Noise (AWGN) channel, but in the presence of interference this assumption is unlikely to hold. Techniques and methods that would normally be applicable to an AWGN channel must be modified or new algorithms adopted in their place when dealing with non-AWGN channels. This dissertation presents novel methods for signal detection and communication under interference that could be applied to the following scenarios.

Future wireless waveforms will need to consider the impact of interference given the amount of growth in wireless communications and the growing scarcity of available spectrum. A large array of multicarrier waveforms have been proposed for 5th generation cellular communications [5], however they are often not designed to be robust to interference. This can lead to wireless networks which are very fragile to interference and unsophisticated attacks [6]. While it can be assumed that the impact of interference to cellular communications in private bands can be minimized through governmental bodies such as the FCC and law enforcement, unlicensed long term evolution (LTE-U) being used in the industrial scientific and medical (ISM) bands will need to be much more robust to such an environment. Both licensed and unlicensed LTE will also need to consider methods for protecting their control channel information given their fragility [7]. A method for building robust OFDM waveforms by exploiting spectral redundancy in repeated data symbols is proposed in Chapter 3.

Increasing the spectral efficiency under interference will also become more important in the future. Unmanned aerial vehicles will experience much more interference due to their vantage point [8], and will need methods to communicate more efficiently under these conditions. Similarly, new methods will be needed to extend the usefulness of error correcting codes to non-white Gaussian noise environments, or new types of codes altogether, to improve their spectral efficiency while under interference. Methods will also be needed to enable full-duplex communications [9] and improve their spectral efficiency by better self-interference rejection techniques. The method for building robust waveforms in Chapter 3 can also be used to improve the spectral efficiency of OFDM under

interference.

Communications co-existence with radar presents a challenge given the large power of radar transmitters, and both co-channel interference and adjacent channel interference must be considered. The unlicensed national information infrastructure (U-NII) bands at 5 GHz must share spectrum with terminal Doppler weather radar [10], affecting WiFi devices in that band. The citizens broadband radio service (CBRS) has been allocated by the Federal Communications Commission (FCC) for wireless broadband access at 3.5 GHz, but its capacity is limited by military radars in this band [11]. Chirped radar waveforms use radio altimeters at 4.2 GHz which also interfere with wireless monitoring services for aircraft [12]. A novel method for mitigating chirped radar interference to OFDM is proposed in Chapter 4.

Given the sensitivity of most waveforms to interference it is important to be able to detect when interference is occurring. The classic scenario for interference detection is the hidden node problem, where two radios who cannot receive one another's transmissions due to their geography, attempt to transmit simultaneously while a third party receives both interfering transmissions. The detection of jamming attacks on control channels, such as in LTE, will enable the waveform to respond and mitigate its impact [13, 14]. A method for detecting interference to cyclostationary signals is proposed in Chapter 5.

1.2 Contributions

Chapter 3 covers the development of paramorphic multicarrier waveforms and demodulators and a description of the contribution is given below in Section 1.2.1. In chapter 4, the TV-FRESH filter is applied to mitigating radar interference to OFDM signals as another method or tool to improve co-existence between the two, described in Section 1.2.2. In chapter 5, a FRESH filter is applied to blind interference detection by whitening the received signal based on the cyclostationary properties of the desired signal. A description of the proposed contribution is given in Section 1.2.3.

1.2.1 Paramorphic Multicarrier Communications for Interference Mitigation

A novel method is presented for enabling communication in cyclostationary interference limited environments by adaptively inserting and exploiting spectral redundancy in an OFDM signal. The redundancy is formed through repeating data symbols across OFDM symbols in both time and frequency. A novel FRESH filter is applied to exploit the time-varying cyclostationary properties, enabling the communication while under interference. Designing spectral redundancy into multicarrier waveforms is referred to as *Paramorphic Multicarrier Waveforms* (PMW) and the corresponding demodulator as a *Paramorphic FRESH Demodulator* (PFD). The term *paramorphic* [1] refers to chemical compositions whose physical structure can be modified without a chemical change, an example being the crystalline structure being re-organized. This term is adopted and used within *Paramorphic Multicarrier Waveform* to refer to multicarrier waveforms whose waveform structure will stay the same, but whose cyclostationary properties are modified through symbol repetition in time and frequency.

Making spectral redundancy a design parameter within the waveform enables a new type of waveform and demodulator and a new performance tradeoff can be established: increasing spectral redundancy for improved CS interference mitigation. A similar trade-off is the foundation for error correcting codes (ECC), increasing the amount of bit-level redundancy for an improvement in the bit error rate (BER) at the receiver. Space-time block codes also increase the amount of redundancy, or transmit diversity, in the transmitted waveform. Long Term Evolution (LTE) uses a similar method, space-frequency block codes, where data symbols are repeated over multiple antennas to increase the transmit diversity which also increases the spectral redundancy.

Simulation results demonstrate the performance gains in both signal to interference and noise ratio (SINR) and BER as compared to traditional time-invariant optimal filtering techniques and ECCs. A method for jointly optimizing the waveform and demodulator is demonstrated which balances the improved BER with the amount of redundancy designed into the signal.

---

[1] The property of changing from one mineral species to another (as from aragonite to calcite) by a change in internal structure and physical characters but not in chemical composition. "Paramorphism", Def., Merriam-Webster, http://www.merriam-webster.com/dictionary/paramorphism

1.2.2 Mitigating Linear Frequency Modulated Pulsed Radar Interference to OFDM to Enable Spectrum Co-Existence

A novel OFDM and radar co-existence method is proposed based on exploiting the spectral redundancies of the combined received signal, rather than avoidance which is much more commonly seen. The difficulty in filtering radar signals is their large power, and with time-invariant filters this is a substantial problem to overcome since their interference mitigation properties come from brute force attenuation. On the other hand time-varying filters, such as the FRESH and TV-FRESH filters, are more robust against large power interferers because they establish a system of equations method of mitigation which is able to invert the interference and reduce its impact at the output of the filter.

Another distinction is prior work with FRESH filtering has typically considered signals which are continuously interfering with one another, where this contribution demonstrates the performance of the FRESH and TV-FRESH filters against a pulsed chirp radar signal. The TV-FRESH filter applies a set of filter weights in a periodically time-varying manner, which improves the SINR and minimizes the BER at the output of the filter when applied to the received signal.

1.2.3 Exploiting Spectral Redundancy in Whitening Filters for Blind Signal Detection

Where the other contributions focus on adapting the filter weights based on the MMSE at the output of the filter to improve the reception of a signal, the third contribution adapts the filter weights such that the FRESH filter whitens the output spectrum to improve the detection of signals. A frequency domain time-invariant whitening filter transforms the output spectrum such that the output power per frequency bin is close to uniform. By then introducing a new signal into the filter it will produce a peak in the frequency response which can be used to blindly detect interfering signals. The limitation with a time-invariant filter is that the whitening effect is only done on the power levels of the signal, and therefore signals which overlap in frequency are more difficult to detect.

The proposed time-varying whitening filter improves the ability to detect interference overlapping

in frequency by exploiting the spectral redundancy of the desired signal. Using a FRESH filter to whiten the spectrum based on the spectral redundancy allows signals which do not have the same cyclostationary properties to pass through the whitening filter, allowing for more sensitivity and higher rate of detection. Simulation is used to show the ability of the time-varying whitening filter to improve the probability of detection over time-invariant whitening filters for the same probability of false alarm. In one simulation scenario the proposed time-varying whitening filter gives an improvement of 20% over the time-invariant filter in detection probability.

1.3 Publications

The following papers have been accepted for publication, drawn from the contributions in this dissertation:

- M. Carrick, J. H. Reed and C. M. Spooner, "Paramorphic multicarrier communications for interference mitigation", *EURASIP Journal on Advances in Signal Processing*, January 2018, pp. 1-18 [15].

- M. Carrick, J. H. Reed and f. harris, "An optimal filter for signals with time-varying cyclostationary statistics", 2017 22nd International Conference on Digital Signal Processing (DSP), London, UK, August 2017, pp. 1-5 [16].

- M. Carrick and J. H. Reed, "Improved GFDM equalization in severe frequency selective fading", 2017 IEEE 38th Sarnoff Symposium, Newark, NJ, September 2017, pp. 1-6 [17].

- M. Carrick and J. H. Reed, "Exploiting the Cyclostationarity of Radar Chirp Signals with Time-Varying Filters", 2017 5th IEEE Global Conference on Signal and Information Processing, Montreal, Canada, pp. 1-4 [18].

Two other co-authored papers have been accepted for publication or submitted during the same course of study, but are independent of the contributions in this dissertation:

- M. Sohul, M. Yao, A. Abdallah, M. Carrick, V. Marojevic and J. Reed, "Quality of service assurance-based auction for spectrum sharing systems", Analog Integrated Circuits and Signal

Processing, May 2017, Volume 91, Issue 2, pp. 203-216.

- T. Koehn, M. Carrick and P. Athanas, "An Efficient Structure for Run-time Configuration of Synthesis and Channelizer Filter Banks", 2015 International Conference on ReConFigurable Computing and FPGAs (Re-ConFig), Mexico City, Mexico, December 2015.

1.4   Patent

A utility patent application has been filed with the Patent and Trademark Office (PTO) as of October 2017, Serial No. 15/565614, and is currently awaiting examination. The patent application in April 2016 [19] passed the Patent Cooperation Treaty (PCT) search report, and was previously submitted as a provisional patent in April 2015 [20].

Chapter 2

Related Work and Background

In this chapter the related work is given in Section 2.1 which includes literature covering the development of the FRESH filter, the cyclostationarity of OFDM and the application of FRESH filtering to OFDM signals. Section 2.2 gives more detailed background information necessary for later chapters, including on cyclostationary signals and FRESH filtering.

2.1   Related Work

There has been much research in the area of cyclostationarity and its applications [21, 22]. The most relevant work within cyclostationarity to the proposed research is given, focusing on the intersection of cyclostationary signals, FRESH filtering and OFDM. Although FRESH filtering is the most popular, there are a number of names used in the theory of optimal time-varying filters and an effort has been made to list them for clarity and distinguish them from works which use similar terminology but are otherwise unrelated [23]. Work related to the applications of the proposed technique are also presented.

Optimal linear time-invariant filtering created independently by Wiener [3] and Kolmogorov, with the difference being Wiener's solution was in the frequency domain where Kolmogorov's was in the time domain [24]. These were the first filters to be designed statistically and may be referred

to as *Wiener-Kolmogorov filters*, although in this document they will be referred to as *Wiener filters* for simplicity. Optimal filtering theory was later expanded through [4, 25] by including the theory for optimal *Linear Periodically Time-Varying* (LPTV) filters for cyclostationary signals although the filter representations and terminology are different than what is used in more recent literature. The development of optimal time-varying filters from then on was very intertwined with the development of the theory of cyclostationary signals. Most advances in the theory of cyclostationary signals came from applications to signal detection, starting with [26] which created the foundational concepts and terminology of second-order periodicity, cyclic autocorrelation, and the cyclic spectrum. Spectral correlation theory was developed within [27], which were also introduced conjugate spectral correlation and almost periodic cyclic autocorrelation functions. The theory was used to characterize the spectral correlation of a large number of analog and digital modulations [28, 29] providing the information needed to implement FRESH filters for these respective signals.

The modern understanding of the FRESH filter using only linear branches was created in [30] which introduced the term *cyclic filtering* and expanded the FRESH filtering theory to Linear Almost Periodically Time-Varying (LAPTV) filters. The incorporation of conjugate-linear filtering [31] into optimal time-varying filtering was done in [32] which coined the term *Frequency-Shift* (FRESH) Filtering, which is also known as *Widely Linear Almost Periodically Time-Varying* (WLAPTV) filtering. A summary of the work to date, including work on cyclostationary signals and FRESH filtering, was developed in [1] which introduced the term *Cyclic Wiener filtering*. The terms cyclic Wiener filtering and FRESH filtering are not equivalent as stated in [1] although today they are used synonymously in practice.

Frequency domain FRESH filtering was developed in [33] and the adaptation of such structures in [34, 35] is referred to as *time-dependent adaptive filters*. The performance of adaptive FRESH filters under cycle frequency error is evaluated in [36] and their ability to compensate for cycle frequency errors is also presented. Self Coherence Restoral (SCORE) is a least-squares blind adaptation algorithm for adapting antenna arrays based on the spectral correlation of a desired signal [37]. The performance of the SCORE algorithm under cycle frequency errors was evaluated in [38], which proposed a method for estimating and updating the cycle frequencies. The computational efficiency

of the method was later improved upon [39]. Similarly in [40] FRESH filter weights are blindly adapted based on the spectral correlation of the desired signal. In [41] a FRESH filter is applied to each receive antenna where all weights are jointly adapted. The foundation for characterization of higher order cyclostationarity using cumulants is presented in [42] and their applications in [43], and the estimation of cyclostationary features through the measurement of cyclic cumulants is presented in [44]. The advantages of cyclostationary signal maximum likelihood detectors was presented in [45] and later the classification and detection of cyclostationary signals using hidden Markov models in [46]. The detection of frequency hopping signals using a frequency-channelized whitening adaptive filter was proposed in [47].

The exploitation of the spectral redundancy in OFDM due to the cyclic prefix was proposed in [48] for its ability to remove channel impairments in Rayleigh fading, and later proposed for doubly selective channels [49] and to mitigate cyclostationary noise in power-line communications [50]. The use of FRESH filtering to correct for center frequency offset and I/Q imbalance is proposed in [51]. Detection of cyclostationary features inherent to OFDM signals is proposed in [52–56]. Creating or improving the cyclostationary characteristics of a single carrier signal has been proposed by [1, 57]. More recently improving the cyclostationary features of OFDM signals has been proposed by [58–60] for network identification and cognitive radio applications. In [59, 61] the cyclostationarity of an OFDM signal is incorporated by repeating symbols in frequency and time, respectively. The use of FRESH filtering to exploit the spectral redundancy due to symbol repetition is suggested in [62] but not explored any further.

Transmitting redundant symbols in OFDM has also been proposed by [63, 64] but without any references to cyclostationarity. In [63] a repetition code is used as an outer code to an inner convolutional code. The receiver corrects for any channel effects and combines the received symbols by weighting them according to their SNR and summing the result. The symbols are repeated across multiple frequencies in a pattern which maximizes their diversity. This is in contrast to [64] where a pseudo-random, non-periodic repetition pattern is used. The randomization avoids the possibility that redundant symbols are affected by frequency selective fading. The redundant symbols are hard decision or soft decision quantized and then combined using Maximal Ratio Combining (MRC). Transmission of redundant information within Long Term Evolution (LTE) exists through the use

of Transmission Time Interval (TTI) bundling [65]. TTI bundling allows for many slots to be sent without waiting for the acknowledgment or negative acknowledgment to return on the reverse link. This proposed approach could be incorporated into a technique like TTI bundling if frequency diversity is forced into the redundant slots.

Radar systems transmit much more power than cellular communication systems, and therefore co-existence approaches often favor interference avoidance rather than interference mitigation or excision. Exclusion zones have been proposed as a way to spatially and geographically separate radar and communications signals to ensure there is no harmful interference however, the exclusion zones within the United States prohibit communications within the coastal areas which are also the locations of the most dense populations [66–68]. An approach for using database-driven spectrum sensing for co-existence with radar was proposed in [69] which improves the flexibility and use of the spectrum for communications. A spectrum access system (SAS) for radar and communications co-existence in the CBRS band is proposed in [70] which presents a tiered spectrum-access architecture. The impact of adjacent channel interference of radar to time division LTE (TD-LTE) systems is measured in [11].

Rather than avoid the interference through exclusions zones, other techniques have been proposed to mitigate the impact of the interference. In [71] a method is presented for projecting the radar interference into the null space of the channel for multiple long term evolution (LTE) basestations. A similar approach is used in [72] although the focus is on resource allocation of LTE-Advanced resources under radar interference. Listen-before-talk and dynamic frequency selection modes for radar avoidance have been proposed for licensed-assisted access (LAA) LTE [73]. An information theoretic approach is described in [74] which jointly considers the communications signal and the radar as components of the same system, rather than treating either as interference, to improve performance. An information theoretic optimization is performed in [75] given a minimum signal to interference and noise ratio (SINR).

2.2 Background

The following sections provide an introduction to the necessary background materials used within the proposed research.

2.2.1 Cyclostationary Signals

First-Order Periodicity

The signal $x(t)$ contains first-order periodicity at frequency α when [26]:

$$m_x^\alpha = \lim_{T \to \infty} \frac{1}{T} \int_{-\frac{T}{2}}^{\frac{T}{2}} x(t) e^{-j2\pi\alpha t} dt \neq 0. \tag{2.1}$$

Second-Order Periodicity

Cyclostationary signals by definition are those which contain second-order periodicity in the time domain and spectral redundancy in the frequency domain [1]. Second-order periodicity is measured by the cyclic autocorrelation function (CAF),

$$R_x^\alpha(\tau) = \lim_{T \to \infty} \frac{1}{T} \int_{-\frac{T}{2}}^{\frac{T}{2}} x\left(t + \frac{\tau}{2}\right) x^*\left(t - \frac{\tau}{2}\right) e^{-j2\pi\alpha t} dt, \tag{2.2}$$

which gives the frequency content of the autocorrelation function of $x(t)$ at some frequency α [76]. Conceptually second-order periodicity is most easily associated with the baud rate of a signal, although it can come from other sources.

Just as the autocorrelation function and power spectral density are related through the Wiener-Khinchin relation, so are the cyclic autocorrelation function and the spectral correlation function [1]. The spectral correlation function [77] is:

$$S_x^\alpha(f) = \lim_{T \to \infty} \lim_{\Delta t \to \infty} \frac{1}{T \Delta t} \int_{-\frac{\Delta t}{2}}^{\frac{\Delta t}{2}} X_T\left(t, f + \frac{\alpha}{2}\right) X_T^*\left(t, f - \frac{\alpha}{2}\right) dt, \tag{2.3}$$

where:

$$X_T(t, v) = \int_{t-\frac{T}{2}}^{t+\frac{T}{2}} x(u) e^{-j2\pi vu} du. \tag{2.4}$$

The spectral correlation function $S_x^\alpha(f)$ is a measure of spectral redundancy at cycle frequency α [1]. A cycle frequency is a relative difference in frequency upon which the signal $x(t)$ spectrally correlates, $S_x^\alpha(f) \neq 0$. All finite power signals have at least one cycle frequency, $\alpha = 0$, however for cyclostationary signals there may be multiple cycle frequencies present in one cyclostationary signal.

Spectral redundancy is rarely referred to directly in regards to signals, although it is implied in many design decisions. Common examples include increasing the excess bandwidth in single carrier systems to improve signal acquisition performance [78] and using a cyclic prefix to avoid inter-symbol interference in OFDM signals [79]. Both of these methods increase spectral redundancy by increasing the bandwidth over the minimum needed to carry the information content. The terms *spectral correlation* and *spectral redundancy* are often used interchangeably.

Figure 2.1 describes how second-order periodicity and spectral redundancy are created in single carrier QAM signals. A series of stationary symbols is created, upsampled and then pulse shaped. In this example the signal has four samples per symbol. In the time domain the upsampling process creates a signal whose distribution of amplitude is periodic or cyclic in nature, yet within each of the four time offsets the distribution is stationary, leading to the name *cyclostationary*. In the frequency domain four perfect images of the original spectrum are created due to the upsampling and the pulse shaping filter reduces their amplitude, forming sidelobes of the signal. The spectral redundancy still exists at these frequencies but at a much lower power.

Cyclostationary signals may also have conjugate second-order periodicity, measured by the conjugate cyclic autocorrelation function,
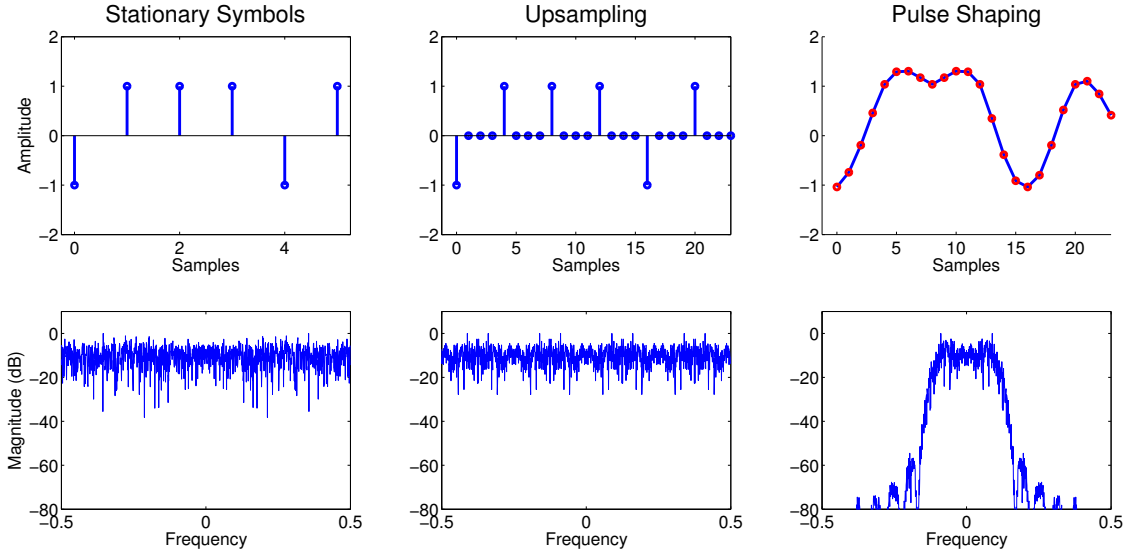
Figure 2.1: A stationary series of symbols is transformed into a cyclostationary signal through the upsampling process.

$$R_{xx^*}^{\beta}(\tau) = \lim_{T \to \infty} \frac{1}{T} \int_{-\frac{T}{2}}^{\frac{T}{2}} x\left(t + \frac{\tau}{2}\right) x\left(t - \frac{\tau}{2}\right) e^{-j2\pi\beta t} dt, \tag{2.5}$$

and conjugate spectral redundancy, measured by the conjugate spectral correlation function,

$$S_{xx^*}^{\beta}(f) = \lim_{T \to \infty} \lim_{\Delta t \to \infty} \frac{1}{T\Delta t} \int_{-\frac{\Delta t}{2}}^{\frac{\Delta t}{2}} X_T\left(t, f + \frac{\beta}{2}\right) X_T\left(t, -f + \frac{\beta}{2}\right) dt. \tag{2.6}$$

The cycle frequencies of the conjugate spectral correlation in (2.6) are denoted by β to distinguish them from the α cycle frequencies of the spectral correlation in (2.3). Therefore a signal is cyclostationary for any combination of $S_x^{\alpha}(f) \neq 0$ for $\alpha \neq 0$ and $S_{xx^*}^{\beta}(f) \neq 0$.

Almost Cyclostationary Signals

The exact type of cyclostationarity a signal possesses can be determined from the second-order periodicities within its autocorrelation and conjugate autocorrelation function. The autocorrelation function is defined by:

$$R_x(\tau) = \mathbb{E}\left\{x\left(t + \frac{\tau}{2}\right)x^*\left(t - \frac{\tau}{2}\right)\right\}, \tag{2.7}$$

and the conjugate autocorrelation function:

$$R_{xx^*}(\tau) = \mathbb{E}\left\{x\left(t + \frac{\tau}{2}\right)x\left(t - \frac{\tau}{2}\right)\right\}. \tag{2.8}$$

The cyclic autocorrelation function $R_x^\alpha(\tau)$ is used to determine second-order periodicity of frequency α is present within $x(t)$, and is also a component of a generalized Fourier Series [30] of the autocorrelation function,

$$R_x(t, \tau) = \sum_\alpha R_x^\alpha(\tau)e^{j2\pi\alpha t}, \tag{2.9}$$

and related through:

$$R_x^\alpha(\tau) = \lim_{T \to \infty} \frac{1}{T}\int_{-\frac{T}{2}}^{\frac{T}{2}} R_x(t, \tau)e^{-j2\pi\alpha t}dt. \tag{2.10}$$

Wide sense stationary signals contain no second-order periodicities, meaning the autocorrelation function does not contain any additive sine wave components of frequency $\alpha \neq 0$. Therefore their autocorrelation function can be written as [80],

$$R_x(t, \tau) = R_{t,x}^0(\tau). \tag{2.11}$$

Wide sense cyclostationary signals contain second-order periodicity, and as such the autocorrelation function is periodic,

$$R_x(t, \tau) = \sum_{n=-\infty}^{\infty} R_x^{\alpha_n}(\tau)e^{j2\pi\alpha_n t}, \tag{2.12}$$

where the cycle frequencies $\{\alpha_n\}$ are all commensurate [80] with period T,

$$\alpha_n = \frac{n}{T}, \; n = 0, \pm 1, \pm 2, \dots . \tag{2.13}$$

This can be interpreted as a Fourier series, with coefficients $R_x^{\frac{n}{T}}(\tau)$ and frequencies $\frac{n}{T}$ [77],

$$R_x(t, \tau) = \sum_{n=-\infty}^{\infty} R_x^{\frac{n}{T}}(\tau) e^{j2\pi \frac{n}{T} t}. \tag{2.14}$$

The cyclostationarity of many analog and digital single carrier signals is described in [28, 29]. A signal is almost cyclostationary when the autocorrelation function is an almost periodic function,

$$R_x(t, \tau) = \sum_{n \in A} R_x^{\alpha_n}(\tau) e^{j2\pi \alpha_n t}. \tag{2.15}$$

where the cycle frequencies $A = \{\alpha_n\}$ may not be commensurate [80].

Generalized Almost Cyclostationary Signals

The signal $x(t)$ is generalized almost cyclostationary (GACS) when the autocorrelation function is an almost periodic function and whose set of cycle frequencies $A_\tau = \{\alpha_n(\tau)\}$ is lag dependent and which may not be commensurate [80],

$$R_x(t, \tau) = \sum_{n \in A_\tau} R_x^{\alpha_n(\tau)}(\tau) e^{j2\pi \alpha_n(\tau) t}. \tag{2.16}$$

An example of a GACS signal is a continuous-time chirped radar signal [81], however periodically and uniformly sampling a continuous-time GACS signal transforms into a discrete-time ACS signal [82].

2.2.2 Wiener Filtering

The Wiener filter is the optimal time invariant filter [1], and the Finite Impulse Response (FIR) variant will be considered here. The filter weights are designed by minimizing the mean squared

error (MSE) of the filter, where the error is the squared difference between the desired signal and the estimate of the desired signal. Knowledge of the entire desired signal is impractical but provides a bound for performance. The received signal $x(t)$ will be modeled as,

$$x(t) = d(t) + i(t) + n(t), \tag{2.17}$$

where $d(t)$ is the desired signal, $i(t)$ is the interference and $n(t)$ is stationary noise. The output of the Wiener filter $\hat{d}(t)$ is therefore,

$$\hat{d}(t) = x(t) \otimes a(t), \tag{2.18}$$

where $a(t)$ are the weights of the Wiener filter and $\otimes$ represents convolution.

Frequency Domain Filtering

Operating a time-invariant filter in the time domain can be computationally intensive for large filter orders. A reduction in complexity can be achieved by filtering in the frequency domain [83]. Rather than implement a convolution in the time domain, the signal and filter weights are transformed into the frequency domain, multiplied, and then transformed back into the time domain. An example of one of these structures is given in Figure 2.2.
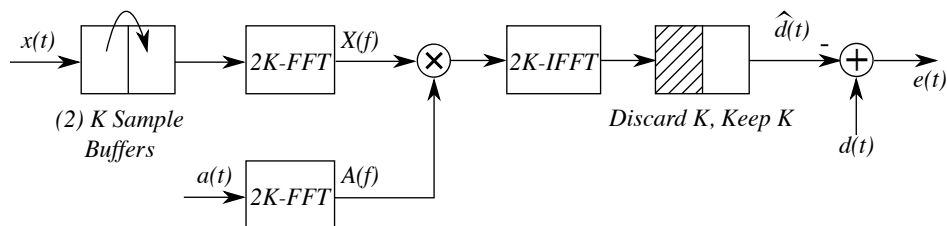
Figure 2.2: An example of an oversampled frequency domain filter using the overlap-save structure.

The MMSE filter weights for the frequency domain filter are found by setting the derivative of the MSE with respect to the filter weights equal to zero. The filter error $E(f)$ is the difference between the desired signal $D(f)$ and its estimate $\hat{D}(f)$,

$$E(f) = D(f) - \hat{D}(f), \tag{2.19}$$

where $D(f) = \mathcal{F}\{d(t)\}$ and $\hat{D}(f) = \mathcal{F}\{\hat{d}(t)\}$. The mean squared error E_{MSE} is minimized by taking the derivative with respect to filter $A^*(f)$,

$$E_{MSE} = \mathbb{E}\left\{|D(f) - \hat{D}(f)|^2\right\}, \tag{2.20}$$

and setting the result equal to zero,

$$\frac{\partial E_{MSE}}{\partial A^*(f)} = 0. \tag{2.21}$$

Solving the derivative (2.21) results in the orthogonal projection:

$$\mathbb{E}\left\{E(f)A^*(f)\right\} = 0, \tag{2.22}$$

which upon substitution of (2.19) results in the design equation for the MMSE filter weights $A(f)$,

$$A(f) = \frac{S_{dx}(f)}{S_x(f)}. \tag{2.23}$$

The solution for the filter weights (2.23) is applied to a system of equations, where L is the number of frequency domain samples,

$$\begin{bmatrix} S_x(f_0) & 0 & 0 & \dots & 0 \\ 0 & S_x(f_1) & 0 & \dots & 0 \\ 0 & 0 & S_x(f_2) & \dots & 0 \\ \dots & \dots & \dots & \dots & \dots \\ 0 & 0 & 0 & \dots & S_x(f_{L-1}) \end{bmatrix} \begin{bmatrix} A(f_0) \\ A(f_1) \\ A(f_2) \\ \dots \\ A(f_{L-1}) \end{bmatrix} = \begin{bmatrix} S_{dx}(f_0) \\ S_{dx}(f_1) \\ S_{dx}(f_2) \\ \dots \\ S_{dx}(f_{L-1}) \end{bmatrix}. \tag{2.24}$$

The system of equations can be simplified and re-written as:

$$\mathbf{S}_x \mathbf{A} = \mathbf{S}_{dx}. \tag{2.25}$$

The filter weights can then be solved according to:

$$\mathbf{A} = \mathbf{S}_x^{-1} \mathbf{S}_{dx}. \tag{2.26}$$

Time Domain Filtering

The time domain Wiener filter output, $\hat{d}[k]$, is described in the time domain by:

$$\hat{d}[k] = a[k] \otimes x[k]. \tag{2.27}$$

The frequency domain MMSE filter weight design equation from (2.23) is translated into the time domain using the inverse Fourier Transform,

$$r_{dx}[k] = a[k] \otimes r_x[k]. \tag{2.28}$$

The autocorrelation $r_x[k]$ and spectral density $S_x(f)$ are related through the Wiener relation [1], where $\mathcal{F}^{-1}\{S_x(f)\} = r_x[k]$. The same is true for the cross correlation $r_{dx}[k]$ and cross spectral density $S_{dx}(f)$ where $\mathcal{F}^{-1}\{S_{dx}(f)\} = r_{dx}[k]$. The convolution in the design equation (2.28) is written explicitly:

$$r_{dx}[k] = \sum_{p=0}^{P-1} a[k] r_x[k-p], \tag{2.29}$$

where the filter $a[k]$ has P filter weights. The convolution in (2.29) is expanded into a system of equations:

$$
\begin{array}{llllll}
a[0]r_x[0] & + & a[1]r_x[-1] & + & \ldots & + & a[P-1]r_x[-P+1] & = & r_{dx}[0] \\
a[0]r_x[-1] & + & a[1]r_x[0] & + & \ldots & + & a[P-1]r_x[-P+2] & = & r_{dx}[1] \\
\ldots & & \ldots & & \ldots & & \ldots & & \ldots \\
a[0]r_x[-P+1] & + & a[1]r_x[-P+2] & + & \ldots & + & a[P-1]r_x[0] & = & r_{dx}[P-1].
\end{array}
\tag{2.30}
$$

The system of linear equations can then be written in matrix form:

$$
\begin{bmatrix}
r_x[0] & r_x[-1] & \ldots & r_x[-P+1] \\
r_x[1] & r_x[0] & \ldots & r_x[-P+2] \\
\ldots & \ldots & \ldots & \ldots \\
r_x[P-1] & r_x[P-2] & \ldots & r_x[0]
\end{bmatrix}
\begin{bmatrix}
a[0] \\
a[1] \\
\ldots \\
a[P-1]
\end{bmatrix}
=
\begin{bmatrix}
r_{dx}[0] \\
r_{dx}[1] \\
\ldots \\
r_{dx}[P-1]
\end{bmatrix}.
\tag{2.31}
$$

The equations can be simplified by writing:

$$
\mathbf{R}_x \mathbf{a} = \mathbf{r}_{dx},
\tag{2.32}
$$

and the filter weights can then be found according to:

$$
\mathbf{a} = \mathbf{R}_x^{-1} \mathbf{r}_{dx}.
\tag{2.33}
$$

2.2.3   FRESH Filtering

Filter Structures

A Frequency Shift (FRESH) filter is the optimal filter for cyclostationary signals [1]. It exploits spectrally redundant information in cyclostationary signals to improve the estimates of the desired signal. The process filters the received signal through a parallel set of frequency shifters, followed by Linear Time-Invariant (LTI) filters and the summation of their parallel outputs. The FRESH filter is defined as:

$$\hat{d}(t) = \sum_{m=0}^{M-1} a_m(t) \otimes x(t) e^{j2\pi\alpha_m t} + \sum_{n=0}^{N-1} b_n(t) \otimes x^*(t) e^{j2\pi\beta_n t}, \tag{2.34}$$

where $\otimes$ is the convolution operator [1], $x(t)$ is the received signal, and $\hat{d}(t)$ is the estimate of the desired signal $d(t)$. The FRESH filter is illustrated in Figure 2.3.
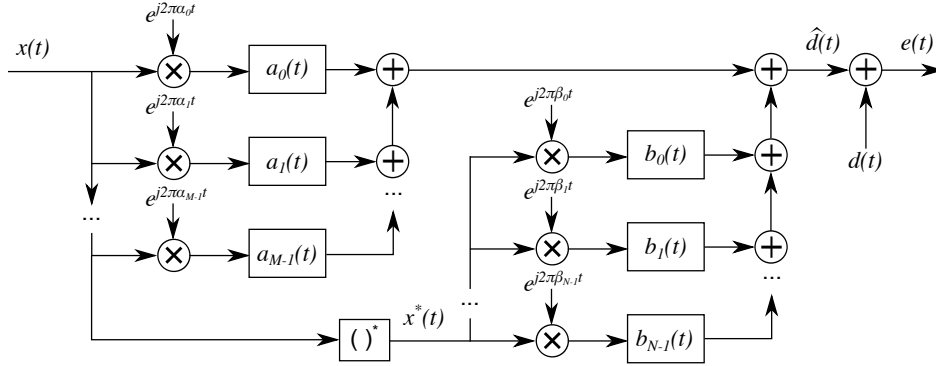
Figure 2.3: The time-domain implementation of the FRESH filter from [1].

Performing filtering in the frequency domain reduces the computational load for time-invariant filters [83] and the same is true for time-varying filters. Frequency domain time-invariant filters operate by transforming the input signal into the frequency domain, filtering by the multiplication of frequency domain weights and then transforming back into the time domain. Frequency domain FRESH filters operate similarly, an example given in Figure 2.4, with frequency shifts performed by circular shifting and where spectrally correlated bins are filtered and summed [33]. While conceptually frequency domain FRESH filters utilize circular shifts, in practice the frequency shifting is done through memory indexing.

The FRESH filter is a Linear-Conjugate Linear (LCL) filter, with the linear branches corresponding to filters $a_m(t)$ and frequency shifts α_m and the conjugate linear branches corresponding to filters $b_n(t)$ and frequency shifts β_n. The FRESH filter is not strictly linear but may be referred to as *widely linear* [31]. The Wiener filter is a degenerate case of the FRESH filter where $\{\alpha\} = \{0\}$ and $\{\beta\} = \{\varnothing\}$. In this case no spectral redundancy is exploited by the filter leading to the decrease in performance relative to the FRESH filter.
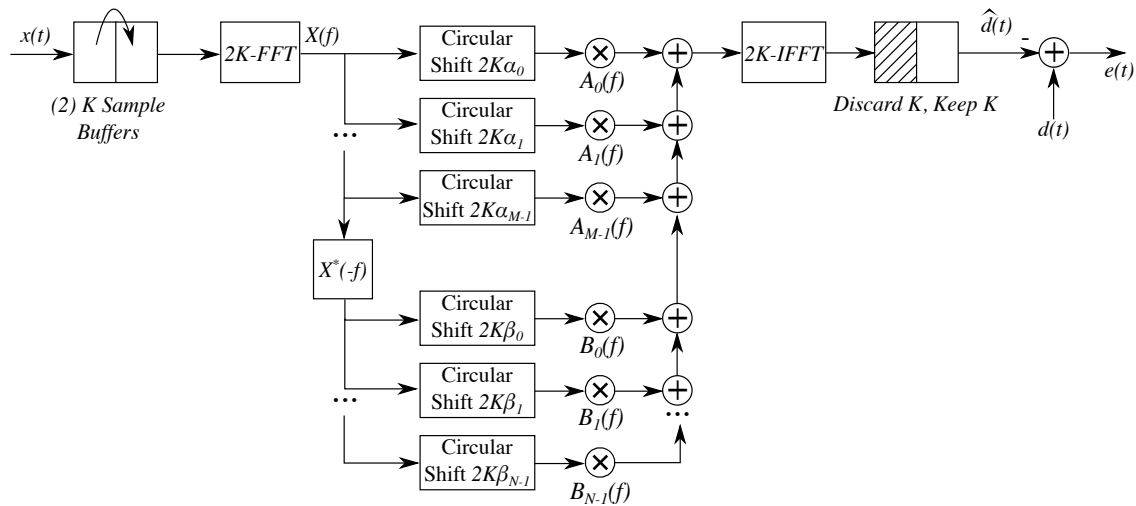
Figure 2.4: An example of an oversampled frequency domain FRESH filter using the overlap-save structure.

Frequency Shifts

The set of frequency shifts $\{\alpha\}$ can come from the desired signal $d(t)$ and cyclostationary interference $i(t)$ within the received signal $x(t)$. Linearly combining $d(t)$ and $i(t)$ creates additional second-order periodicities within $x(t)$ from their cycle frequency differences which can be exploited by the FRESH filter [1]. The set of cycle frequencies corresponding to the desired signal is given by $\{\gamma_d\} = \{\gamma_{d,0}, \gamma_{d,1}, \gamma_{d,2}, \ \ldots\}$ and the set for the interference is given by $\{\gamma_i\} = \{\gamma_{i,0}, \gamma_{i,1}, \gamma_{i,2}, \ \ldots\}$. The set of all frequency shifts $\{\alpha\}$ is therefore:

$$\{\alpha\} = \{\gamma_{d,0}, \ \gamma_{d,1}, \ \gamma_{d,2}, \ \cdots \ ,$$
$$\gamma_{i,0}, \ \gamma_{i,1}, \ \gamma_{i,2}, \ \cdots \ ,$$
$$\gamma_{d,0} - \gamma_{i,0}, \ -\gamma_{d,0} + \gamma_{i,0},$$
$$\gamma_{d,0} - \gamma_{i,1}, \ -\gamma_{d,0} + \gamma_{i,1},$$
$$\cdots \ ,$$
$$\gamma_{d,1} - \gamma_{i,0}, \ -\gamma_{d,1} + \gamma_{i,0},$$
$$\gamma_{d,1} - \gamma_{i,1}, \ -\gamma_{d,1} + \gamma_{i,1},$$
$$\cdots \ \}. \tag{2.35}$$

The frequency shift α_m is therefore the mth element of the set $\{\alpha\}$, and $\{\alpha\}$ does not have to be ordered in a specific manner. The set $\{\beta\}$ is formed similarly. If $\{\zeta_d\}$ is the set of cycle frequencies of the conjugate spectral redundancy for the desired signal, and $\{\zeta_i\}$ for the interference, then:

$$\{\beta\} = \{\zeta_{d,0}, \ \zeta_{d,1}, \ \zeta_{d,2}, \ \cdots \ ,$$
$$\zeta_{i,0}, \ \zeta_{i,1}, \ \zeta_{d,2}, \ \cdots \ ,$$
$$\zeta_{d,0} - \zeta_{i,0}, \ -\zeta_{d,0} + \zeta_{i,0},$$
$$\zeta_{d,0} - \zeta_{i,1}, \ -\zeta_{d,0} + \zeta_{i,1},$$
$$\cdots \ ,$$
$$\zeta_{d,1} - \zeta_{i,0}, \ -\zeta_{d,2} + \zeta_{i,0},$$
$$\zeta_{d,1} - \zeta_{i,1}, \ -\zeta_{d,2} + \zeta_{i,1},$$
$$\cdots \ \}. \tag{2.36}$$

The frequency shifts $e^{j2\pi\alpha_m t}$ align the spectral redundancies within $x(t)$, which are then combined using the filters $a_m(t)$. Similarly, the frequency shifts $e^{j2\pi\beta_n t}$ align the conjugate spectral redundancies within $x^*(t)$, which are combined using the filters $b_n(t)$.

MMSE Filter Weights

One method for determining the optimal filters $a_m(t)$ and $b_n(t)$ is to minimize the Mean Squared Error (MSE) produced by the FRESH filter, where the error is the difference between the desired signal $d(t)$ and its estimate, $\hat{d}(t)$. Finding the filter weights which minimize the MSE is simpler mathematically in the frequency domain, therefore the filter estimate $\mathcal{F}\{\hat{d}(t)\}$ is transformed into the frequency domain in (2.37),

$$\hat{D}(f) = \sum_{m=0}^{M-1} A_m(f) X\left(f - \alpha_m\right) + \sum_{n=0}^{N-1} B_n(f) X^*\left(-f + \beta_n\right), \tag{2.37}$$

where $\mathcal{F}\{a_m(t)\} = A_m(f)$ and $\mathcal{F}\{b_n(t)\} = B_n(f)$. The filter error $E(f)$ is given by (2.38), where $\mathcal{F}\{d(t)\} = D(f)$ and the mean squared error $E_{MSE}(f)$ is given by (2.39),

$$E(f) = D(f) - \hat{D}(f), \tag{2.38}$$

$$E_{MSE}(f) = \mathbb{E}\left\{E(f)E^*(f)\right\}. \tag{2.39}$$

To find the filters $A_m(f)$ and $B_n(f)$ that minimize the MSE, the derivative of the MSE is taken with respect to both sets of filters and set equal to zero as in (2.40) and (2.41),

$$\frac{\partial E_{MSE}(f)}{\partial A_p^*(f)} = 0, \tag{2.40}$$

$$\frac{\partial E_{MSE}(f)}{\partial B_q^*(f)} = 0. \tag{2.41}$$

Performing the derivatives of the MSE results in two orthogonal projections as expected for a Minimum Mean Squared Error (MMSE) filter, (2.42) and (2.43). The projections state that the filter error $E(f)$ is orthogonal to the input $X(f)$ and $X^*(f)$ at each of the frequency shifts,

$$\mathbb{E}\left\{E(f)X^*\left(f - \alpha_p\right)\right\} = 0, \tag{2.42}$$

$$\mathbb{E}\left\{E(f)X\left(-f + \beta_q\right)\right\} = 0. \tag{2.43}$$

The filter error $E(f)$ (2.38) is substituted into the orthogonal projections (2.42) and (2.43), resulting in the FRESH filter design equations in [1],

$$S_{dx}^{\alpha_p}\left(f - \frac{\alpha_p}{2}\right) = \sum_{m=0}^{M-1} S_x^{\alpha_p - \alpha_m}\left(f - \frac{\alpha_m + \alpha_p}{2}\right) A_m(f) + \sum_{n=0}^{N-1} S_{xx^*}^{\beta_n - \alpha_p}\left(f - \frac{\beta_n + \alpha_p}{2}\right)^* B_n(f),$$

$$p = 0, 1, \ldots, M - 1, \tag{2.44}$$

$$S_{dx^*}^{\beta_q}\left(f - \frac{\beta_q}{2}\right) = \sum_{m=0}^{M-1} S_{xx^*}^{\beta_q - \alpha_m}\left(f - \frac{\alpha_m + \beta_q}{2}\right) A_m(f) + \sum_{n=0}^{N-1} S_x^{\beta_q - \beta_n}\left(-f + \frac{\beta_n + \beta_q}{2}\right) B_n(f),$$

$$q = 0, 1, \ldots, N - 1. \tag{2.45}$$

A system of linear equations is desired to solve for the frequency domain filter weights, similar to that of (2.24). A compact matrix representation, analogous to (2.25), is given by:

$$\begin{bmatrix} \mathbf{S}_x(f) & \mathbf{S}_{xx^*}(f)^* \\ \mathbf{S}_{xx^*}(f) & \mathbf{S}_x(-f) \end{bmatrix} \begin{bmatrix} \mathbf{A} \\ \mathbf{B} \end{bmatrix} = \begin{bmatrix} \mathbf{S}_{dx} \\ \mathbf{S}_{dx^*} \end{bmatrix}. \tag{2.46}$$

The correlation matrices $\mathbf{S}_x(f)$, $\mathbf{S}_{xx^*}(f)^*$, $\mathbf{S}_{xx^*}(f)$, and $\mathbf{S}_x(-f)$ contain the spectral correlation of $x(t)$ and $x^*(t)$ at a series of combinations of cycle frequencies α and β. The correlation matrices are:

$$
\mathbf{S}_x(f) = \begin{bmatrix}
\mathbf{S}_x^{\alpha_0-\alpha_0}\left(f-\frac{\alpha_0+\alpha_0}{2}\right) & \mathbf{S}_x^{\alpha_0-\alpha_1}\left(f-\frac{\alpha_1+\alpha_0}{2}\right) & \cdots & \mathbf{S}_x^{\alpha_0-\alpha_{M-1}}\left(f-\frac{\alpha_{M-1}+\alpha_0}{2}\right) \\
\mathbf{S}_x^{\alpha_1-\alpha_0}\left(f-\frac{\alpha_0+\alpha_1}{2}\right) & \mathbf{S}_x^{\alpha_1-\alpha_1}\left(f-\frac{\alpha_1+\alpha_1}{2}\right) & \cdots & \mathbf{S}_x^{\alpha_1-\alpha_{M-1}}\left(f-\frac{\alpha_{M-1}+\alpha_1}{2}\right) \\
\cdots & \cdots & \cdots & \cdots \\
\mathbf{S}_x^{\alpha_{M-1}-\alpha_0}\left(f-\frac{\alpha_0+\alpha_{M-1}}{2}\right) & \mathbf{S}_x^{\alpha_{M-1}-\alpha_1}\left(f-\frac{\alpha_1+\alpha_{M-1}}{2}\right) & \cdots & \mathbf{S}_x^{\alpha_{M-1}-\alpha_{M-1}}\left(f-\frac{\alpha_{M-1}+\alpha_{M-1}}{2}\right)
\end{bmatrix}, \quad (2.47)
$$

$$
\mathbf{S}_{xx^*}(f)^* = \begin{bmatrix}
\mathbf{S}_{xx^*}^{\beta_0-\alpha_0}\left(f-\frac{\beta_0+\alpha_0}{2}\right)^* & \mathbf{S}_{xx^*}^{\beta_1-\alpha_0}\left(f-\frac{\beta_1+\alpha_0}{2}\right)^* & \cdots & \mathbf{S}_{xx^*}^{\beta_{N-1}-\alpha_0}\left(f-\frac{\beta_{N-1}+\alpha_0}{2}\right)^* \\
\mathbf{S}_{xx^*}^{\beta_0-\alpha_1}\left(f-\frac{\beta_0+\alpha_1}{2}\right)^* & \mathbf{S}_{xx^*}^{\beta_1-\alpha_1}\left(f-\frac{\beta_1+\alpha_1}{2}\right)^* & \cdots & \mathbf{S}_{xx^*}^{\beta_{N-1}-\alpha_1}\left(f-\frac{\beta_{N-1}+\alpha_1}{2}\right)^* \\
\cdots & \cdots & \cdots & \cdots \\
\mathbf{S}_{xx^*}^{\beta_0-\alpha_{N-1}}\left(f-\frac{\beta_0+\alpha_{N-1}}{2}\right)^* & \mathbf{S}_{xx^*}^{\beta_1-\alpha_{N-1}}\left(f-\frac{\beta_1+\alpha_{N-1}}{2}\right)^* & \cdots & \mathbf{S}_{xx^*}^{\beta_{N-1}-\alpha_{N-1}}\left(f-\frac{\beta_{N-1}+\alpha_{N-1}}{2}\right)^*
\end{bmatrix}, \quad (2.48)
$$

$$
\mathbf{S}_{xx^*}(f) = \begin{bmatrix}
\mathbf{S}_{xx^*}^{\beta_0-\alpha_0}\left(f-\frac{\alpha_0+\beta_0}{2}\right) & \mathbf{S}_{xx^*}^{\beta_0-\alpha_1}\left(f-\frac{\alpha_1+\beta_0}{2}\right) & \cdots & \mathbf{S}_{xx^*}^{\beta_0-\alpha_{M-1}}\left(f-\frac{\alpha_{M-1}+\beta_0}{2}\right) \\
\mathbf{S}_{xx^*}^{\beta_1-\alpha_0}\left(f-\frac{\alpha_0+\beta_1}{2}\right) & \mathbf{S}_{xx^*}^{\beta_1-\alpha_1}\left(f-\frac{\alpha_1+\beta_1}{2}\right) & \cdots & \mathbf{S}_{xx^*}^{\beta_1-\alpha_{M-1}}\left(f-\frac{\alpha_{M-1}+\beta_1}{2}\right) \\
\cdots & \cdots & \cdots & \cdots \\
\mathbf{S}_{xx^*}^{\beta_{N-1}-\alpha_0}\left(f-\frac{\alpha_0+\beta_{N-1}}{2}\right) & \mathbf{S}_{xx^*}^{\beta_{N-1}-\alpha_1}\left(f-\frac{\alpha_1+\beta_{N-1}}{2}\right) & \cdots & \mathbf{S}_{xx^*}^{\beta_{N-1}-\alpha_{M-1}}\left(f-\frac{\alpha_{M-1}+\beta_{N-1}}{2}\right)
\end{bmatrix}, \quad (2.49)
$$

$$
\mathbf{S}_x(-f) = \begin{bmatrix}
\mathbf{S}_x^{\beta_0-\beta_0}\left(-f+\frac{\beta_0+\beta_0}{2}\right) & \mathbf{S}_x^{\beta_0-\beta_1}\left(-f+\frac{\beta_1+\beta_0}{2}\right) & \cdots & \mathbf{S}_x^{\beta_0-\beta_{N-1}}\left(-f+\frac{\beta_{N-1}+\beta_0}{2}\right) \\
\mathbf{S}_x^{\beta_1-\beta_0}\left(-f+\frac{\beta_0+\beta_1}{2}\right) & \mathbf{S}_x^{\beta_1-\beta_1}\left(-f+\frac{\beta_1+\beta_1}{2}\right) & \cdots & \mathbf{S}_x^{\beta_1-\beta_{N-1}}\left(-f+\frac{\beta_{N-1}+\beta_1}{2}\right) \\
\cdots & \cdots & \cdots & \cdots \\
\mathbf{S}_x^{\beta_{N-1}-\beta_0}\left(-f+\frac{\beta_0+\beta_{N-1}}{2}\right) & \mathbf{S}_x^{\beta_{N-1}-\beta_1}\left(-f+\frac{\beta_1+\beta_{N-1}}{2}\right) & \cdots & \mathbf{S}_x^{\beta_{N-1}-\beta_{N-1}}\left(-f+\frac{\beta_{N-1}+\beta_{N-1}}{2}\right)
\end{bmatrix}. \quad (2.50)
$$

Each of the correlation matrices (2.47)-(2.50) themselves is comprised of submatrices, each submatrix corresponding to a different cycle frequency. The submatricies are given by:

$$
\mathbf{S}_x^{\alpha_p-\alpha_m}\left(f-\frac{\alpha_m+\alpha_p}{2}\right) = \begin{bmatrix}
S_x^{\alpha_p-\alpha_m}\left(f_0-\frac{\alpha_m+\alpha_p}{2}\right) & 0 & \cdots & 0 \\
0 & S_x^{\alpha_p-\alpha_m}\left(f_1-\frac{\alpha_m+\alpha_p}{2}\right) & \cdots & 0 \\
\cdots & \cdots & \cdots & \cdots \\
0 & 0 & \cdots & S_x^{\alpha_p-\alpha_m}\left(f_{L-1}-\frac{\alpha_m+\alpha_p}{2}\right)
\end{bmatrix}, \quad (2.51)
$$

$$\mathbf{S}_{xx^*}^{\beta_n-\alpha_p}\left(f-\tfrac{\beta_n+\alpha_p}{2}\right)^* = \begin{bmatrix} S_{xx^*}^{\beta_n-\alpha_p}\left(f_0-\tfrac{\beta_n+\alpha_p}{2}\right)^* & 0 & \cdots & 0 \\ 0 & S_{xx^*}^{\beta_n-\alpha_p}\left(f_1-\tfrac{\beta_n+\alpha_p}{2}\right)^* & \cdots & 0 \\ \cdots & \cdots & \cdots & \cdots \\ 0 & 0 & \cdots & S_{xx^*}^{\beta_n-\alpha_p}\left(f_{L-1}-\tfrac{\beta_n+\alpha_p}{2}\right)^* \end{bmatrix}, \quad (2.52)$$

$$\mathbf{S}_{xx^*}^{\beta_q-\alpha_m}\left(f-\tfrac{\alpha_m+\beta_q}{2}\right) = \begin{bmatrix} S_{xx^*}^{\beta_q-\alpha_m}\left(f_0-\tfrac{\alpha_m+\beta_q}{2}\right) & 0 & \cdots & 0 \\ 0 & S_{xx^*}^{\beta_q-\alpha_m}\left(f_1-\tfrac{\alpha_m+\beta_q}{2}\right) & \cdots & 0 \\ \cdots & \cdots & \cdots & \cdots \\ 0 & 0 & \cdots & S_{xx^*}^{\beta_q-\alpha_m}\left(f_{L-1}-\tfrac{\alpha_m+\beta_q}{2}\right) \end{bmatrix}, \quad (2.53)$$

$$\mathbf{S}_{x}^{\beta_q-\beta_n}\left(-f+\tfrac{\beta_n+\beta_q}{2}\right) = \begin{bmatrix} S_{x}^{\beta_q-\beta_n}\left(-f_0+\tfrac{\beta_n+\beta_q}{2}\right) & 0 & \cdots & 0 \\ 0 & S_{x}^{\beta_q-\beta_n}\left(-f_1+\tfrac{\beta_n+\beta_q}{2}\right) & \cdots & 0 \\ \cdots & \cdots & \cdots & \cdots \\ 0 & 0 & \cdots & S_{x}^{\beta_q-\beta_n}\left(-f_{L-1}+\tfrac{\beta_n+\beta_q}{2}\right) \end{bmatrix}. \quad (2.54)$$

The coefficient vectors $\mathbf{A}$ and $\mathbf{B}$ in (2.46) are comprised of sub-vectors,

$$\mathbf{A} = \begin{bmatrix} \mathbf{A}_0 \\ \mathbf{A}_1 \\ \mathbf{A}_2 \\ \cdots \\ \mathbf{A}_{M-1} \end{bmatrix}, \quad (2.55)$$

$$\mathbf{B} = \begin{bmatrix} \mathbf{B}_0 \\ \mathbf{B}_1 \\ \mathbf{B}_2 \\ \cdots \\ \mathbf{B}_{N-1} \end{bmatrix}. \quad (2.56)$$

Each sub-vector in (2.55) and (2.56) is a set of filter coefficients,

$$
\mathbf{A}_0 = \begin{bmatrix} A_0(f_0) \\ A_0(f_1) \\ A_0(f_2) \\ \dots \\ A_0(f_{L-1}) \end{bmatrix}, \tag{2.57}
$$

$$
\mathbf{B}_0 = \begin{bmatrix} B_0(f_0) \\ B_0(f_1) \\ B_0(f_2) \\ \dots \\ B_0(f_{L-1}) \end{bmatrix}. \tag{2.58}
$$

The vectors $\mathbf{S}_{dx}$ and $\mathbf{S}_{dx^*}$ from (2.46) contain the spectral cross correlations of $d(t)$ and $x(t)$ at all cycle frequencies $\{\alpha\}$, and the spectral cross correlations of $d(t)$ and $x^*(t)$ at all cycle frequencies $\{\beta\}$. The vectors are given by:

$$
\mathbf{S}_{dx} = \begin{bmatrix} \mathbf{S}_{dx}^{\alpha_0}(f) \\ \mathbf{S}_{dx}^{\alpha_1}(f) \\ \dots \\ \mathbf{S}_{dx}^{\alpha_{M-1}}(f) \end{bmatrix}, \tag{2.59}
$$

$$
\mathbf{S}_{dx^*} = \begin{bmatrix} \mathbf{S}_{dx^*}^{\beta_0}(f) \\ \mathbf{S}_{dx^*}^{\beta_1}(f) \\ \dots \\ \mathbf{S}_{dx^*}^{\beta_{N-1}}(f) \end{bmatrix}. \tag{2.60}
$$

The sub-vectors are the spectral cross correlations at each cycle frequency,

$$\mathbf{S}_{dx}^{\alpha_0}(f) \begin{bmatrix} S_{dx}^{\alpha_0}\left(f - \frac{\alpha_0}{2}\right) \\ S_{dx}^{\alpha_1}\left(f - \frac{\alpha_1}{2}\right) \\ \dots \\ S_{dx}^{\alpha_{M-1}}\left(f - \frac{\alpha_{M-1}}{2}\right) \end{bmatrix}, \tag{2.61}$$

$$\mathbf{S}_{dx^*}^{\beta_0}(f) \begin{bmatrix} S_{dx^*}^{\beta_0}\left(f - \frac{\beta_0}{2}\right) \\ S_{dx^*}^{\beta_1}\left(f - \frac{\beta_1}{2}\right) \\ \dots \\ S_{dx^*}^{\beta_{N-1}}\left(f - \frac{\beta_{N-1}}{2}\right) \end{bmatrix}. \tag{2.62}$$

Once all of the matrices and vectors are populated with the spectral autocorrelation and spectral cross correlation values the filter weights can be solved according to:

$$\begin{bmatrix} \mathbf{A} \\ \mathbf{B} \end{bmatrix} = \begin{bmatrix} \mathbf{S}_x(f) & \mathbf{S}_{xx^*}(f)^* \\ \mathbf{S}_{xx^*}(f) & \mathbf{S}_x(-f) \end{bmatrix}^{-1} \begin{bmatrix} \mathbf{S}_{dx} \\ \mathbf{S}_{dx^*} \end{bmatrix}. \tag{2.63}$$

2.2.4 Matrix-Based Whitening Filter

A whitening filter transforms a colored signal into one whose spectrum is white. The filter weights of such a transform are dependent on the received signal, and the method of [84] uses a Cholesky decomposition of the covariance matrix to find such filter weights.

The time-domain received signal, $x[k]$, is transformed into the frequency domain using a discrete Fourier transform (DFT) with size N_{FFT}, resulting in a matrix of frequency domain samples:

$$\mathbf{X} = \begin{bmatrix} \mathbf{X}_0 \\ \mathbf{X}_1 \\ \mathbf{X}_2 \\ \vdots \\ \mathbf{X}_{N_{FFT}-1} \end{bmatrix}. \tag{2.64}$$

The entries $\mathbf{X}_l$ are row vectors of the frequency domain samples,

$$\mathbf{X}_l = \begin{bmatrix} X[0,l], & X[1,l], & X[2,l] & \dots \end{bmatrix}, \tag{2.65}$$

where $X[f,l]$ is the fth frequency bin within the lth set of frequency domain samples. The time-series and frequency domain samples are related through:

$$\mathcal{F} \left\{ \begin{bmatrix} x\left[lN_{FFT}\right] \\ x\left[lN_{FFT}+1\right] \\ x\left[lN_{FFT}+2\right] \\ \vdots \\ x\left[(l+1)N_{FFT}-1\right] \end{bmatrix} \right\} = \begin{bmatrix} X[0,l] \\ X[1,l] \\ X[2,l] \\ \vdots \\ X[N_{FFT}-1,l] \end{bmatrix}, \tag{2.66}$$

where $\mathcal{F}$ is the DFT operator.

The covariance matrix $\mathbf{C}$ of $x[k]$ is found according to:

$$C[r,c] = \mathbb{E}\left\{ (\mathbf{X}_r - \mu_r)(\mathbf{X}_c - \mu_c)^* \right\}, \tag{2.67}$$

where $\mu_r = \mathbb{E}\left\{\mathbf{X}_r\right\}$, $r = 0,1,2,\dots N_{FFT} - 1$ and $c = 0,1,2,\dots N_{FFT} - 1$. Using the Cholesky decomposition the inverse of the correlation matrix can then be represented by [84],
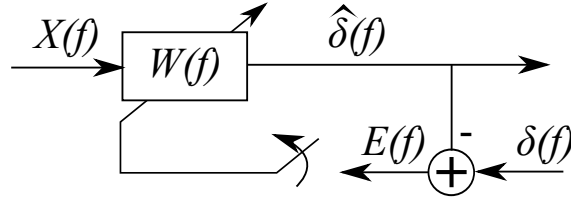
Figure 2.5: The frequency domain implementation of the TIW. The feedback switch is opened once the filter is trained, and the weights are no longer adapted so the signal detection can occur.

$$\mathbf{C}^{-1} = \mathbf{W}_{chol}^{\dagger}\mathbf{W}_{chol}, \tag{2.68}$$

where $\mathbf{W}_{chol}$ are the weights for the whitening filter and $\dagger$ is the Hermitian operator.

2.2.5 Time-Invariant Whitening Filter

Rather than adapt according to a communications signal, the filter weights can be adapted in order to whiten the spectrum when the desired signal is an impulse, $d[k] = \delta[k]$. The filter structure will be referred to as a TIW under these circumstances. Figure 2.5 gives the block diagram for the TIW. The design equations for the TIW then become:

$$\mathbf{W}_{TIW} = \frac{\mathbf{S}_{\delta x}}{\mathbf{S}_x} = \frac{diag\left(\mathbb{E}\{\boldsymbol{\delta}\mathbf{X}^{\dagger}\}\right)}{diag\left(\mathbb{E}\{\mathbf{X}\mathbf{X}^{\dagger}\}\right)}. \tag{2.69}$$

The matrix $\boldsymbol{\delta}$ is formed by the DFT of $\delta[k]$, and substituting in results in a simpler design equation:

$$\begin{aligned}
\mathbf{W}_{TIW} &= \frac{\mathbf{X}_0^*}{diag\left(\mathbb{E}\{\mathbf{X}\mathbf{X}^{\dagger}\}\right)} \\
&= diag\left(\mathbb{E}\{\mathbf{X}\mathbf{X}^{\dagger}\}\right)^{-1}\mathbf{X}_0^*,
\end{aligned} \tag{2.70}$$

analogous to the results of the Cholesky decomposition in (2.68).

The filter weights minimize the error between the received signal spectrum and a spectrum that is

perfectly flat, since $\mathcal{F}\{\delta[k]\} = 1$. Although implemented differently, this is the same effect from the Cholesky decomposition in Section 2.2.4. The filter weights of (2.68) and (2.70) are both derived from the product of a matrix and its Hermitian, one being the inverse covariance matrix and one being the inverse power spectral density matrix, respectively.

2.2.6   Orthogonal Frequency Division Multiplexing

The most relevant multicarrier modulation today is Orthogonal Frequency Division Multiplexing (OFDM), and while proposed in 1966 by [85] it is most known for its recent use in WiFi and Long Term Evolution (LTE). OFDM derives its name from modulating its information upon orthogonal subcarriers with the most common implementation of the modulation and demodulation coming from the Inverse Fast Fourier Transform (IFFT) and the Fast Fourier Transform (FFT) [86]. While a computationally efficient modulation and demodulation scheme, OFDM has high sidelobes which can result in high intercarrier-interference if the orthogonality between subcarriers is broken. In addition, a cyclic prefix is used to avoid intersymbol-interference in the presence of a multi-path channel [87]. Multiplexing the signal in frequency over low-bandwidth subcarriers can allow a frequency selective channel to be modeled as flat fading with respect to each individual subcarrier, enabling a very efficient single-tap equalization method.

OFDM has been used to provide LTE with a large increase in data rate over prior 3G Code Division Multiple Access (CDMA) systems yet there are still drawbacks, potentially limiting its use in future standardization [88]. The orthogonality of subcarriers within OFDM is created due to the perfect reconstruction properties of the Discrete Fourier Transform (DFT) and Inverse Discrete Fourier Transform (IDFT) filter banks [89] of which the FFT and IFFT are built. The orthogonality is very fragile and can be destroyed with any disturbance such as Doppler shifts coming in a mobile environment. The use of a cyclic prefix to avoid intersymbol-interference introduces redundancy into the signal and reduces its spectral efficiency.

2.2.7   Simulated Annealing

Simulated annealing [90] is a meta-heuristic optimization approach that has been applied to Cognitive Radio [91]. Simulated annealing derives its technique from metallurgy, where the temperature of a metal is high while being shaped and is gradually cooled as it takes its final shape. In our context, this process is simulated by testing a series of candidate solutions (heating and forging), measuring their performance, and gradually narrowing down the scope of potential solutions over time (cooling). To avoid focusing on a local maxima, simulated annealing uses a probabilistic function to determine if a solution with relatively worse performance will be accepted. Over time, this probability is decreased, allowing the algorithm to find the global maximum.

Simulated annealing is used in Chapter 3 to optimize the waveform parameters which minimize the BER while maximizing the spectral efficiency, subject to an objective function. The multi-objective non-linear optimization problem makes deriving an analytic solution difficult, and therefore simulated annealing is used to approximate the optimal solutions.

Chapter 3

Paramorphic Multicarrier Communications for Interference Mitigation

3.1 Publications

Elements of this chapter have been included in the following publications:

- M. Carrick, J. H. Reed and C. M. Spooner, "Paramorphic multicarrier communications for interference mitigation", *EURASIP Journal on Advances in Signal Processing*, January 2018, pp. 1-18 [15].

- M. Carrick, J. H. Reed and f. harris, "An optimal filter for signals with time-varying cyclostationary statistics", 2017 22nd International Conference on Digital Signal Processing (DSP), London, UK, August 2017, pp. 1-5 [16].

- M. Carrick and J. H. Reed, "Improved GFDM equalization in severe frequency selective fading", 2017 IEEE 38th Sarnoff Symposium, Newark, NJ, September 2017, pp. 1-6 [17].

3.2 Introduction

In this chapter a method is proposed where spectral redundancy is adaptively designed into a multicarrier signal for communicating in cyclostationary (CS) interference limited environments. Investing into redundancies within a signal to produce a gain at the receiver is a common trade-off in wireless communication system design. Common examples of this trade-off include trading bandwidth for robustness by using coding to improve the bit error rate, and using a larger cyclic prefix on an orthogonal frequency division multiplexing (OFDM) signal to improve the signal to noise ratio (SNR) at the receiver. These two solutions overcome traditional problems in wireless communications: communicating in noise limited environments and the affects of multipath channels. This chapter focuses on the separate but related problem of communicating within cyclostationary interference limited environments, where other communication signals are directly in-band of the desired signal. Simulation results demonstrate that under the given interference scenarios, transmitting redundant spectra at selected positions in the overall spectrum and optimally combining the redundancies at the receiver enables reliable communication which is otherwise not possible using error correcting codes alone.

The novelty of the proposed method includes:

- Implements a method for communicating in cyclostationary interference limited environments.
- Adaptable and dynamic, adjusts the waveform parameters and locations of redundancies to the spectral environment on the fly.
- Implements a novel filter for exploiting time-varying cyclostationary properties of signals.
- Provides more than 16.5 dB worth of SNR gain at a BER of 10^{-5} within the given simulation as compared to low density parity check (LDPC) error correcting codes.

The proposed method introduces redundancies into the signal, analogous to an error correcting code (ECC). The proposed method is explicitly designed for cyclostationary interference, in direct contrast to ECCs which are designed for stationary noise. The performance of ECCs degrades quickly under wideband cyclostationary interference because the assumption is not valid, however

the paramorphic waveform is much more robust under the same conditions because it is specifically designed for the signal environment at hand.

A FRESH filter is applied to mitigate the interference and reduce the expanded bandwidth to its nominal value, analogous to a direct sequence spread spectrum (DSSS) receiver. The bandwidth expansion of the DSSS signal is fixed, a function of the spreading sequence. The distribution of the signal energy is inefficient as it is smeared across the spectrum due to the spreading operation, requiring bandwidth expansion factors of 15 or 31 for short code DSSS [92]. The proposed technique only requires a bandwidth expansion factor of K to mitigate the impact of $K-1$ full bandwidth interferers because the redundancies are optimally combined at the receiver [1]. The method allows for more flexibility, placing redundancies across the spectrum with finer detail and adapting their location and power levels according to the interference.

Simulated Annealing is used to optimize the waveform parameters in light of the interference rejection capability, balancing the improved BER with the reduction in spectral efficiency, approximating an optimal solution to a non-linear multi-objective optimization problem.

Multicarrier waveforms designed with spectral redundancy are referred to as *paramorphic multi-carrier waveforms* (PMW), requiring new adaptive demodulators to incorporate the redundancy into the estimate of the desired signal, referred to as *paramorphic FRESH demodulators* (PFD).

3.2.1   Outline

The remainder of the chapter is outlined as follows. In Section 3.3 the proposed approach is described, including the signal model, improved demodulator and its optimal weights, and the optimization of the waveform design and demodulator. Simulation results and a complexity analysis are presented in Section 3.4, and the conclusion is given in Section 3.5.

3.3   Paramorphic Multicarrier Waveform and Demodulator

The proposal is to insert spectral redundancy into an OFDM signal through data-symbol repetition to form a *paramorphic multicarrier waveform*. A *paramorphic FRESH demodulator* is then

developed to exploit the time-varying spectral redundancy designed into the signal. A signal model is created in Section 3.3.1 to describe the nature of the symbol repetition, and the resulting CS properties are described in Section 3.3.2. The novel demodulator which exploits the time-varying spectral redundancy is proposed in Section 3.3.4 and its MMSE filter weights are derived in Section 3.3.5. The theoretical SINR at the output of the novel FRESH filter is derived in Section 3.3.6, and a joint optimization is proposed in Section 3.3.7 to select the best operating parameters of the new paramorphic waveform.

3.3.1 Signal Model

The received signal model used within this chapter is described by:

$$x(t) = (d(t) \otimes \phi(t)) + (\psi(t) \otimes i(t)) + n(t), \tag{3.1}$$

where $x(t)$ is the received signal, $d(t)$ is the desired signal and its channel is $\phi(t)$, $i(t)$ is CS interference and its channel is $\psi(t)$, $n(t)$ is stationary white noise. The convolution operator is represented by $\otimes$, defined as:

$$a(t) \otimes b(t) = \int_{-\infty}^{\infty} a(\tau) b(t - \tau) d\tau. \tag{3.2}$$

The analytic expressions in the remainder of this chapter often use the frequency domain representation, which is given by:

$$X(f) = D(f)\Phi(f) + I(f)\Psi(f) + N(f), \tag{3.3}$$

where $X(f) = \mathcal{F}\{x(t)\}$.

The standard OFDM signal model is provided and adapted to include symbol repetition that creates exploitable spectral redundancy. An OFDM signal with N subcarriers is represented by (3.4) and (3.5) in the time and frequency domains, respectively [59]:

$$\tilde{d}(t) = \sum_{l=0}^{L-1} \sum_{n=0}^{N-1} a_{l,n} q\left(t - lT\right) e^{j2\pi \frac{n}{N} t}, \tag{3.4}$$

$$\tilde{D}(f) = \sum_{l=0}^{L-1} \sum_{n=0}^{N-1} a_{l,n} Q\left(f - \frac{n}{N}\right) e^{-j2\pi\left(f - \frac{n}{N}\right) lT}. \tag{3.5}$$

In these models $a_{l,n}$ is the data-symbol of the lth OFDM symbol applied to subcarrier n, and $q(t)$ is the rectangular pulse shape, where $Q(f) = \mathcal{F}\{q(t)\}$. T is the length of the window, including the cyclic prefix time, where $T = T_{CP} + T_s$.

The OFDM model in (3.4) and (3.5) is modified by incorporating data-symbol repetition across both time and frequency, requiring block-based transmissions of B OFDM symbols. The data-symbols to be transmitted within each block are represented by $a_{l,0}, a_{l,1}, \ldots, a_{l,M-1}$, and the mth symbol $a_{l,m}$ is repeated $R(m)$ times within the block. The data-symbol $a_{l,m}$ is mapped onto the subcarrier at frequency $f_{m,r}$ where $r = 0, 1, \ldots, R(m) - 1$. The signal model for the cth OFDM symbol within the lth block for the proposed technique is therefore [16]:

$$d_{l,c}(t) = \sum_{m=0}^{M-1} \sum_{r=0}^{R(m)-1} a_{l,m} q(t - (Bl + c)T) e^{j2\pi f_{m,r} t}, \tag{3.6}$$

$$D_{l,c}(f) = \sum_{m=0}^{M-1} \sum_{r=0}^{R(m)-1} a_{l,m} Q(f - f_{m,r}) e^{-j2\pi(f - f_{m,r})(Bl+c)T}. \tag{3.7}$$

The symbols $a_{l,n}$ of (3.4) are typically assumed to be independent and identically distributed (IID) [56, 93]. The symbols applied to the subcarriers are no longer independent, as correlation has been introduced into the signal by design in (3.6).

The signals over all time are therefore $d(t) = \sum_l \sum_{c=0}^{B-1} d_{l,c}(t)$ and $D(f) = \sum_l \sum_{c=0}^{B-1} D_l(f)$.

3.3.2 Cycle Frequencies of Paramorphic Waveform

The cycle frequencies of the received signal must be known to the receiver when constructing the PFD. As in (2.35) and (2.36), the cycle frequencies come from the desired signal and the interference. In this section the cycle frequencies of the desired signal are described, while the cycle frequencies of the interference are described in Section 3.3.3.

The PMW is able to independently select any linear modulation format on each of its subcarriers; however, the type of modulation will have an impact on the cyclostationary properties of the signal. Formats such as quadrature amplitude modulation (QAM) and phase shift keying (PSK) will induce spectral redundancy when their symbols are repeated across the spectrum, while others such as pulse amplitude modulation (PAM) and binary phase shift keying (BPSK) in addition will induce conjugate spectral redundancy. The impact of these formats is highlighted here because they are commonly used, but it does not preclude the use of other constellations.

The CFs corresponding to the repetitions of symbol $a_{l,m}$ must be known to the receiver so the spectral redundancy, which is derived from the repetition patterns of the data-symbols, can be exploited. Examples of repetition patterns are given in Figures 3.1 and 3.2.

While repeating data-symbols creates spectral redundancy, some modulations have inherent conjugate spectral redundancy which can also be exploited. The test for spectral redundancy is given by [28]:

$$\mathbb{E}\{vv^*\} \neq 0, \tag{3.8}$$

and the test for conjugate spectral redundancy is given by:

$$\mathbb{E}\{vv\} \neq 0, \tag{3.9}$$

where v is the set of all constellation points within a modulation. A modulation format contains spectral redundancy when (3.8) is true and and conjugate spectral redundancy when (3.9) is true.

For QPSK, $v = \{-1 - j, -1 + j, 1 - j, 1 + j\}$, and from (3.8),

$$\mathbb{E}\{|-1-j|^2 + |-1+j|^2 + |1-j|^2 + |1+j|^2\} \neq 0, \tag{3.10}$$

and according to (3.9),

$$\mathbb{E}\{(-1-j)^2 + (-1+j)^2 + (1-j)^2 + (1+j)^2\} = 0, \tag{3.11}$$

therefore QPSK only contains spectral redundancy. For BPSK, $\mathbb{E}\{(-1)^2 + (1)^2\} \neq 0$ and $\mathbb{E}\{|-1|^2 + |1|^2\} \neq 0$, thus BPSK has both spectral correlation and conjugate spectral correlation. Other modulations can be tested for spectral redundancy and conjugate spectral redundancy by applying (3.8) and (3.9). Once the type of redundancy is known, its cycle frequencies can be incorporated into the PFD as in (3.16) and (3.17).

The CFs are therefore defined according to the modulation and their location within the repetition pattern. As data-symbols can be repeated in time, new notation is needed to capture the now time-varying spectral redundancy. The notation $\gamma_{c,b,u}$ is described in Figure 3.1, showing how the cycle frequencies align spectral redundancies in time. For example, $\gamma_{2,1,k}$ frequency shifts OFDM symbol 1 to align the redundancies in OFDM symbol 2. The k index represents the kth cycle frequency between OFDM symbol 1 and 2. The same is true for $\zeta_{c,b,v}$ which represents the CFs of the conjugate spectral redundancy.

There is a trade-off when selecting the modulation format for each of the subcarriers. QAM has a better BER than PAM for the same modulation order under stationary white noise [92], however PAM includes conjugate spectral redundancy which can be incorporated into the PFD for a signal processing gain over using QAM. The selection of the modulation format for each of the subcarriers is dependent on the requirements for the communication link and the characteristics of the received signal including the type and parameters of the interference and the SNR. The optimization in Section 3.4.5 provides one set of results where these trade-offs are incorporated by minimizing the BER while maximizing the spectral redundancy.
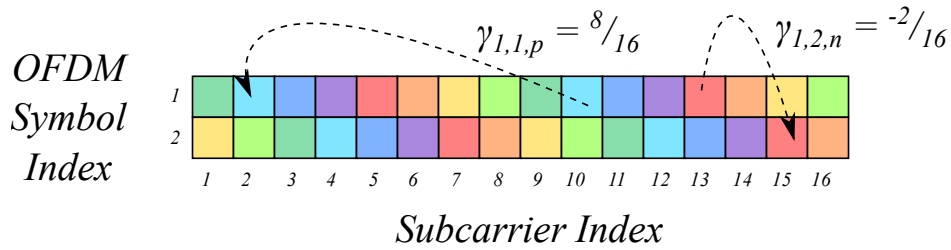
Figure 3.1: Spectral redundancy is distributed across both time and frequency within this pattern of $B = 2$ OFDM symbols, $N = 16$ subcarriers and $M = 8$ data-symbols. Two CFs illustrate the time-varying spectral redundancy. The arrows indicate in which direction the FS is performed.
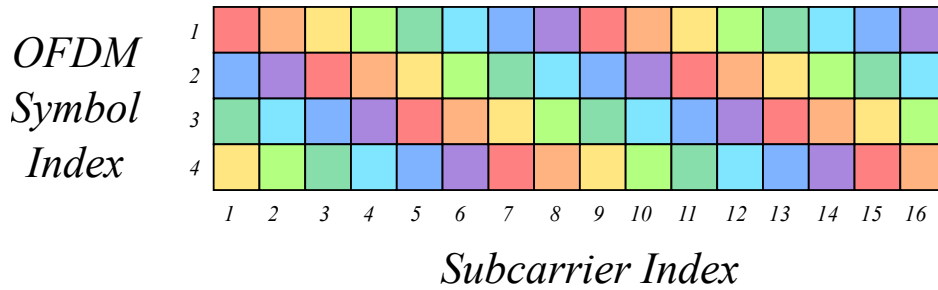
Figure 3.2: An example of a repetition pattern for $B = 4$ OFDM symbols, $N = 16$ subcarriers and $M = 8$ data-symbols.

3.3.3 Interference Model

A single carrier 16-QAM signal is used as interference to show the ability of the PFD to mitigate wideband heterogeneous interference. The analytic representation for the interference is [92]:

$$i(t) = \sum_{k=-\infty}^{+\infty} s_k p(t - kT) e^{j2\pi f_0 t}, \tag{3.12}$$

where s_k is the kth 16-QAM symbol and $p(t)$ is a square-root raised cosine (SRRC) pulse shaping filter with roll-off factor 0.35, and f_0 is the center frequency of the signal. Specific parameters for the interference such as the power and bandwidth are specified in Section 3.4.1.

The cycle frequencies of a 16-QAM signal are [28]:

$$\alpha = \frac{k}{T}, \ k = 0, \pm 1, \pm 2, \ \dots \ . \tag{3.13}$$

The SRRC pulse shaping reduces the energy of the spectral copies beyond the symbol rate, therefore for practicality the cycle frequencies are limited to:

$$\alpha = \left\{ 0, \frac{1}{T}, -\frac{1}{T} \right\}. \tag{3.14}$$

3.3.4 Paramorphic FRESH Demodulator

The analytic representation of the PFD is given in this section. The PFD structure only requires knowledge of the cycle frequencies within the received signal as in (3.16) and (3.17). The cycle frequencies $\alpha_{c,b,u}$ and $\beta_{c,b,u}$ determine how many filtering branches are located within the PFD. The cycle frequencies of the PMW can be determined from Section 3.3.2 and the cycle frequencies of the interference from Section 3.3.3. The additional knowledge required for MMSE filter weights is described in Section 3.3.5.

The fast Fourier transform (FFT) is used to demodulate the OFDM signal, transforming the time domain signal into frequency domain symbols. A novel FRESH filter is employed in the frequency domain to exploit the time-varying spectral redundancy of the received signal. Each block of B OFDM symbols is buffered in memory using a series of delay lines which allows them to be jointly filtered. The estimate $\hat{D}_{l,c}$ of the cth symbol of the lth block $D_{l,c}$ is given in (3.15) and the filtering structure is illustrated in Figures 3.3 and 3.4 [16],

$$\hat{D}_{l,c}(f) = \sum_{b=0}^{B-1} \left(\sum_{u=0}^{U_{c,b}-1} G_{c,b,u}(f) X_{l,b}(f - \alpha_{c,b,u}) + \sum_{v=0}^{V_{c,b}-1} H_{c,b,v}(f) X_{l,b}^*(-f + \beta_{c,b,v}) \right). \tag{3.15}$$

$U_{c,b}$ is the number of FS's in the FRESH filter between OFDM symbol c and OFDM symbol b. Similarly $V_{c,b}$ is the number of FS's in the FRESH filter corresponding to the conjugate spectrally redundant symbols in OFDM symbol c and OFDM symbol b.

The estimate of the PMW (3.15) is a function of the FS's $\{\alpha_{c,b,u}\}$ and $\{\beta_{c,b,v}\}$ in the FRESH filter. The set of CFs of the spectral correlation for the PMW, $\{\gamma_{d,c,b,u}\}$, and interference, $\{\gamma_{i,c,b,u}\}$, as well as their differences are included in the set of FS's $\{\alpha_{c,b,u}\}$ as in (2.35):
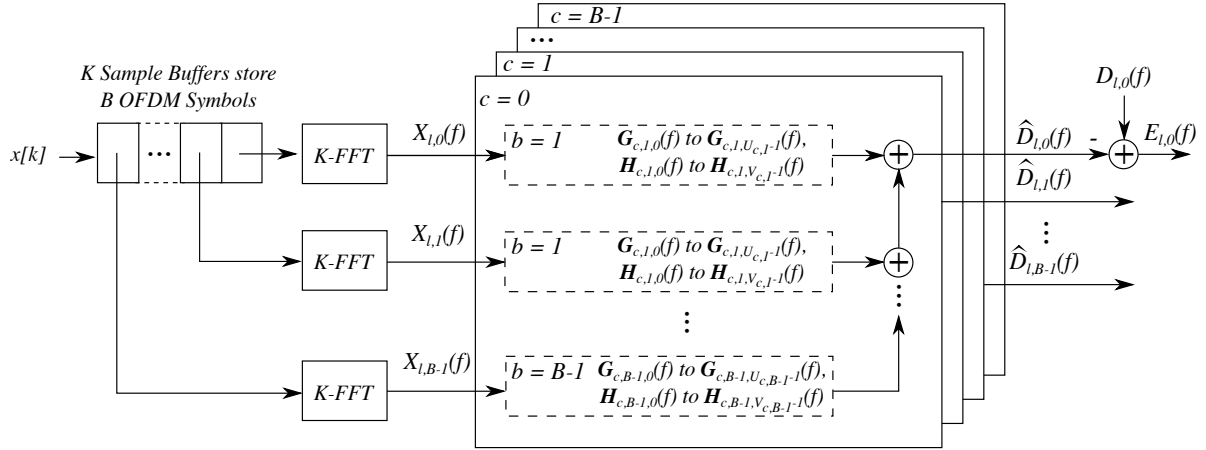
Figure 3.3: The PFD structure that exploits spectral redundancy across time and frequency by demodulating and applying a novel FRESH filter. The depth in the image indicates a similar filtering structure with different filter weights for each of the sets of OFDM symbols.
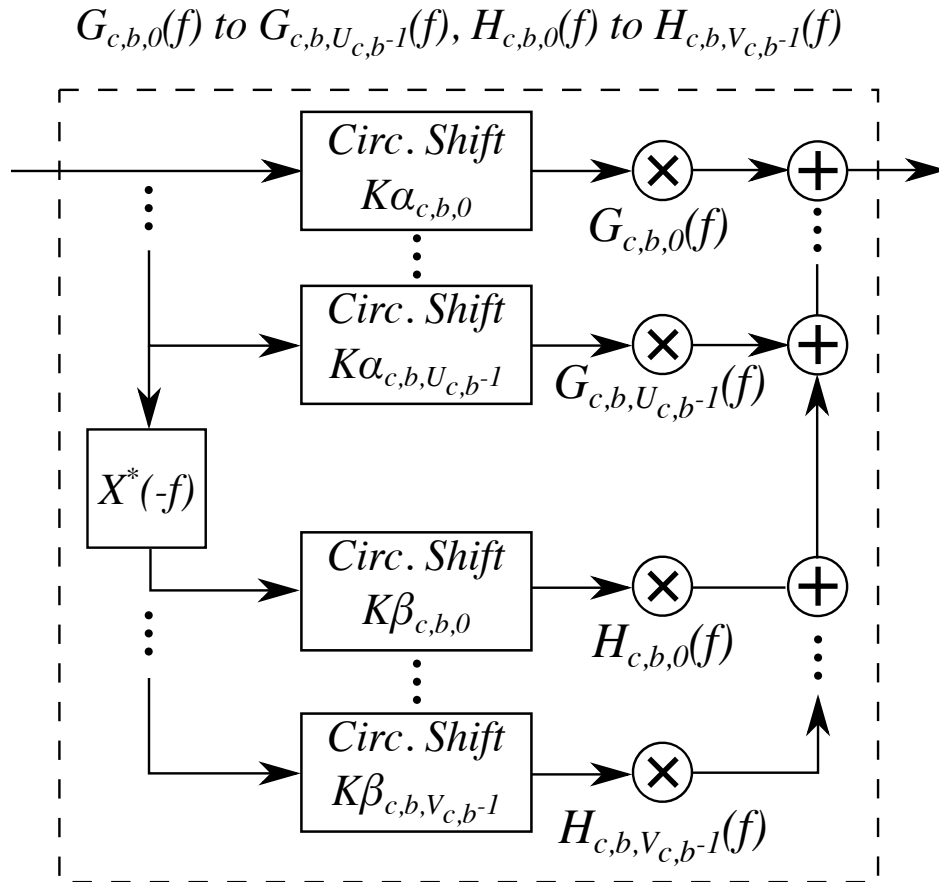
Figure 3.4: Each sub-filter is a linear combination of a series of frequency domain filters and circular shifts, which implement the FS's.

$$\begin{aligned}
\{\alpha_{c,b,u}\} = \{ & \gamma_{d,c,b,0}, \ \gamma_{d,c,b,1}, \ \gamma_{d,c,b,2}, \ \cdots, \\
& \gamma_{i,c,b,0}, \ \gamma_{i,c,b,1}, \ \gamma_{i,c,b,2}, \ \cdots, \\
& \gamma_{d,c,b,0} - \gamma_{i,c,b,0}, \ -\gamma_{d,c,b,0} + \gamma_{i,c,b,0}, \\
& \gamma_{d,c,b,0} - \gamma_{i,c,b,1}, \ -\gamma_{d,c,b,0} + \gamma_{i,c,b,1}, \\
& \cdots, \\
& \gamma_{d,c,b,1} - \gamma_{i,c,b,0}, \ -\gamma_{d,c,b,1} + \gamma_{i,c,b,0}, \\
& \gamma_{d,c,b,1} - \gamma_{i,c,b,1}, \ -\gamma_{d,c,b,1} + \gamma_{i,c,b,1}, \\
& \cdots \ \}.
\end{aligned} \tag{3.16}$$

The set of FS's $\{\beta_{c,b,v}\}$ is formed using the set of CFs of the conjugate spectral correlation for the PMW, $\{\zeta_{d,c,b,u}\}$, and interference, $\{\zeta_{i,c,b,v}\}$, and their differences:

$$\begin{aligned}
\{\beta_{c,b,v}\} = \{ & \zeta_{d,c,b,0}, \ \zeta_{d,c,b,1}, \ \zeta_{d,c,b,2}, \ \cdots, \\
& \zeta_{i,c,b,0}, \ \zeta_{i,c,b,1}, \ \zeta_{i,c,b,2}, \ \cdots, \\
& \zeta_{d,c,b,0} - \zeta_{i,c,b,0}, \ -\zeta_{d,c,b,0} + \zeta_{i,c,b,0}, \\
& \zeta_{d,c,b,0} - \zeta_{i,c,b,1}, \ -\zeta_{d,c,b,0} + \zeta_{i,c,b,1}, \\
& \cdots, \\
& \zeta_{d,c,b,1} - \zeta_{i,c,b,0}, \ -\zeta_{d,c,b,1} + \zeta_{i,c,b,0}, \\
& \zeta_{d,c,b,1} - \zeta_{i,c,b,1}, \ -\zeta_{d,c,b,1} + \zeta_{i,c,b,1}, \\
& \cdots \ \}.
\end{aligned} \tag{3.17}$$

It is assumed that the cycle frequencies, and thus the signaling rate, of the interference is known. This information can be arrived at through spectrum sensing, or if the interference is a legacy user in a shared spectrum band it will already be known. Mismatches or errors in the estimated cycle frequencies and the true cycle frequencies due to real world impairments can be corrected through adaptive algorithms [36].

Spectrally redundant information which does not vary with time, either present in the PMW or the interference, can be included in (3.16) and (3.17) by setting the FS's appropriately. Consider the example of a single-carrier QPSK interferer with symbol period T, whose CFs are $\{0, \pm\frac{1}{T}, \pm\frac{2}{T}, \ldots\}$ [28]. The CFs do not vary with time, thus $\gamma_{i,c,b,u} = \varnothing$ when $c \neq b$, and $\gamma_{i,c,b,0} = 0$, $\gamma_{i,c,b,1} = \frac{1}{T}$, $\gamma_{i,c,b,2} = -\frac{1}{T}$, $\ldots$, for $c = b$.

3.3.5 MMSE Filter Weights

The MMSE filter weights for $G_{c,b,u}(f)$ and $H_{c,b,u}(f)$ of the PFD from (3.15) are derived within this section. The MMSE filter weights are optimal as they require knowledge of the desired signal, a common assumption used in the Wiener filter [94] derivation and previous MMSE FRESH filter weight derivations [1, 32, 95]. The MMSE filter weights are derived to find an upper bound on the performance of the filtering which future work can use as a reference. LMS algorithms for FRESH filters such as [34, 35] can be incorporated to adapt the filter weights using preambles for training or blind adaptation [40], such as decision directed training or property restoration, and whose performance can be measured against the MMSE filter weights derived here.

The derivation of the MMSE filter weights [16] for $G_{c,b,u}(f)$ and $H_{c,b,v}(f)$ of the paramorphic FRESH demodulator proceeds in the same fashion as the derivation for the time-domain FRESH filter from Section 2.2.3. The filter error is established in (3.18) and the MSE in (3.19):

$$E_{l,c}(f) = D_{l,c}(f) - \hat{D}_{l,c}(f), \tag{3.18}$$

$$E_{MSE}(f) = \mathbb{E}\left\{E_{l,c}(f)E_{l,c}^*(f)\right\}. \tag{3.19}$$

The MSE is minimized by taking its derivative with respect to both $G_{c,b,u}(f)$ and $H_{c,b,v}(f)$ and setting equal to zero in (3.20) and (3.21):

$$\frac{\partial E_{MSE}(f)}{\partial G_{c,p,k}^*(f)} = 0, \tag{3.20}$$

$$\frac{\partial E_{MSE}(f)}{\partial H_{c,m,n}^*(f)} = 0. \tag{3.21}$$

Solving for the derivatives results in two orthogonal projections, (3.22) and (3.23):

$$\mathbb{E}\left\{E_{l,c}(f)X_{l,p}^*\left(f - \alpha_{c,p,k}\right)\right\} = 0, \tag{3.22}$$

$$\mathbb{E}\left\{E_{l,c}(f)X_{l,m}\left(-f + \beta_{c,m,n}\right)\right\} = 0. \tag{3.23}$$

The first projection states that the filter error of the cth OFDM symbol is orthogonal to the conjugate of the received p^{th} OFDM symbol when frequency-shifted by $\alpha_{c,p,k}$.

The frequency domain error (3.18) is then substituted into the projections (3.22) and (3.23) to produce the optimal filter design equations (3.26) and (3.27). The design equations include new ways of representing the spectral correlation. For example, $S_{d_c,x_p}^{\alpha_{c,p,k}}\left(f - \frac{\alpha_{c,p,k}}{2}\right)$ is the cross spectral correlation of the cth desired OFDM symbol from each block with the pth received OFDM symbol from each block at FS $\alpha_{c,p,k}$, represented by:

$$S_{d_c,x_p}^{\alpha_{c,p,k}}\left(f - \frac{\alpha_{c,p,k}}{2}\right) = \lim_{L\to\infty} \frac{1}{L} \sum_{l_1,l_2=0}^{L-1} D_{l_1,c}(f)X_{l_2,p}^*\left(f - \alpha_{c,p,k}\right). \tag{3.24}$$

3.3.6 Theoretical SINR

In order to validate the simulation results, the theoretical signal to interference and noise ratio (SINR) at the output of the PFD is derived. The theoretical SINR (3.25) for the cth OFDM symbol is:

$$\lambda_l = \frac{\mathbb{E}\left\{|D_{l,c}(f)|^2\right\}}{\mathbb{E}\left\{\left|D_{l,c}(f) - \hat{D}_{l,c}(f)\right|^2\right\}}, \tag{3.25}$$

$$S_{d_c,x_p}^{\alpha_{c,p,k}}\left(f - \frac{\alpha_{c,p,k}}{2}\right) = \sum_{b=0}^{B-1}\left(\sum_{u=0}^{U_{c,b}-1} G_{c,b,u}(f)S_{x_c,x_b}^{\alpha_{c,p,k}-\alpha_{c,b,u}}\left(f - \frac{\alpha_{c,p,k}+\alpha_{c,b,u}}{2}\right)\right.$$
$$\left. + \sum_{v=0}^{V_{c,b}-1} H_{c,b,v}(f)\, S_{x_c,x_b^*}^{\beta_{c,b,v}-\alpha_{c,p,k}}\left(f - \frac{\beta_{c,b,v}+\alpha_{c,p,k}}{2}\right)^*\right) \tag{3.26}$$

$$p = 0, 1, \ldots, B-1; \quad k = 0, 1, \ldots, U_{c,p}-1$$

$$S_{d_c,x_m^*}^{\beta_{c,m,n}}\left(f - \frac{\beta_{c,m,n}}{2}\right) = \sum_{b=0}^{B-1}\left(\sum_{u=0}^{U_{c,b}-1} G_{c,b,u}(f)S_{x_c,x_b^*}^{\beta_{c,m,n}-\alpha_{c,b,u}}\left(f - \frac{\beta_{c,m,n}+\alpha_{c,b,u}}{2}\right)\right.$$
$$\left. + \sum_{v=0}^{V_{c,b}-1} H_{c,b,v}(f)\, S_{x_c,x_b}^{\beta_{c,m,n}-\beta_{c,b,v}}\left(-f + \frac{\beta_{c,m,n}+\beta_{c,b,v}}{2}\right)\right) \tag{3.27}$$

$$m = 0, 1, \ldots, B-1; \quad n = 0, 1, \ldots, V_{c,m}-1$$

$$\mathbb{E}\left\{\left|D_{l,c} - \hat{D}_{l,c}\right|^2\right\} = S_d(f) - 2\Re\left(\mathbb{E}\left\{D_{l,c}(f)\hat{D}_{l,c}^*(f)\right\}\right) + \mathbb{E}\left\{\hat{D}_{l,c}(f)\hat{D}_{l,c}^*(f)\right\} \tag{3.28}$$

$$\mathbb{E}\left\{D_{l,c}(f)\hat{D}_{l,c}^*(f)\right\} = \sum_{b=0}^{B-1}\left(\sum_{u=0}^{U_{c,b}-1} G_{c,b,u}^*(f)S_{d_c,x_b}^{\alpha_{c,b,u}}\left(f - \frac{\alpha_{c,b,u}}{2}\right) + \sum_{v=0}^{V_{c,b}-1} H_{c,b,v}^*(f)S_{d_c,x_b^*}^{\beta_{c,b,v}}\left(f - \frac{\beta_{c,b,v}}{2}\right)\right) \tag{3.29}$$

$$\mathbb{E}\left\{\hat{D}_{l,c}(f)\hat{D}_{l,c}^*(f)\right\} = \sum_{b=0}^{B-1}\sum_{z=0}^{B-1}\sum_{u=0}^{U_{c,b}-1}\sum_{m=0}^{U_{c,b}-1} G_{c,b,u}(f)G_{c,z,m}^*(f) \cdot\; S_{x_b,x_z}^{\alpha_{c,z,m}-\alpha_{c,b,u}}\left(f - \frac{\alpha_{c,b,u}+\alpha_{c,z,m}}{2}\right)$$

$$+2\Re\left\{\sum_{b=0}^{B-1}\sum_{z=0}^{B-1}\sum_{u=0}^{U_{c,b}-1}\sum_{n=0}^{V_{c,b}-1} G_{c,b,u}(f)H_{c,z,n}^*(f)S_{x_b,x_z}^{\beta_{c,z,n}-\alpha_{c,b,u}}\left(f - \frac{\beta_{c,b,n}+\alpha_{c,b,u}}{2}\right)\right\}$$

$$+\sum_{b=0}^{B-1}\sum_{z=0}^{B-1}\sum_{v=0}^{V_{c,b}-1}\sum_{n=0}^{V_{c,b}-1} H_{c,b,v}(f)H_{c,z,n}^*(f)S_{x_b,x_z}^{\beta_{c,z,n}-\beta_{c,b,v}}\left(-f + \frac{\beta_{c,b,v}+\beta_{c,z,n}}{2}\right) \tag{3.30}$$

where $D(f)$ is from (3.7) and $\hat{D}_{l,c}(f)$ is from (3.15). The denominator is the MSE, and is expanded in (3.28), with additional terms given in (3.29) and (3.30), and where $\Re$ is the real operator. The analytical SINR from (3.25) is used to validate the simulation results for the PFD in Section 3.4.

3.3.7   Joint Optimization of Waveform and Demodulator

Cognitive radios most commonly adapt waveform parameters such as transmit power, modulation type and order, and code rate and type to satisfy objectives of BER, throughput and spectral efficiency [91, 96]. The ability to design the waveform for interference mitigation using symbol repetition allows for another degree of freedom within the optimization.

The fitness function is used to combine the performance of several objectives into a single number where a larger fitness function directly translates to a more suitable solution to the optimization. In this approach a linear fitness function (3.26),

$$\phi = w_1\phi_1 + w_2\phi_2, \tag{3.31}$$

combines the objective of the BER, ϕ_1, and the objective of the spectral efficiency, ϕ_2. The weights w_1 and w_2 are set such that $w_1 + w_2 = 1$. The objectives ϕ, ϕ_1 and ϕ_2 are all bounded by $[0, 1]$. The objective functions for the BER and spectral efficiency are given by (3.32) and (3.33) [97]:

$$\phi_1 = \frac{log_{10}\left(0.5\right) - log_{10}\left(BER_M\right)}{log_{10}\left(0.5\right) - log_{10}\left(BER_T\right)}, \tag{3.32}$$

$$\phi_2 = \frac{\eta}{\eta_{max}}. \tag{3.33}$$

BER_T is a target BER and BER_M is the measured BER. The target BER is a minimum BER threshold, where if the threshold is not met the solution is penalized by reducing the fitness of the solution. The measured BER is the actual BER of the PMW, requiring knowledge of the desired signal, which is compared against the BER threshold when computing the fitness function. Knowledge of the desired signal is also needed in order to form the MMSE filter weights of the

PFD. In practical systems, training sequences or pilot sequences are transmitted to provide a known signal. The average information bits per symbol, η, comes from the modulation and incorporates the reduction in spectral efficiency due to coding as well as symbol repetition. The weights are set to $w_1 = \frac{2}{3}$ and $w_2 = \frac{1}{3}$ to ensure the optimization does not select a solution which produces a poor BER but has an abnormally high spectral efficiency.

3.4 Simulation Results

Simulation results are used to show the ability of the PMW and PFD to mitigate interference and make comparisons to traditional filtering techniques and ECC. The simulated scenario is motivated by the co-existence of 5G cellular systems and satellite communications within the same band [98]. The SINR is used to compare against filtering techniques in Section 3.4.2 and the BER is used to compare against ECCs in Section 3.4.3. Simulated annealing is used in Section 3.4.5 to optimize the BER and spectral efficiency when under interference. A detailed complexity analysis of the PFD is given in Section 3.4.6.

3.4.1 Simulation Parameters

In Sections 3.4.2 and 3.4.3, five different techniques are compared for their ability to mitigate interference. The techniques are Wiener filtering, maximal ratio combining (MRC), the proposed PFD, soft decision convolutional codes, and soft decision LDPC codes. The spectral redundancy of the interferer is exploited within the PFD results, but for no other methods. The LDPC codes used are those defined in the digital video broadcasting second generation (DVB-S2) standard [99]. The SINR and BER are computed within the same set of Monte Carlo simulations. The length of the input signal to the FRESH filter is a minimum of 10^5 samples for each run of the simulation, and the simulations continue until a minimum of 1000 bit errors is observed.

The 16-QAM interference model from Section 3.3.3 is used in all of the following simulations, although the power and bandwidth are varied. The interference has high SIR values within the passband of the desired signal, and examples of the received spectrum under these conditions are given in Figures 3.5a and 3.5b.
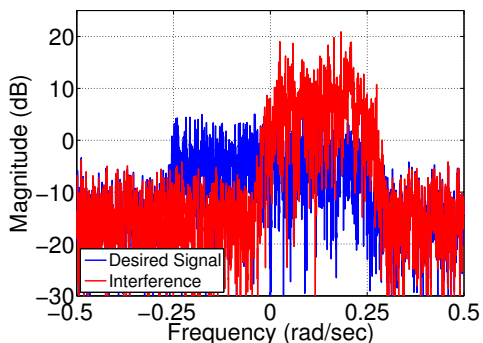
(a) An example of the spectrum when the interference covers 1/2 of the bandwidth.
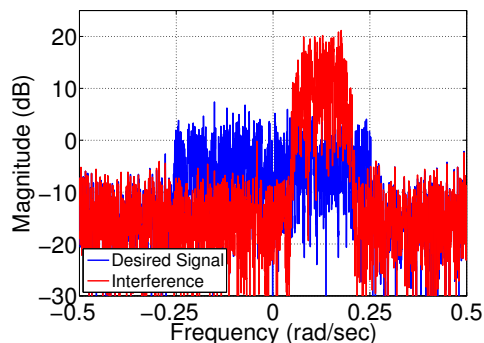
(b) An example of the spectrum when the interference covers 1/4 of the bandwidth.

Figure 3.5: Two plots showing the spectrum of the received signal when $E_b/N_0 = 7$ dB and $P_i/N_0 = 20$ dB.

3.4.2 SINR Performance

The SINR after the Wiener filter, MRC and the PFD are all compared using the simulation parameters referenced in Section 3.4.1. The SINR is simulated for a series of E_b/N_0 values where the interference to noise ratio is fixed at $P_i/N_0 = 20$ dB, and the interference bandwidth covers 1/2 and 1/4 of that of the OFDM signal. The energy per bit E_b/N_0 is in relation to information bits, with QPSK being used on each of the 64 subcarriers of the OFDM signal.

The SINR is plotted in Figures 3.6a and 3.6b, and it can be seen that significant gains can be achieved by using the PFD over MRC and the Wiener filter. The gains over the Wiener filter are about 6 and 4 dB at $E_b/N_0 = 10$ dB when the interference covers 1/2 and 1/4 of the PMW bandwidth. The gains over MRC are about 1.5 dB and 1 dB when the interference covers 1/2 and 1/4 of the PMW bandwidth.

To cancel K cyclostationary interferers in the absence of noise each symbol must be repeated $K+1$ times [1], thus for the single interferer case each symbol only needs to be repeated twice. Repeating each symbol four times or more will improve the estimate of the received signal as it will still mitigate the stationary white noise but it is subject to diminishing returns. Increasing from 1/2 rate symbol repetition to 1/4 rate produces only a small improvement in SINR.
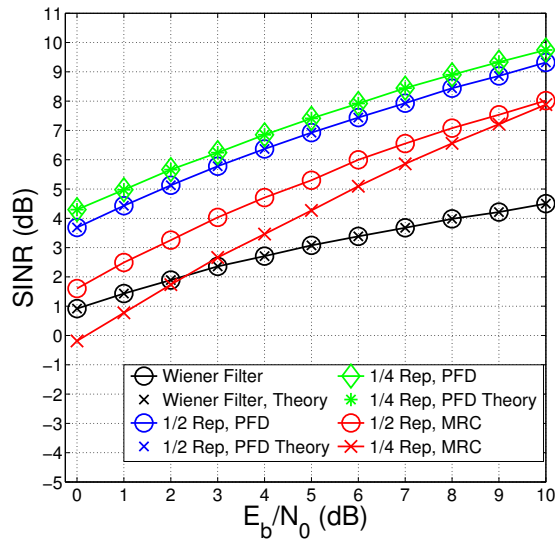
(a) Bandwidth overlap of 1/2.
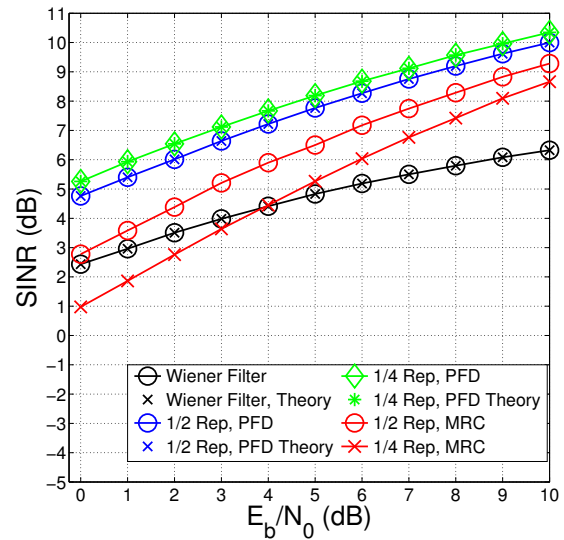
(b) Bandwidth overlap of 1/4.

Figure 3.6: The SINR plots comparing the performance of the Wiener filter, MRC and Symbol Repetition (PFD). The abbreviation *Rep.* refers to symbol repetition.

3.4.3 BER versus Desired Signal E_b/N_0

The results of the BER being simulated for the Wiener filter, PFD, convolutional coding and LDPC are given in Figures 3.7a and 3.7b using the simulation parameters and interference model of Section 3.4.1. For these results, the PMW uses QPSK on each of its 64 subcarriers, the interference power is $P_i/N_0 = 20$ dB and the bandwidth of the interference is 1/2 and 1/4 that of the PMW in Figures 3.7a and 3.7b, respectively.

The PFD outperforms both the Wiener filter, the LDPC, and the convolutional codes in these two scenarios due to its optimal combining of spectral redundancy, even with only 1/2 rate symbol repetition. The PFD can improve the BER further by using 1/4 rate symbol repetition but with diminishing returns. Since the received signal is dominated by cyclostationary interference and not stationary noise, assumptions built into LDPC and convolutional codes break down and thus produce BERs of worse than 10^{-1} for the considered values of E_b/N_0. However, using a hybrid approach of the PFD and an ECC can improve the BER more than either method alone, by reducing the BER by $1000x$ in comparison to the next best method at high E_b/N_0 values.

(a) Bandwidth overlap of 1/2.

(b) Bandwidth overlap of 1/4.
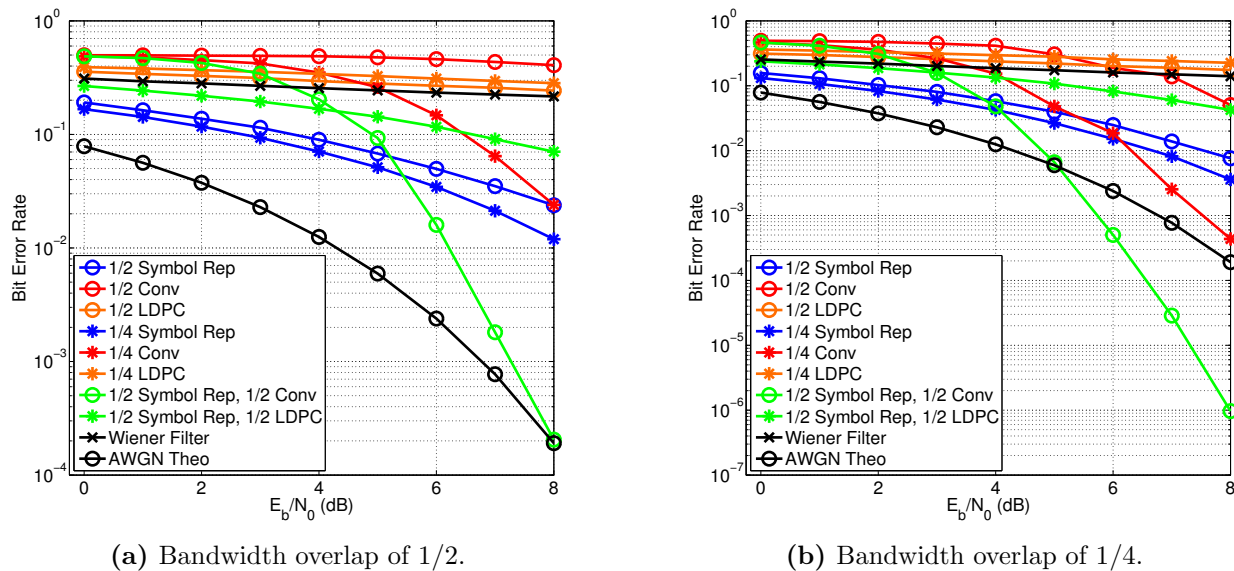
Figure 3.7: The BER curves comparing the performance of the Wiener filter, PFD, LDPC and convolutional codes as a function of E_b/N_0.

With the hybrid approach the PFD is able to mitigate a large portion of the CS interference allowing the convolutional code to operate on the resulting signal which is mostly corrupted by stationary noise. It is for this reason that the hybrid approach exceeds the BER for the theoretical AWGN curve in Figure 3.7b. Enough CS interference is mitigated by the PFD that the convolutional code can then correct residual bit errors caused by the stationary noise. Both the convolutional codes and LDPC codes would be well below a BER of 10^{-4} at $E_b/N_0 = 8$ dB.

The received signal is dominated by cyclostationary interference, and the time-varying nature of the PFD transforms the stationary white noise into time-varying noise. Additionally, the frequency shifts within the PFD color the white noise within the signal. The resulting noise at the output of the PFD is now non-stationary, periodically time-varying, and colored, and it will include any remaining cyclostationary interference that was unable to be removed by the PFD. All of these qualities severely violate the assumptions of stationary white Gaussian noise built into the standard BER equations, which accounts for the distance between the theoretical BER curves and the Monte Carlo results. The violation of the assumptions also prevent an approximation of the theoretical BER by using the SINR results obtained in Section 3.4.2.

As the PFD is able to exploit the spectral redundancy, the $\frac{1}{4}$-rate convolutional code is also able to exploit the frequency diversity to achieve some improvement in BER. The encoded bits are interleaved across all of the OFDM subcarriers and as such some bits will be noise limited and others interference limited. As the E_b/N_0 values increase the BER improves due to the higher SNR for some of the bits, which is the mechanism by which the convolutional decoder exploits the frequency diversity of the OFDM signal.

The expected reason for the bad performance of LDPC codes comes from the shape of the BER curve, or the thresholding effect. While above this threshold LDPC codes perform well in AWGN, but below it the codes provide no error correction capability. In [100] it is shown that cyclostationary noise can have a dramatic affect on the performance of LDPC codes at much smaller interference powers than what has been simulated in this chapter.

Figures 3.8a and 3.8b show the BER when under a frequency selective channel, the magnitude of the frequency response is given in Figure 3.9. The desired signal channel is $\Phi(z) = (-0.35 - 1.06j) + (-0.84 + 0.69j)z^{-1} + (0.03 - 0.01j)z^{-2}$ and the interference channel is $\Psi(z) = (-0.004 + 0.09j) + (-0.80 + 1.26j)z^{-1} + (0.02 - 0.74j)z^{-2}$. The delay z^{-1} is defined according to the sampling rate. The simulated results use a normalized sampling frequency, with the ratio of the bandwidth of the PMW to the sampling ratio being $\frac{1}{2}$. The BER for the paramorphic approach actually improves relative to the case in which there is no frequency selectivity. The FRESH filter can be thought of as an improved fractionally spaced equalizer [1], providing resistance to the frequency selective effects. Additionally, the interference channel reduces the power of the interference on its left side, effectively reducing the bandwidth of the interference. Therefore, both BER curves are close to the case in which the bandwidth only covers 1/4 of the bandwidth, Figure 3.7b.

Another simulation is run for the channel in Figure 3.9, but whose spectral null is on the left side of DC. Figures 3.10a and 3.10b show a substantial loss in BER due to the channel impairment. The null causes a near total loss in the symbols on the left half of the OFDM signal, effectively destroying the spectral redundancy that has been included in the signal. The remaining symbols to the right of DC are therefore left to contend with the interference with very little help from the spectral redundancy. The BER for the paramorphic approach is reduced to nearly 10^{-1} in both cases. Although this is a substantial loss in BER, the proposed approach outperforms all other

(a) Bandwidth overlap of 1/2.

(b) Bandwidth overlap of 1/4.
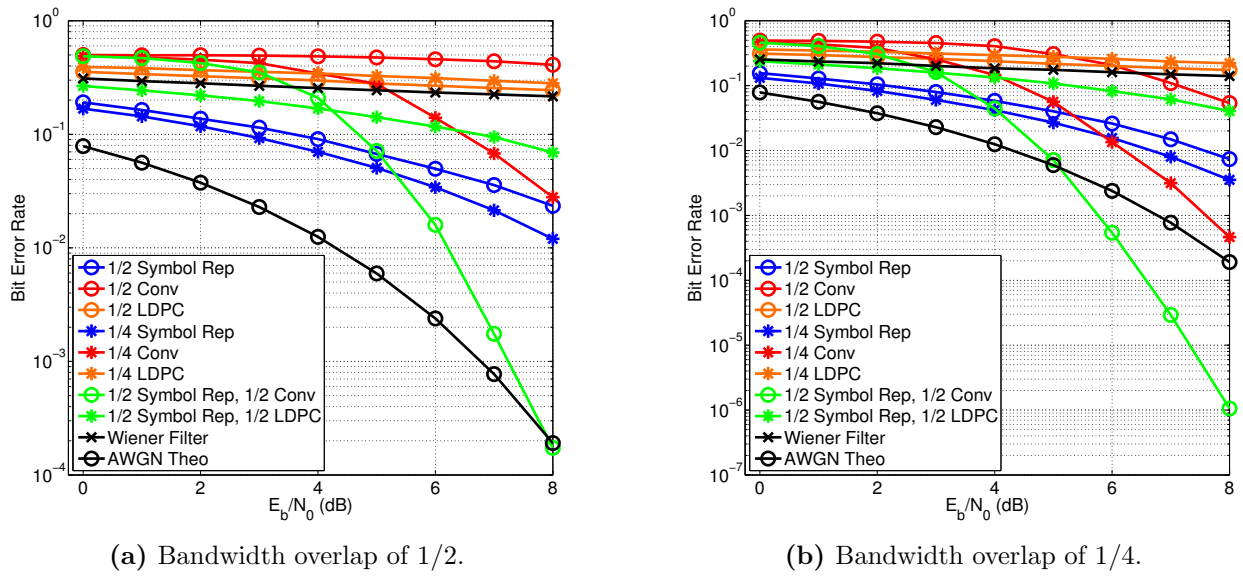
Figure 3.8: The BER curves for the filtering methods and error correcting codes while under a frequency selective channel from Figure 3.9.
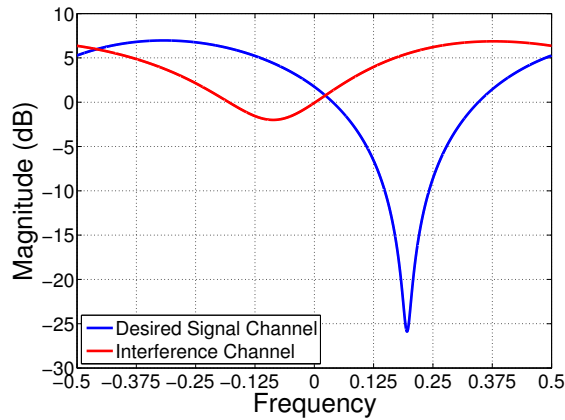
Figure 3.9: The magnitude of the frequency response for the channel on the desired signal and interference.

(a) Bandwidth overlap of 1/2.

(b) Bandwidth overlap of 1/4.
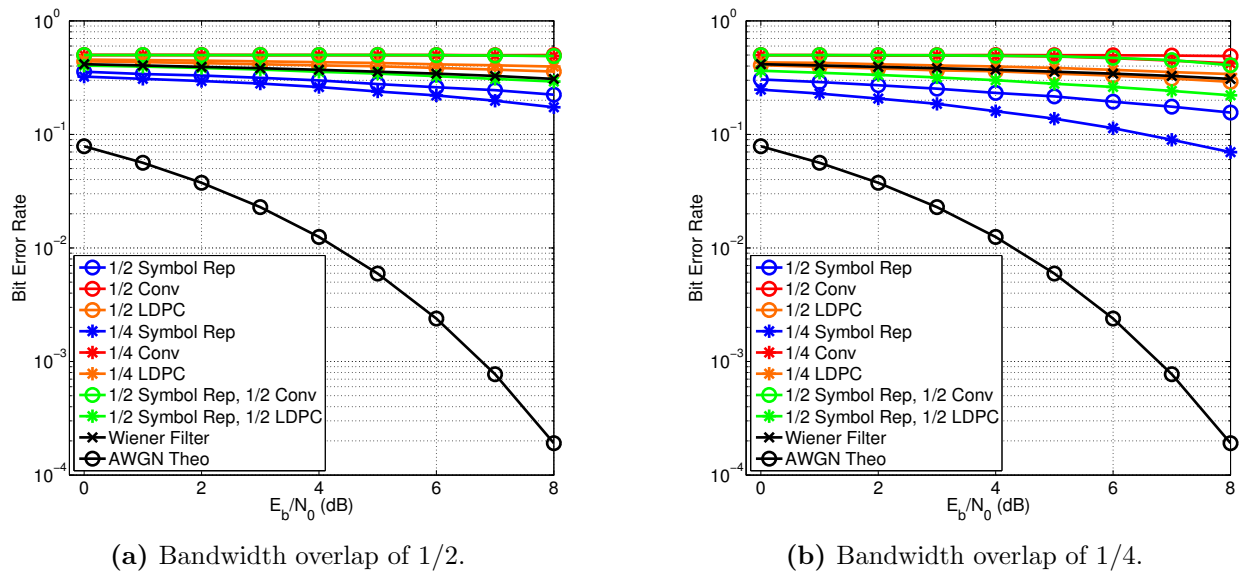
Figure 3.10: The BER curves for the filtering methods and error correcting codes while under a frequency selective channel from Figure 3.11.

methods for its ability to optimally combine the redundancies in the signal.

3.4.4   BER versus Interference Power

The impact of the interference power on the BER is given in Figures 3.12a and 3.12b, as the bandwidth of the interference is 1/2 and 1/4 that of the desired signal, respectively. In these results the power of the desired signal is held constant at $E_b/N_0 = 7$ dB with QPSK being used on each of the 64 subcarriers and the interference power is varied. As the interference power increases all approaches show a BER degradation but the PFD has the most graceful degradation, reducing the BER by less than an order of magnitude as the interference power is increased by 20 dB.

The hybrid approach of using the PFD and a convolutional code works better than each approach alone for almost all interference power values. The PFD is resilient to the increases in interference power and mitigates enough of the CS interference that the convolutional code can be used to correct the bit errors caused by the residual noise. This results in the hybrid approach producing a better BER that also degrades slowly as a function of interference power.
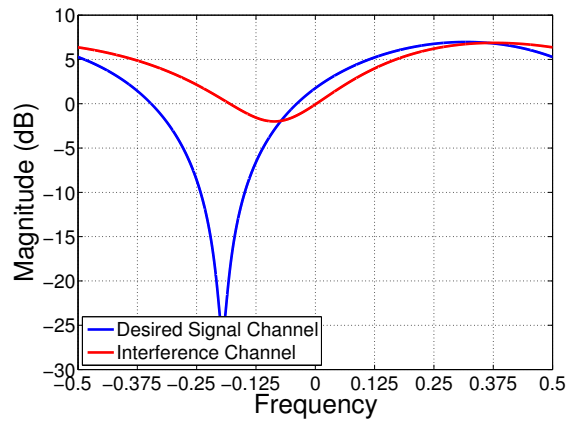
Figure 3.11: The magnitude of the frequency response for the channel on the desired signal and interference.
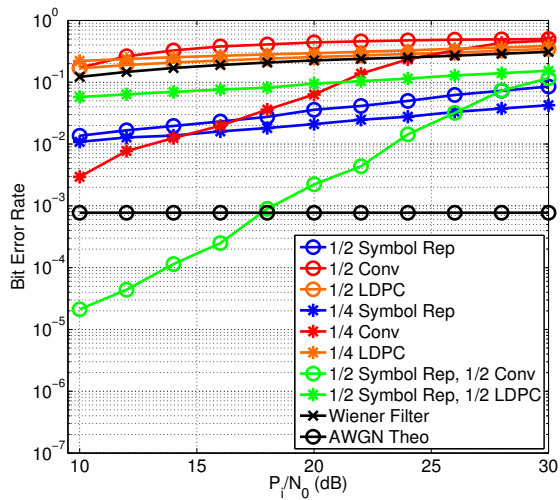
(a) Bandwidth overlap of 1/2.
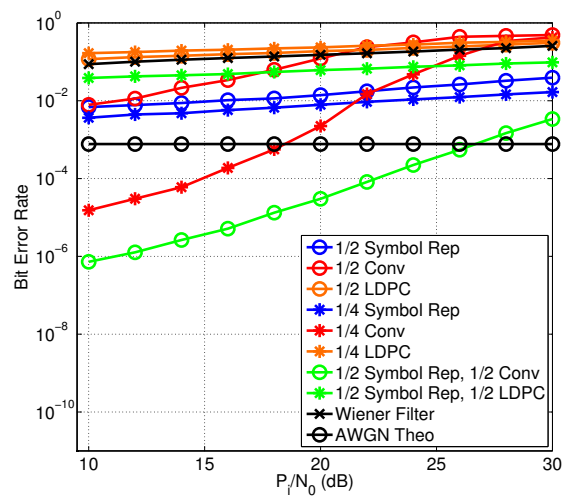
(b) Bandwidth overlap of 1/4.

Figure 3.12: The BER curves for the performance of the Wiener filter, Symbol Repetition (PFD), LDPC and convolutional codes as a function of interference to noise power P_i/N_0 when $E_b/N_0 = 7$ dB.

Modulations:	BPSK, QPSK, 8-PSK, 16-PSK, 16-QAM																									
Symbol Rep. Rates:	none, 1/2, 1/4, 1/8, 1/16																									
Conv. Code Rates:	none,	$\frac{1}{1}$,	$\frac{2}{3}$,	$\frac{3}{4}$,	$\frac{4}{5}$,	$\frac{5}{6}$,	$\frac{6}{7}$,	$\frac{7}{8}$,	$\frac{1}{2}$,	$\frac{1}{3}$,	$\frac{1}{4}$,	$\frac{1}{5}$,	$\frac{1}{6}$,	$\frac{1}{7}$,	$\frac{1}{8}$,	$\frac{3}{5}$,	$\frac{4}{7}$,	$\frac{5}{9}$,	$\frac{5}{8}$,	$\frac{5}{7}$,	$\frac{6}{11}$,	$\frac{7}{13}$,	$\frac{7}{12}$,	$\frac{7}{11}$,	$\frac{7}{10}$,	$\frac{7}{9}$

Table 3.1: The list of options for the modulation, symbol repetition and convolutional code rates from which the optimization can select.

The results demonstrate how an adaptive approach can be beneficial as the spectral environment changes. The PMW and PFD perform well in strong, wideband interference but do not perform as well as ECCs in purely AWGN channels. Balancing the redundancy used within ECCs and symbol repetition can therefore maximize the spectral efficiency while minimizing the BER as the spectral environment changes.

3.4.5 Optimization Results

The optimization in Section 3.4.5 is used to maximize the spectral efficiency while minimizing the BER. The optimization of the PMW selects the symbol repetition rate, coding rate and modulation order for each of the 64 occupied subcarriers. The parameters of the 16-QAM interference described in Section 3.4.1 are used in this optimization, and the interference covers 1/2 of the OFDM signal bandwidth. The power of both the desired signal and interference are both fixed for SIR = -20 dB, along with a fixed SNR = 10 dB. This leaves the selection of the waveform parameters as the only variables, which will also set the E_b/N_0.

The optimization is designed to meet the target BERs 10^{-1} to 10^{-5} while maximizing the spectral efficiency of the waveform. Each optimization is run for 500 iterations of the simulated annealing algorithm, and each iteration is run until 10 bit errors are simulated. Due to computational and memory constraints within the simulation 16 occupied subcarriers are used and spectral redundancy is only used across a single OFDM symbol, $B = 1$. The amplitude of each subcarrier is selected to be within $(0, 1]$ and Table 3.1 gives all options for the modulations, symbol repetition and convolutional code rates available for selection.

Figure 3.13 demonstrates how the simulated annealing algorithm balances the BER and the spectral efficiency to maximize the objective function. The initial iterations have the optimization looking
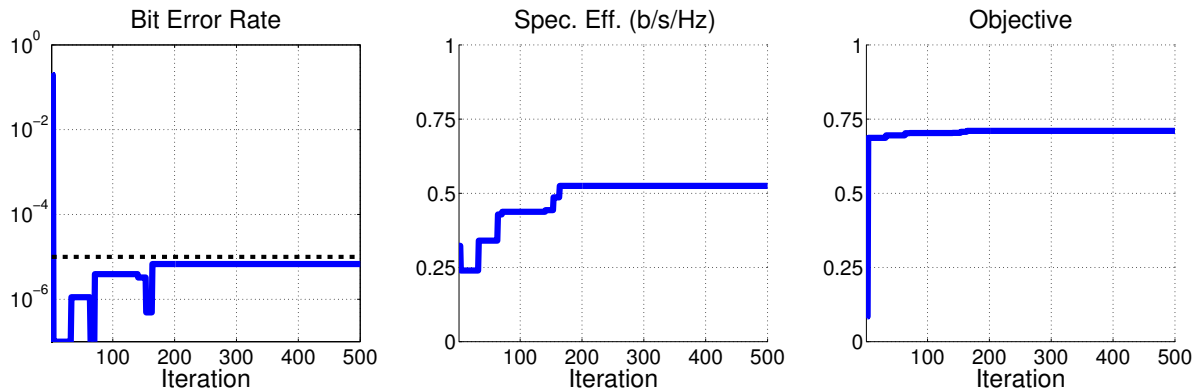
Figure 3.13: The BER, spectral efficiency, and objective, per iteration for the simulated annealing algorithm with a target BER of 10^{-4}.

BER_T	BER_M	Symbol Rep.	Conv. Code	Avg. Info. Bits	Spectral Eff.
10^{-5}	$6.78 * 10^{-6}$	1/4	3/5	0.88	0.53
10^{-4}	$8.86 * 10^{-5}$	1/2	3/5	1.18	0.75
10^{-3}	$1.98 * 10^{-4}$	1/2	5/9	1.50	0.83
10^{-2}	$5.21 * 10^{-3}$	1/2	3/5	1.56	0.94
10^{-1}	$8.22 * 10^{-2}$	1/2	None	1.69	1.69

Table 3.2: The results from the simulated annealing optimization using the PMW and PFD approach. *Avg. Info. Bits* is the average number of information bits per data symbol.

for parameters which meet or exceed the target BER, and then the spectral efficiency is improved through additional iterations. A record of the best set of outcomes is kept, which is represented by the blue line. The parameters which produced the maximum objective during the optimizations is given in Table 3.2. Table 3.3 contains the results of the optimizations when the symbol repetition is disabled.

Tables 3.2 and 3.3 list the parameters and outcomes for the optimizations. Each row lists the target BER, BER_T, and the measured BER, BER_M. The symbol repetition rate and the code rate for the convolutional codes is also given. The average number of information bits per data-symbol is given, which takes into account the repetition rate and the modulation order of the data symbols. The spectral efficiency includes the the average number of information bits per data-symbol and the code rate.

BER_T	BER_M	Symbol Rep.	Conv. Code	Avg. Info. Bits	Spectral Eff.
10^{-5}	$3.95 * 10^{-1}$	None	None	3.12	3.12
10^{-4}	$3.78 * 10^{-1}$	None	None	3.25	3.25
10^{-3}	$3.71 * 10^{-1}$	None	None	3.19	3.19
10^{-2}	$3.75 * 10^{-1}$	None	None	3.12	3.12
10^{-1}	$9.14 * 10^{-2}$	None	$\frac{1}{8}$	2.88	0.36

Table 3.3: The results from the simulated annealing optimization without using the PMW and PFD approach. *Avg. Info. Bits* is the average number of information bits per data symbol.

It is seen in Figure 3.7a that using 1/2 rate symbol repetition provides the largest improvement in BER for the smallest amount of overhead, and a similar effect can be seen in Table 3.2. For the target BERs 10^{-1} to 10^{-4}, the 1/2 rate symbol repetition is used, while for the BER 10^{-5} the 1/4 rate symbol repetition is needed to meet the BER.

When the PMW and PFD is not used the BER approaches 0.5 for most target BERs as seen in Table 3.3. As the BER cannot be controlled, the only way to maximize the objective function is therefore to maximize the spectral efficiency. The coding is able to meet the target BER for 10^{-1}, however its spectral efficiency is worse than using the PFD as it requires a $\frac{1}{8}$ code to do so. The PMW and PFD provides 16.5 dB, 12.3 dB, 11.2 dB, 11.0 dB, 10.7 dB worth of SNR gain from BERs 10^{-5} to 10^{-1}.

3.4.6   Complexity Analysis

The improved performance of the PFD over traditional filtering methods comes at the cost of increased transform and filtering complexity, although clever design decisions can be made to minimize the complexity increases. A traditional FFT-based OFDM demodulator and one-tap equalizer is used as the baseline for comparison. The OFDM receiver discards the N_{CP} samples of the cyclic prefix, transforms the remaining signal using an N-point FFT and then applies N complex weights to the frequency domain samples. The increases to the complexity of the PFD due to additional discrete Fourier transforms (DFT) is presented in Section 3.4.6 and the increases in complexity within the filtering operation is given in Section 3.4.6.

Complexity of Additional DFTs

Traditional OFDM receivers discard the cyclic prefix before taking the FFT over the OFDM symbol. This creates distortion when the received signal is affected by a large power interferer because it generates phase discontinuities, resulting in additional distortion. The increased complexity comes from taking a DFT over the entire OFDM symbol, N samples, along with the cyclic prefix N_{CP} samples, which allows the phase to remain continuous. The additional complexity comes from this larger DFT, applying an IDFT to transform back to the time domain to discard the cyclic prefix after filtering, and a final FFT applied at the nominal size to obtain the frequency domain symbols.

The cyclic prefix length is often represented as a fraction of the number of samples within the body of the OFDM symbol, $N_{CP} = N/4$ for example. Efficiently computing the FFT requires a transform size that is a power of 2, however the total input length of $N + N_{CP} = 5N/4$ is unlikely to be a power of 2. In this case, another DFT implementation is needed.

It is more likely that the longer input sequence can be decomposed into two relative primes allowing use of the prime factorization algorithm (PFA) [101] to efficiently implement the DFT. When $N = 1024$ and $N_{CP} = N/4$, $N + N_{CP} = 1280$ and can be factored into the relative primes of 256 and 5. Similarly, when $N = 1024$ and $N_{CP} = N/2$, $N + N_{CP} = 1536$ and can be factored into the relative primes of 512 and 3. Although a closed-form expression does not exist for the complexity of the PFA, [101] lists the number of complex multiplies required for various transform sizes between 30 and 2520. From the given results, it can be generally stated that for large transform sizes, $N > 128$, the number of complex multiplies required by the PFA for a transform of size $3N/2$ requires about the same number of complex multiplies as the Radix-2 FFT of transform size N. The use of the PFA does not result in a substantial increase in complexity for a single transform, and in some circumstances may decrease it.

The number of complex multiplies needed to implement the Radix-2 N-point FFT is [102]:

$$\frac{N}{2}\log_2(N). \tag{3.34}$$

With the simplifying assumption that the PFA algorithm can implement the $N + N_{CP}$ sized DFT

with approximately the same number of multiplies as the Radix-2 N-point FFT, the relative increase in complexity is approximately 3 times the number of multiplies required.

Complexity of Filtering

Any FRESH filter, including the PFD, is able to exploit the cycle frequencies within the desired signal and any interference, described by (3.16) and (3.17) of (3.15). Each frequency bin is now the summation of multiple complex weighted bins equivalent to the number of cycle frequencies over B OFDM symbols. The redundant bins can be utilized to our advantage by avoiding duplicate work and only computing the summation of correlated bins for a set of cycle frequencies one time.

The maximum number of complex multiplies needed to execute the PFD is:

$$(N + N_{CP}) \left(\sum_{c=0}^{B-1} \sum_{b=0}^{B-1} (U_{c,b} + V_{c,b}) \right). \tag{3.35}$$

However, only $N + N_{cp}$ of the frequency bins need to be estimated due to the redundancies built into the signal. A reasonable simplifying assumption is made that the number of cycle frequencies is consistent across all B OFDM symbols:

$$U = U_{c,b} \; \forall c = 0, 1, \; \ldots \; , B - 1$$
$$b = 0, 1, \; \ldots \; , B - 1, \tag{3.36}$$

$$V = U_{c,b} \; \forall c = 0, 1, \; \ldots \; , B - 1$$
$$b = 0, 1, \; \ldots \; , B - 1. \tag{3.37}$$

The PFD therefore requires:

$$(N + N_{CP}) (U + V), \tag{3.38}$$

multiplies to weight the redundant OFDM symbols and:

$$(N + N_{CP})(U + V) B, \tag{3.39}$$

additions to perform the summation across the B OFDM symbols. The relative increase in complexity over the one-tap equalization to implement the filtering is therefore:

$$\frac{(N + N_{CP})}{N}(U + V), \tag{3.40}$$

complex multiplies and:

$$\frac{(N + N_{CP})}{N}(U + V) B, \tag{3.41}$$

complex additions. The relative complexity increase of (3.40) can be separated into two terms: $\frac{N+N_{CP}}{N}$ due to the larger FFT size and $U + V$ due to the exploitation of the spectral redundancies and conjugate spectral redundancies. The one-tap equalization uses $N_{CP} = 0$ since it discards the cyclic prefix before the FFT, and $U = 1$ and $V = 0$ because it does not exploit any spectral redundancies.

An example is provided to demonstrate the increase in complexity in using the PFD, or any FRESH filter, relative to the one-tap equalizer. In this example the PMW transmits QPSK data symbols which have been repeated twice, represented by 2 cycle frequencies, and the 16-QAM interferer of Section 3.3.3 uses 3 frequencies in (3.14), therefore $U = 5$. Neither of the two signals have conjugate spectral redundancy, therefore $V = 0$. When $N_{CP} = \frac{N}{4}$, then $\frac{N+N_{CP}}{N} = \frac{5}{4}$. The relative increase in number of complex multiplies is therefore $\frac{5}{4}5 = 6.25$, representative of all FRESH filters, including the PFD. The number of complex additions is increased by $6.25B$.

3.5 Conclusion

A novel method has been proposed for creating interference mitigation properties in paramorphic multicarrier waveforms to enable communication in cyclostationary interference limited environments. Spectral redundancy is formed through repeating data symbols in both time and frequency within OFDM symbols, which is exploited at the receiver for a signal processing gain. The method provides a new way to design signals to be robust against cyclostationary interference, while simultaneously producing a better BER than ECCs for similar overhead rates under the simulated scenarios.

Future work would include using more generalized repetition patterns, both varying the amount of repetition per symbol and its placement in time and frequency. The spectral redundancy could also be designed across multiple antennas, including the development of the appropriate array processing algorithms to exploit the spatially distributed spectral redundancy. A real-time cognitive engine could also be developed which takes into account the proposed waveform adaptation techniques.

Chapter 4

Mitigating Linear Frequency Modulated Pulsed Radar Interference to OFDM to Enable Spectrum Co-Existence

4.1 Publications

Elements of this chapter have been included in the following publication:

- M. Carrick and J. H. Reed, "Exploiting the Cyclostationarity of Radar Chirp Signals with Time-Varying Filters", 2017 5th IEEE Global Conference on Signal and Information Processing, Montreal, Canada, pp. 1-4 [18].

4.2 Introduction

This chapter presents a novel method for the co-existence of Orthogonal Frequency Division Multiplexing (OFDM) signals with radar signals using a Time-Varying Frequency Shift (TV-FRESH) filter. The co-existence of communications signals with radar signals presents a difficult problem as the large power of radar systems is concentrated in a short pulse, virtually guaranteeing a spike in Bit Error Rate (BER). The proposed solution can be applied ad-hoc in a decentralized manner because it is implemented within a filter at the receiver, in direct comparison to other centralized and controlled methods such as exclusion zones and database access systems. The method also provides a protocol-agnostic method for co-existence, where others have only considered specific technologies such as Long Term Evolution (LTE).

The contributions described in this chapter include:

- The application of FRESH filters for mitigating linear frequency modulated radar interference.

- A novel filtering structure for mitigating pulsed chirp radar signals for improving the BER of an OFDM signal.

- A processing gain of more than 8 dB, and an improvement in BER by more than 10 times, with respect to the optimal time-invariant filter when the SIR = -20 dB.

- Derivation of the cycle frequencies of a linear frequency modulated radar signal.

- A decentralized, flexible and ad-hoc solution to OFDM and radar co-existence.

Whereas a time-invariant filter can only mitigate interference by attenuating selected subbands, a TV-FRESH filter effectively estimates and subtracts the interferer, leaving the signal of interest intact and with an improved SINR. The mitigation performance TV-FRESH structure is less dependent on the interference power than the time-invariant filter, which is especially important for interferers that can have transmit powers in the megawatt range. Powerful short-duration interferers can induce significant bit errors for victim radios over a large geographical area, so that mitigating such interference has a significant impact on overall co-existence of the communication and radar systems.

The impact of the TV-FRESH filter can be the reduction of exclusion zones [66, 67] and as a way to improve the transition of spectrum from legacy radar users to co-existence bands. By rejecting interference with the TV-FRESH filter, rather than avoiding it as in prior work, the geographical area for exclusions zones can be decreased which improves the spectral efficiency of the new co-existence bands. The TV-FRESH filter can also be applied as an additional layer of protection for communications users as the bands are phased out from single-use only into dual use or co-existence.

The proposed method applies a TV-FRESH filter which jointly exploits the spectral redundancies of the OFDM and radar signals. The TV-FRESH filter partitions the received signal into multiple time segments and exploits the spectral redundancies between them, allowing for improved interference rejection as compared to a FRESH filter alone. Where the FRESH filter is a periodically time-varying filter due to the frequency shifters, the TV-FRESH filter includes additional periodicities due to the time-varying application of filter weights. This is in direct contrast to the Wiener filter, a time-invariant filter, which is unable to exploit any spectral redundancies of the received signal thereby limiting its performance.

The TV-FRESH filter creates its signal processing gain over other methods through additional computation, however it can be implemented efficiently within a vectorized structure for general purpose graphics processing units, or in a parallel structure for Field Programmable Gate Arrays (FPGAs).

4.2.1   Outline

Optimal filtering of radar and OFDM signals with the TV-FRESH is proposed in Section 4.3. Simulation results are presented in Section 4.4 and the conclusion in Section 4.5.

4.3   Optimal Filtering for OFDM and Radar Signals

The intent of this section is to describe the cyclostationary nature of radar signals, and then to present optimal filters. This is first introduced through describing the cyclostationarity of a complex

sinusoid and its optimal filtering. The methods are then generalized to include a sinusoid with a swept frequency: a chirp signal. The cycle frequencies of the chirp signal are derived and the optimal filtering of the joint radar and OFDM received signal is presented. The chirp radar signal is considered here to develop a foundation for which other radar signals can be considered, such as OFDM-based radar signals [103, 104].

4.3.1   FRESH Filtering of a Complex Exponential

The following example is intended to provide intuition for the filtering of a pulsed chirp radar signal, and how the conjugate spectral redundancy can be exploited. A complex exponential is used for simplicity, with the intent that the procedure can be extrapolated easily for more complicated signals such as chirp pulse trains.

The spectral redundancy inherent in a complex exponential can be exploited by an Almost Cyclostationary (ACS) FRESH filter [1] by linearly combining the exponential with its conjugate. A complex exponential carries redundant information on its real and imaginary components,

$$z(t) = e^{j2\pi ft} = \cos\left(2\pi ft\right) + j\sin\left(2\pi ft\right). \tag{4.1}$$

The cycle frequencies of (4.1) are $\alpha = 0$ and $\beta = 2f$, therefore the FRESH filter for this case is:

$$\hat{z}(t) = (a(t) \; \circledast \; x(t)) + \left(b(t) \otimes x^*(t)e^{j2\pi(2f)t}\right). \tag{4.2}$$

Since $\alpha = 0$, the linear path of the FRESH filter will not perform any frequency shifting on $x(t)$. The conjugate-linear path however will perform a spectral flip due to the conjugation and a frequency shift of $\beta = 2f$ to align the linear and conjugate-linear paths in frequency. The multiplication by the complex term within the frequency shifter,

$$e^{j2\pi(2f)t} = \cos\left(2\pi(2f)t\right) + j\sin\left(2\pi(2f)t\right), \tag{4.3}$$

will switch the real and imaginary channels of the received signal $x(t)$. The redundant information on the real and imaginary channels of $x(t)$ have now been aligned with one another and filtering by $a(t)$ and $b(t)$ can combine the spectrally redundant information.

4.3.2 Cyclic Autocorrelation of Frequency Swept Signals

A chirped signal is a sinusoid whose frequency is changed over time, which creates beneficial properties for radar systems. Where a sinusoid of frequency f_o has spectral redundancy for $\alpha = 0$ and $\beta = 2f_o$ for all time, the frequency sweep of a chirp signal distributes spectral redundancy across a set of frequencies. The signal model assumes that the radar signal is already at complex baseband [105]:

$$c(t) = e^{j2\pi\left(\frac{-\Delta ft}{2} + \frac{\Delta ft^2}{2T_c}\right)}, \tag{4.4}$$

where the sweep rate in frequency of the chirp is defined by Δf, while T_c is the length of the pulse. The chirp pulse train is given by:

$$\tilde{c}(t) = \sum_k c(t - kT_{PRI}), \tag{4.5}$$

where T_{PRI} is the pulse repetition interval (PRI).

The frequency sweep translates energy of the chirp across a band, forming a type of diversity which can be exploited. The chirp signal is in direct contrast to the complex exponential in (4.1) whose spectral redundancy is constant over all time. The signal model of (4.4) and the following analysis is left symbolic in order that the filtering can be adapted as the radar parameters change in real time. Similarly, the signal representation (4.4) and its analysis can be modified to represent other radar waveforms as in [105] to develop the cyclostationarity statistics so they too can be FRESH filtered.

Before the filter can be described, the cyclostationarity of the chirp signal must be derived. The modulated signal $\tilde{d}(t)$ is represented by a product,

$$\tilde{d}(t) = \sum_k z(t)c(t - kT_{PRI}), \tag{4.6}$$

where $c(t)$ is the deterministic modulating chirp, and $z(t)$ is the signal to be modulated. When considering only a chirp signal then $z(t)$ can be replaced by a ramping frequency, however it is left symbolic so the results can be more general. For generality, it is assumed that $z(t)$ is ACS.

The time-varying transformation of $\tilde{d}(t)$ by modulation with the chirp train signal $\tilde{c}(t)$ results in a generalized almost cyclostationary signal [106]. However, the sampling process transforms a continuous time generalized almost cyclostationary signal into a discrete time ACS signal [107]. The discrete time signal $\tilde{d}[k]$ is produced by sampling with period T_s,

$$\tilde{d}[k] = \tilde{d}(kT_s) = z(kT_s)\tilde{c}(kT_s). \tag{4.7}$$

The cyclic autocorrelation and conjugate cyclic autocorrelation of $\tilde{d}(kT_s)$ after sampling are [30],

$$R_d^\alpha[l] = \sum_\gamma R_z^{\alpha-\gamma}[l]R_c^\gamma[l], \tag{4.8}$$

$$R_{dd^*}^\beta[l] = \sum_\zeta R_{zz^*}^{\beta-\zeta}[l]R_{cc^*}^\zeta[l]. \tag{4.9}$$

The discrete time chirp $\tilde{c}(kT_s)$ can be represented by the generalized Fourier Series,

$$\tilde{c}(kT_s) = \sum_\gamma c_\gamma e^{j2\pi\gamma kT_s}. \tag{4.10}$$

The frequencies of the Fourier series representation are:

$$\gamma = \frac{n}{T_{PRI}/T_s}, \ n = 0, \pm 1, \pm 2, \ \dots \ , \frac{T_{PRI}/T_s}{2}, \tag{4.11}$$

$$\zeta = \frac{p}{T_{PRI}/T_s}, \; p = 0, \pm 1, \pm 2, \; \ldots \; , \frac{T_{PRI}/T_s}{2}, \tag{4.12}$$

where it is assumed that $\frac{T_{PRI}}{T_s}$ is an integer. The frequencies from the Fourier series of the cyclic autocorrelation and conjugate cyclic autocorrelation are therefore the cycle frequencies of the chirp pulse train [30, 43]. The cyclic autocorrelation and conjugate cyclic autocorrelation functions of $\tilde{c}(kT_s)$ are therefore [30],

$$R_c^\gamma[l] = \sum_\zeta c_\zeta c_{\gamma - \zeta} e^{j\pi(2\zeta - \gamma)lT_s}, \tag{4.13}$$

$$R_{cc^*}^\gamma[l] = \sum_\zeta c_\zeta c_{\zeta - \gamma}^* e^{j\pi(2\zeta - \gamma)lT_s}. \tag{4.14}$$

When $z(kT_s) = e^{j2\pi f_z kT_s}$, $R_z^{\alpha - \gamma}[l] \neq 0$ for $\alpha - \gamma = 0$. Therefore $R_d^\alpha[l] \neq 0$ for $\alpha = \gamma$, and the discrete time cycle frequencies of $\tilde{d}(kT_s)$ become [18],

$$\alpha = \frac{n}{T_{PRI}/T_s}, \; n = 0, \pm 1, \pm 2, \; \ldots \; , \frac{T_{PRI}/T_s}{2}. \tag{4.15}$$

As $R_{zz^*}^{\beta - \zeta}[l] \neq 0$ for $\beta - \zeta = 2f_z$, therefore $R_{dd^*}^\beta[l] \neq 0$ for $\beta = 2f_z + \zeta$, and the discrete time conjugate cycle frequencies of $\tilde{d}(kT_s)$ become [18],

$$\beta = 2f_z + \frac{p}{T_{PRI}/T_s}, p = 0, \pm 1, \pm 2, \; \ldots \; , \frac{T_{PRI}/T_s}{2}. \tag{4.16}$$

The complex exponential $z(kT_s)$ has only two cycle frequencies, $\alpha = 0$ and $\beta = 2f_z$. The harmonics of the pulse length T_{PRI} of the chirp signal $\tilde{d}(kT_s)$ form many more cycle frequencies.

The cyclic spectrum and conjugate cyclic spectrum for a chirp signal with a pulse repetition interval of 16 samples and a duty cycle of 50% is given in Figures 4.1a and 4.1b. The parameters are chosen exclusively for their illustrative purposes, such that the reader may extrapolate the intuition into more realistic scenarios. Similar cyclic spectrum plots for other radar waveforms can be found in
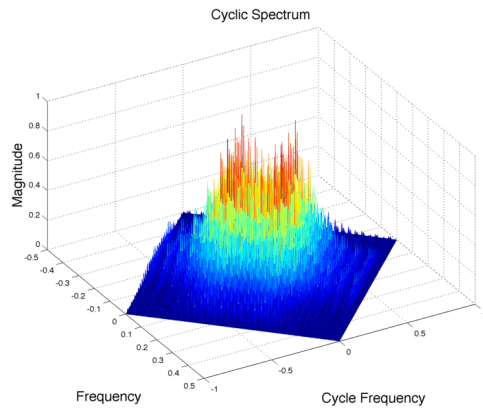
(a) An example cyclic spectrum.
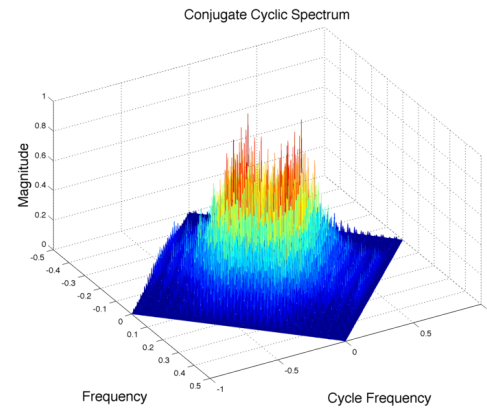
(b) An example conjugate cyclic spectrum.

Figure 4.1: The cyclic and conjugate cyclic spectra for a pulsed chirp radar signal whose PRI is 32 samples and whose duty cycle is 50%.
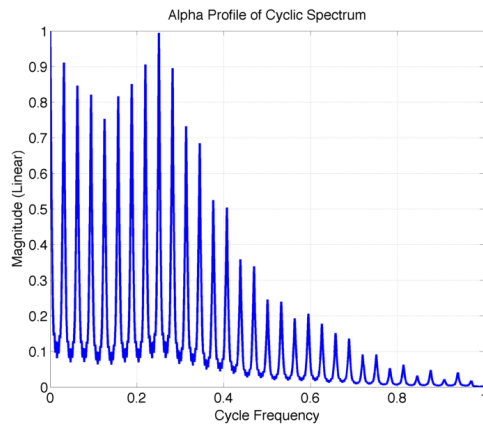
(a) An example alpha profile of the cyclic spectrum for a chirp pulse train.
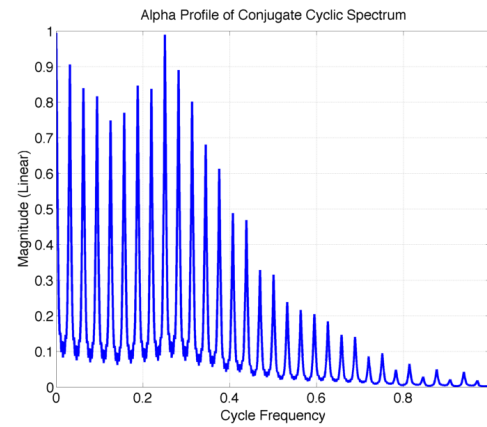
(b) An example alpha profile of the conjugate cyclic spectrum for a chirp pulse train.

Figure 4.2: The alpha profile of the cyclic and conjugate cyclic spectrum shown in Figures 4.1a and 4.1b.

[105]. The alpha profile of the cyclic spectra is presented in Figures 4.2a and 4.2b. The alpha profile plots the maximum value across all frequency values for each cyclic frequency, collapsing the three-dimensional cyclic spectrum plot into a two-dimensional one [108].

The initial representations of cyclostationary signals deal with vectorized stationary signal forms [4] produced by applying a rotating set of filter weights to each of the different samples in the received signal, similar to a decimating polyphase filter bank [109]. The segmentation of the time domain signal using FFTs performs a similar vectorization of the signal, and applies periodically time-varying filter weights to the received signal.

Errors in the PRI due to hardware imperfections, mismatches between the transmitter and receiver or Doppler shift will lead to cycle frequency error, where the frequency shifts in the branches of the TV-FRESH do not match perfectly with the cycle frequencies in the received signal. An adaptive FRESH filter will correct for some of the cycle frequency errors as presented in [36]. Adaptations to a varying PRI can also be incorporated into an adaptive FRESH structure.

The cycle frequencies of the perfectly downconverted OFDM signal with a cyclic prefix are known to be $\alpha = 0, \pm\frac{1}{N}, \pm\frac{2}{N}, \ldots$ where N is the length of the OFDM symbol in number of samples, including the cyclic prefix [48]. The conjugate cycle frequencies are $\beta = 0, \pm\frac{1}{N}, \pm\frac{2}{N}, \ldots$ when any OFDM subcarriers use BPSK or any other modulation with co-linear constellation points. Although not considered here, redundant symbols transmitted across multiple subcarriers in LTE can produce additional cycle frequencies and result in better interference mitigation [15].

4.3.3 Optimal Filtering with the TV-FRESH Filter

The TV-FRESH filter includes a time resolution as a design parameter. The receive signal is divided into multiple, identical-length time segments. The TV-FRESH filter jointly filters the block of time segments, increasing the time resolution while still filtering a large number of samples. Each time segment is transformed into the frequency domain, time aligned with a tapped delay line, and filtered.

The number of time segments defines the time resolution for the TV-FRESH filter, with more time segments resulting in better time resolution. Increasing the time resolution allows time-varying
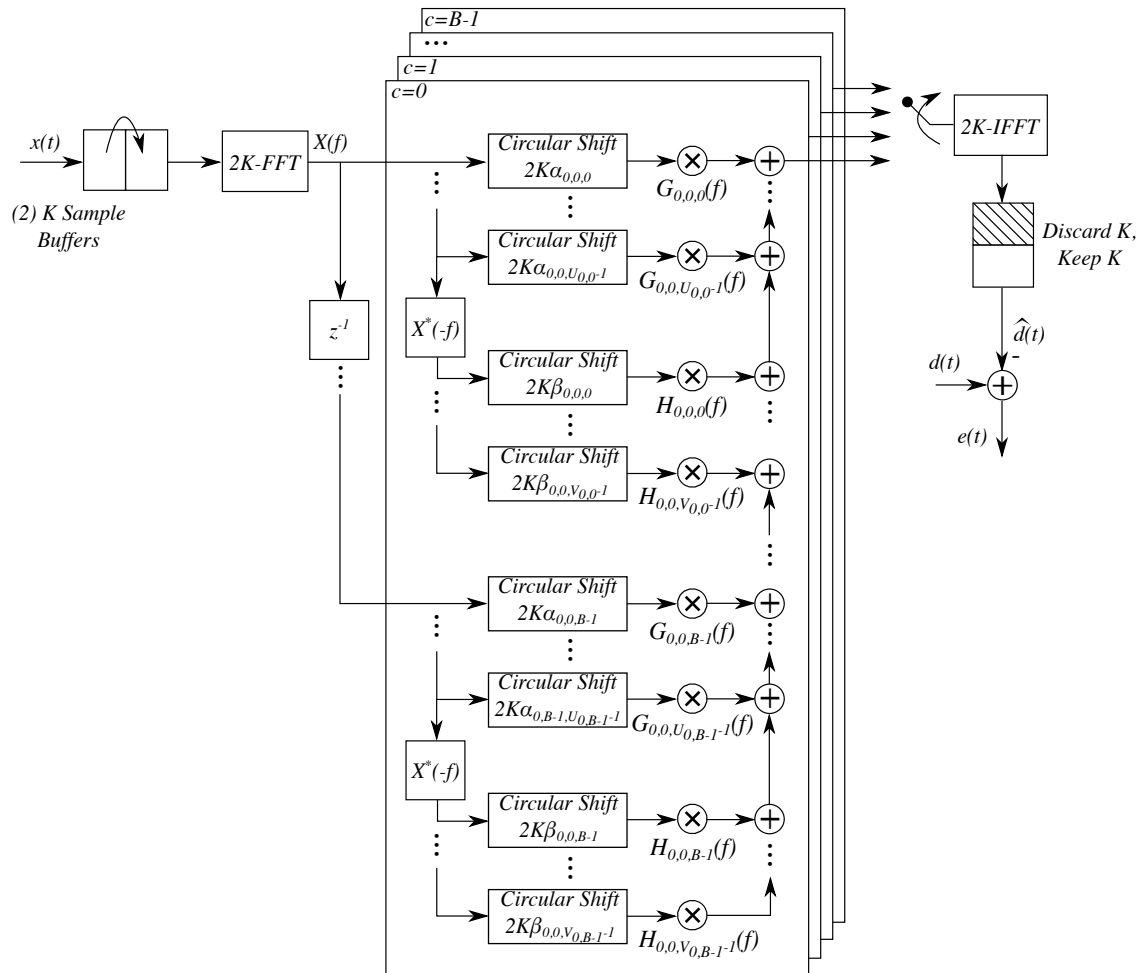
Figure 4.3: The frequency domain TV-FRESH filter uses overlap-save input and output sample buffering to implement linear convolution.

parameters to be better approximated as slowly varying, or constant, over a small time scale which allows better tracking for the filter. Each segment will therefore have its own set of filter weights, matching the time-varying nature of the TV-FRESH to that of the received signal.

The signal $x[k]$ is segmented into B segments of K time domain samples and transformed into the frequency domain using a $2K$-point FFT, $X(f)$. The group of B segments, forming a total of BK samples, is referred to as a *block*.

The TV-FRESH filter exploits the periodic nature of the pulsed radar by jointly filtering across a tapped delay line of length B, each delay element containing a sequential set of frequency domain samples. The lth block of B OFDM symbols is fed into the memory, $X_{l,0}(f), X_{l,1}(f), \ldots, X_{l,B-1}(f)$. It is assumed that the OFDM symbols are time aligned at the receiver such that the B OFDM symbols fit within the proper time-window. The filter then estimates the cth time segment within the lth block, $\hat{D}_{l,c}(f)$, for the desired signal according to [18]:

$$\hat{D}_{l,c}(f) = \sum_{b=0}^{B-1} \left[\sum_{u=0}^{U_{c,b}-1} G_{c,b,u}(f) X_{l,b}(f - \alpha_{c,b,u}) + \sum_{v=0}^{V_{c,b}-1} H_{c,b,v}(f) X_{l,b}^*(-f + \beta_{c,b,v}) \right]. \qquad (4.17)$$

Figure 4.3 gives a graphical representation of the TV-FRESH filter, whose commutator is analogous to the vector stationary signal model of [4]. The frequency domain filter weights $G_{c,b,u}(f)$ correspond to the linear portion which exploits the spectral redundancy with the uth frequency shift of the bth time segment with respect to the cth segment. The filter $H_{c,b,v}(f)$ is part of the conjugate linear portion, which exploits the conjugate spectral redundancy with the vth frequency shift of the bth time segment with respect to the cth segment. There are $U_{c,b}$ frequency shifts for the spectral redundancy of the bth time segment with respect to the cth time segment. Likewise, there are $V_{c,b}$ frequency shifts for the conjugate spectral redundancy of the bth time segment with respect to the cth segment.

The number of frequency shifts in (4.17) defines a trade-off between the computational complexity and the output SINR. Including more frequency shifts in the TV-FRESH filter increases the potential SINR gain [1], with the cost that additional linear time-invariant filters will be needed to

optimally align the amplitude and phase of the different frequency shifted versions of the received signal.

Where frequency shifts were described by α and β for the ACS FRESH filter, a notation is needed to describe spectral redundancy over time. Subscripts are now used for $\alpha_{c,b,u}$ which is the uth cycle frequency of the bth time segment with respect to the cth segment. The vth frequency shift of the conjugate spectral redundancy in the bth time segment with respect to the cth segment is represented by $\beta_{c,b,v}$.

The sums and differences of the cycle frequencies for the desired signal and interference can be used within the TV-FRESH filter as in [15]. Whereas the frequency shifts of the desired signal are represented by $\{\gamma_{d,c,b,u}\}$, and the interference by $\{\gamma_{i,c,b,u}\}$, the entire set of frequency shifts for $\{\alpha_{c,b,u}\}$ is found according to [15]:

The frequency shifts $\{\beta_{c,b,v}\}$ can be found in a similar manner as (4.24).

The cycle frequencies for CS and ACS signals can be represented within the notation of $\alpha_{c,b,u}$. Taking the sample of a BPSK signal with symbol interval T, the cycle frequencies are $\{\alpha\} = \frac{n}{T}$ for $n = 0, \pm1, \pm2, \ldots$. Therefore, $\{\alpha_{c,b,u}\} = \varnothing$ when $c \neq b$ and $\{\alpha_{c,b,u}\} = \frac{n}{T}$ as $c = b$.

The MMSE weights of the TV-FRESH filter can be found using the same process outlined in Section 2.2.3, and are derived in [18]. The design equations are presented in (4.19) and (4.20).

The theoretical SINR at the output of the TV-FRESH filter can also be found in [18]. The output SINR is given by (4.25), the details of which are described in (4.21)-(4.23).

$$\lambda_l = \frac{\mathbb{E}\left\{|D_{l,c}(f)|^2\right\}}{\mathbb{E}\left\{\left|D_{l,c}(f) - \hat{D}_{l,c}(f)\right|^2\right\}}. \tag{4.18}$$

4.3.4 Computation Complexity

The ability to mitigate the radar interference comes at the cost of additional computation complexity. The complexity here will be measured as a relative increase with respect to the Wiener filter, and a similar analysis can be found in [15].

$$S_{d_c,x_p}^{\alpha_{c,p,k}}\left(f - \frac{\alpha_{c,p,k}}{2}\right) = \sum_{b=0}^{B-1}\left[\sum_{u=0}^{U_{c,b}-1} G_{c,b,u}(f)S_{x_c,x_b}^{\alpha_{c,p,k}-\alpha_{c,b,u}}\left(f - \frac{\alpha_{c,p,k}+\alpha_{c,b,u}}{2}\right)\right.$$
$$\left. + \sum_{v=0}^{V_{c,b}-1} H_{c,b,v}(f)\, S_{x_c,x_b^*}^{\beta_{c,b,v}-\alpha_{c,p,k}}\left(f - \frac{\beta_{c,b,v}+\alpha_{c,p,k}}{2}\right)^*\right] \tag{4.19}$$

$$p = 0,1,\ldots,B-1; \quad k = 0,1,\ldots,U_{c,p}-1$$

$$S_{d_c,x_m^*}^{\beta_{c,m,n}}\left(f - \frac{\beta_{c,m,n}}{2}\right) = \sum_{b=0}^{B-1}\left[\sum_{u=0}^{U_{c,b}-1} G_{c,b,u}(f)S_{x_c,x_b^*}^{\beta_{c,m,n}-\alpha_{c,b,u}}\left(f - \frac{\beta_{c,m,n}+\alpha_{c,b,u}}{2}\right)\right.$$
$$\left. + \sum_{v=0}^{V_{c,b}-1} H_{c,b,v}(f)\, S_{x_c,x_b}^{\beta_{c,m,n}-\beta_{c,b,v}}\left(-f + \frac{\beta_{c,m,n}+\beta_{c,b,v}}{2}\right)\right] \tag{4.20}$$

$$m = 0,1,\ldots,B-1; \quad n = 0,1,\ldots,V_{c,m}-1$$

$$\mathbb{E}\left\{\left|D_{l,c} - \hat{D}_{l,c}\right|^2\right\} = S_d(f) - 2\Re\left(\mathbb{E}\left\{D_{l,c}(f)\hat{D}_{l,c}^*(f)\right\}\right) + \mathbb{E}\left\{\hat{D}_{l,c}(f)\hat{D}_{l,c}^*(f)\right\} \tag{4.21}$$

$$\mathbb{E}\left\{D_{l,c}(f)\hat{D}_{l,c}^*(f)\right\} = \sum_{b=0}^{B-1}\left(\sum_{u=0}^{U_{c,b}-1} G_{c,b,u}^*(f)S_{d_c,x_b}^{\alpha_{c,b,u}}\left(f - \frac{\alpha_{c,b,u}}{2}\right) + \sum_{v=0}^{V_{c,b}-1} H_{c,b,v}^*(f)S_{d_c,x_b^*}^{\beta_{c,b,v}}\left(f - \frac{\beta_{c,b,v}}{2}\right)\right)$$
$$\tag{4.22}$$

$$\mathbb{E}\left\{\hat{D}_{l,c}(f)\hat{D}_{l,c}^*(f)\right\} = \sum_{b=0}^{B-1}\sum_{z=0}^{B-1}\sum_{u=0}^{U_{c,b}-1}\sum_{m=0}^{U_{c,b}-1} G_{c,b,u}(f)G_{c,z,m}^*(f)S_{x_b,x_z}^{\alpha_{c,z,m}-\alpha_{c,b,u}}\left(f - \frac{\alpha_{c,b,u}+\alpha_{c,z,m}}{2}\right)$$
$$+2\Re\left\{\sum_{b=0}^{B-1}\sum_{z=0}^{B-1}\sum_{u=0}^{U_{c,b}-1}\sum_{n=0}^{V_{c,b}-1} G_{c,b,u}(f)H_{c,z,n}^*(f)S_{x_b,x_z}^{\beta_{c,z,n}-\alpha_{c,b,u}}\left(f - \frac{\beta_{c,b,n}+\alpha_{c,b,u}}{2}\right)\right\}$$
$$+\sum_{b=0}^{B-1}\sum_{z=0}^{B-1}\sum_{v=0}^{V_{c,b}-1}\sum_{n=0}^{V_{c,b}-1} H_{c,b,v}(f)H_{c,z,n}^*(f)S_{x_b,x_z}^{\beta_{c,z,n}-\beta_{c,b,v}}\left(-f + \frac{\beta_{c,b,v}+\beta_{c,z,n}}{2}\right) \tag{4.23}$$

$$\{\alpha_{c,b,u}\} = \{\gamma_{d,c,b,0},\ \gamma_{d,c,b,1},\ \gamma_{d,c,b,2},\ \cdots\ ,\gamma_{i,c,b,0},\ \gamma_{i,c,b,1},\ \gamma_{i,c,b,2},\ \cdots\ ,$$
$$\gamma_{d,c,b,0} - \gamma_{i,c,b,0}, -\gamma_{d,c,b,0} + \gamma_{i,c,b,0}, \gamma_{d,c,b,0} - \gamma_{i,c,b,1}, -\gamma_{d,c,b,0} + \gamma_{i,c,b,1},$$
$$\gamma_{d,c,b,1} - \gamma_{i,c,b,0}, -\gamma_{d,c,b,1} + \gamma_{i,c,b,0}, \gamma_{d,c,b,1} - \gamma_{i,c,b,1}, -\gamma_{d,c,b,1} + \gamma_{i,c,b,1}, \cdots\ \}. \tag{4.24}$$

The frequency domain implementation of the Wiener filter, shown in Figure 2.2, transforms the signal into the frequency domain using a $2K$-point FFT. The $2K$ complex weights are then multiplied against the frequency bins and transformed back into the time domain using a $2K$-point IFFT. The TV-FRESH operates similarly, shown in Figure 4.3, however it multiplies frequency shifted versions of the frequency domain samples before summing the result. The additional complexity is proportional to the number of frequency shifts implemented in the TV-FRESH filter.

The simplifying assumption is made that the number of frequency shifts $U_{c,b}$ and $V_{c,b}$ from (4.17) is constant for all c and b, represented by U and V. The number of complex multiplies due to the weighting of the frequency bins, $G_{c,b,u}X_{l,b}(f - \alpha_{c,b,u})$ and $H_{c,b,v}X^*_{l,b}(-f + \beta_{c,b,v})$ is then:

$$2KB(U + V). \tag{4.25}$$

The Wiener filter implements $2K$ complex multiples for its frequency domain filter, therefore the TV-FRESH increases the number of complex multiples by a factor of:

$$B(U + V). \tag{4.26}$$

While the radar signal can have a large number of cycle frequencies as see in Figures 4.2a and 4.2b, the TV-FRESH is not required to implement them all as frequency shifts. Experimentation has been used to develop a heuristic, where the cycle frequencies corresponding to the largest values in the spectral correlation function should be prioritized as they will contribute the most to the output of the TV-FRESH filter. The results in the following section implement a limited number of frequency shifts to keep the computational complexity reasonable while still mitigating the interference to a significant extent.

4.4 Simulation Results

Simulation results are presented for the scenario for which a radar signal is interfering with an OFDM signal. The mitigation of radar interference to an OFDM signal shows the ability to exploit
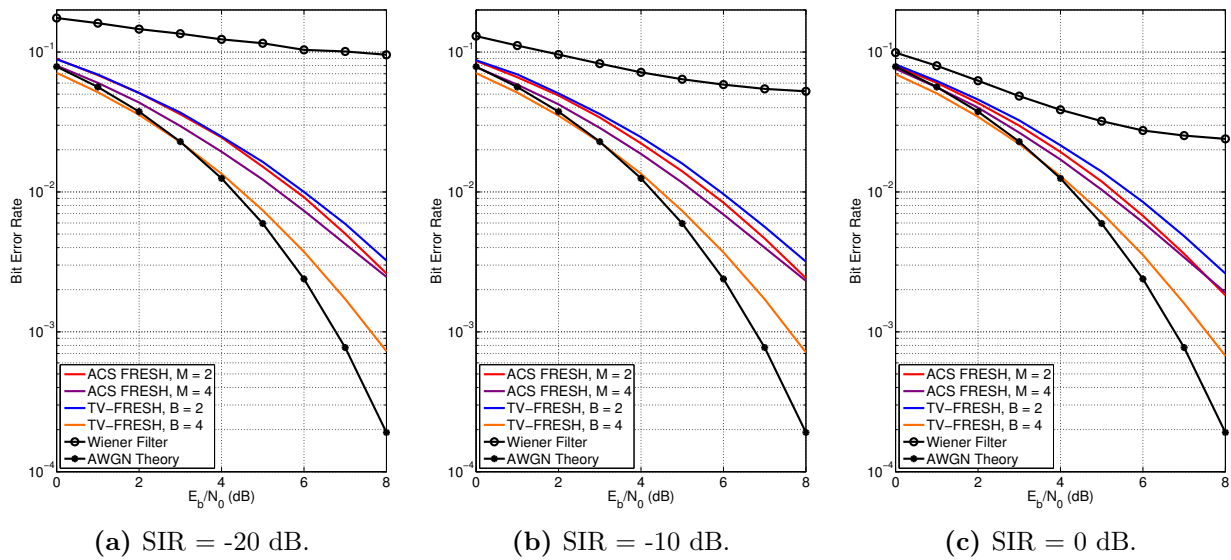
Figure 4.4: The BER curves when chirped radar interferes with OFDM, when using QPSK subcarriers.
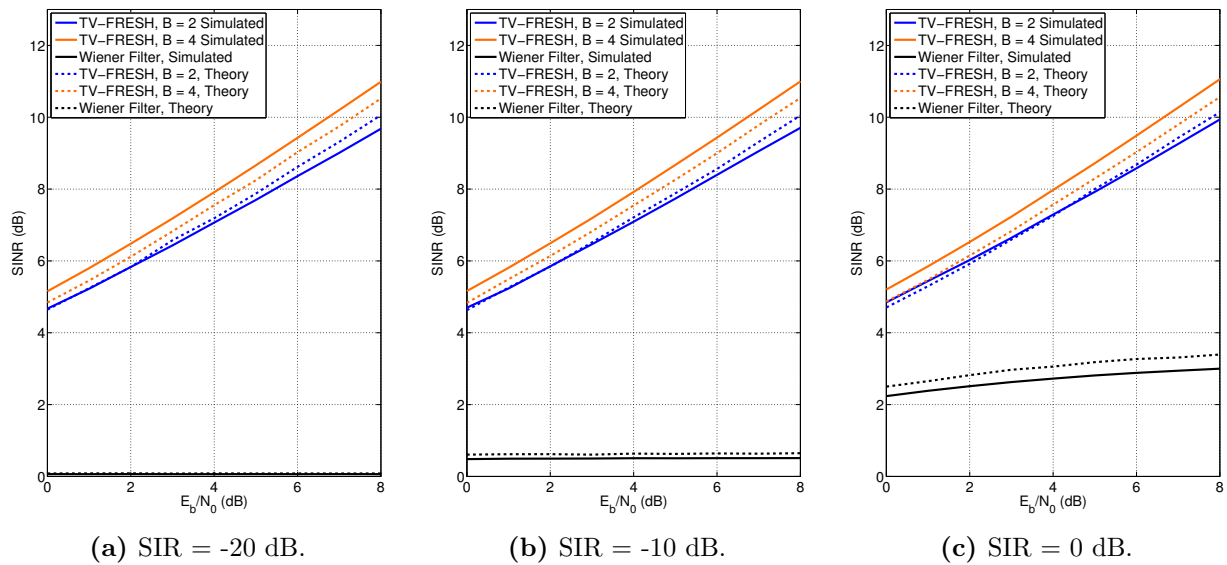
Figure 4.5: The SINR curves when chirped radar interferes with OFDM, when using QPSK subcarriers.

(a) SIR = -20 dB. **(b)** SIR = -10 dB. **(c)** SIR = 0 dB.
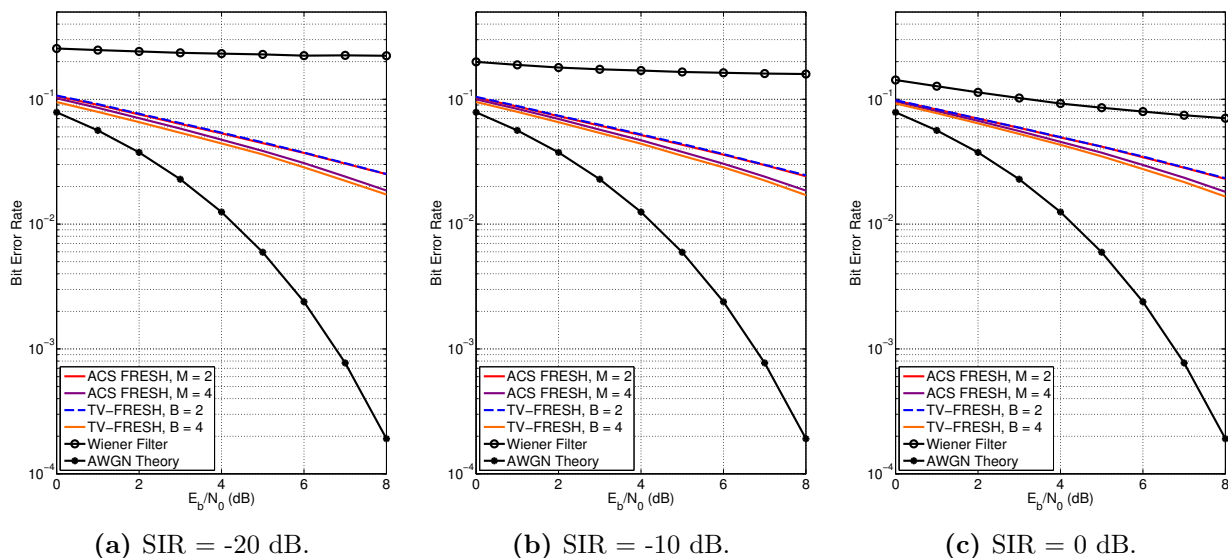
Figure 4.6: The BER curves when chirped radar interferes with OFDM, when using QPSK subcarriers and with an example multipath channel.

time-varying spectral redundancy, in this case for two heterogeneous signals. The theoretical SINR plots are created using the theoretical SINR equation (4.25).

The simulation scenario is that a chirp radar signal is interfering with an OFDM signal, with signal to interference ratios (SIR) of -20, -10 and 0 dB. The SIR is defined as the ratio of the power of the entire OFDM signal to that of the entire radar signal. The OFDM signal uses 16 occupied subcarriers out of 32 total, and has a cyclic prefix length of 8 samples. The subcarriers all use QPSK as the modulation. The radar pulse length is 4 OFDM symbols, with the PRI being 40 OFDM symbols long. The frequency of the chirp sweeps across the full bandwidth of the 16 occupied subcarriers over the PRI. It is assumed that the PRI is known to the receiver for these simulations.

The BER and SINR is measured for the Wiener filter, the ACS FRESH filter, and the TV-FRESH filter, in Figures 4.4a-4.5c. Both the BER and SINR are measured for the full duration of the received signal, including the "on" and "off" times of the radar signal. When $B = 2$ and $B = 4$, the amount of data jointly filtered by the TV-FRESH is increased by the same factor. The amount of data in the ACS FRESH filter is increased by the factor $M = 2$ and $M = 4$ in the plots. The number of input samples for the TV-FRESH filter is $40\frac{MB}{2}$, where 40 comes from the total length
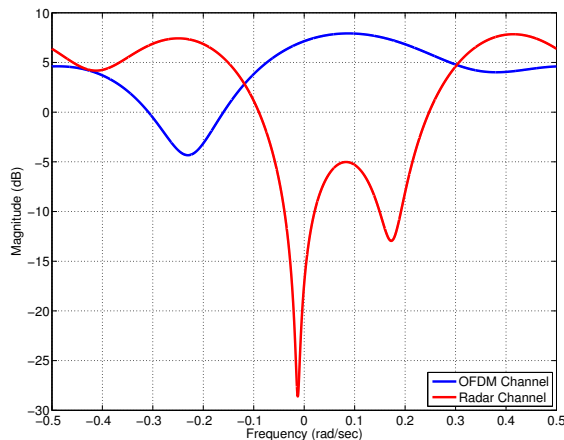
Figure 4.7: The magnitude of the frequency response for the multipath fading channel applied to the OFDM and radar signals.

of each OFDM symbol.

The cyclic prefix introduces a large number of cycle frequencies into the OFDM signal, but each of them corresponds to a small amount of spectral redundancy [48]. A similar effect occurs with the radar signal, where the many cycle frequencies contain a small piece of the spectral redundancy. Since including more frequency shifts in the TV-FRESH filter increases the computations required, the number of frequency shifts in the filter have been limited to keep the simulation length reasonable. The number of frequency shifts in the TV-FRESH filter is therefore limited to $20/B$. The division by B is to balance the amount of computation for different values of B to make a valid comparison across all results.

Figures 4.4a-4.4c show the BER curves for each of the different filtering methods for SIR = -20, -10, and 0 dB. Both types of FRESH filters are able to reject the radar interference well, such that the BER curves are consistent even for large changes in the SIR. The largest gain is provided by the TV-FRESH with $B = 4$, where it is within 1 dB of the AWGN theoretical curve at $E_b/N_0 = 8$ dB. However, the ACS FRESH outperforms the TV-FRESH for $B = 2$ when $M = 2$ and $M = 4$. The Wiener filter performs the worst, even for SIR = 0 dB the BER approaches a performance floor of 10^{-2} and is 5 dB worse than the TV-FRESH with $B = 4$.

Figures 4.5a-4.5c plot the measured and theoretical SINR curves for the Wiener filter and TV-FRESH filter. Similar to the BER curves, the output SINR for the TV-FRESH filter is largely

(a) SIR = -20 dB. **(b)** SIR = -10 dB. **(c)** SIR = 0 dB.
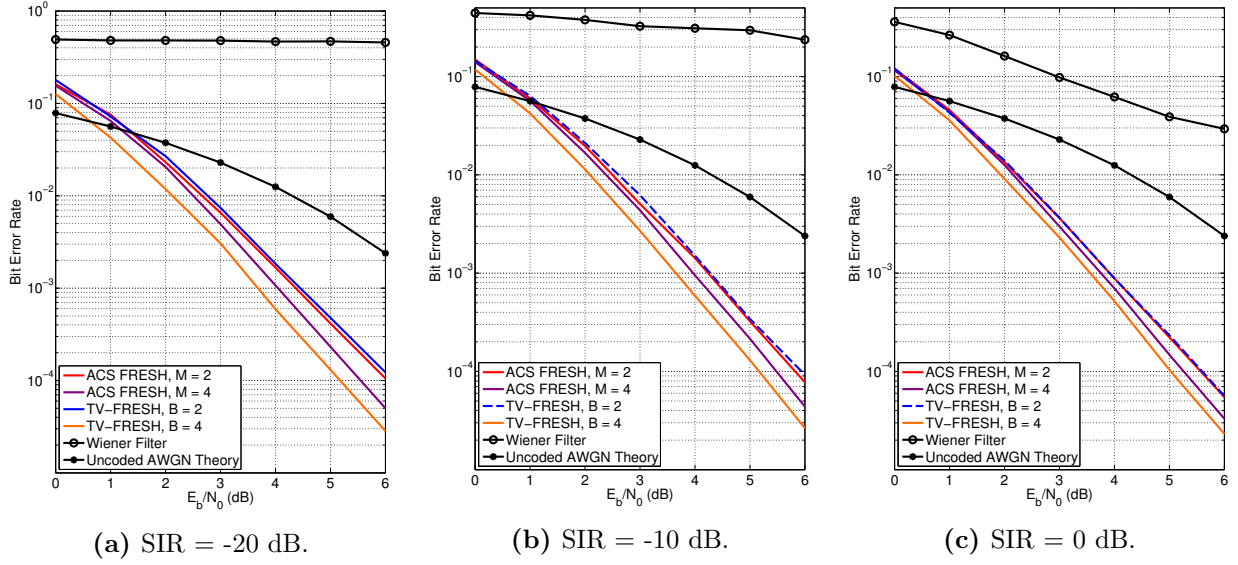
Figure 4.8: The $\frac{1}{2}$-rate convolutionally encoded BER curves when chirped radar interferes with OFDM for SIR = -20 dB, when using QPSK subcarriers and with an example multipath channel. All BER curves, except the theoretical AWGN curve, include the convolutional code.

independent of the input SIR value. The largest gains are seen by the Wiener filter, however it is still at least 10 dB worse than the TV-FRESH filter for all of the simulated SIR values.

There is some distance between the theoretical and simulated SINR curves for Figures 4.5a-4.5c, which is also present in [18]. The theoretical output SINR is based on the received signal $x(t)$ and the MMSE filter weights from (4.19) and (4.20). The input formatting required by the overlap-save algorithm modifies the underlying cyclostationarity, creating a distance between the two curves. The formatting of the input samples could be undone, but the MMSE filter weights would no longer correspond to such an input signal. The theoretical output SINR for circular convolution does not show this distance between the curves because the input samples are not distorted in the same way [15].

The BER under the same simulation scenario with an example multipath channel is given in Figures 4.6a-4.6c. A Rayleigh multipath channel is simulated by a tapped delay line whose weights for the desired OFDM signal η_d and radar interference η_i are:

$$\eta_d(z) = (0.581 - 0.15j) + (0.653 - 1.023j)z^{-1}$$
$$+(0.957 + 0.568j)z^{-2} + (-0.001 - 0.007j)z^{-3}, \tag{4.27}$$

$$\eta_i(z) = (0.864 - 0.707j) + (-1.054 + 0.276j)z^{-1}$$
$$+(-0.031 - 0.01)z^{-2} + (0.356 + 0.423j)z^{-3}. \tag{4.28}$$

The magnitude of the frequency responses for the two multipath channels is given in Figure 4.7.

The BER for the $B = 4$ TV-FRESH is better than the other FRESH filtering variants, a similar effect seen in the AWGN channel results, but increases the BER by about an order of magnitude. The FRESH filter can exploit spectral redundancy to mitigate interference as well as multipath fading, however adding the multipath fading increases the BER to nearly 10^{-2} from about 10^{-3} in the AWGN case. The impact could be counter-balanced by increasing the amount of spectral redundancy in the OFDM signal through increasing the cyclic prefix or through designing in spectral redundancy [15].

The TV-FRESH filter is able to mitigate a large portion of the radar interference because it is able to exploit the periodic chirp structure. When a sinusoid is interfering with a cyclostationary signal, an ACS FRESH filter is able to reject the interference because its bandwidth is approaching zero, while the cyclostationary signal will have a non-zero amount of excess bandwidth. In this case the segment of corrupted spectrum can simply be replaced with the redundant spectrum. Similarly by providing the TV-FRESH with the periodicities of the chirp signal, it can transform the received signal into a vectorized cyclostationary signal which accounts for the sweeping frequency of the tone and then exploit the spectral redundancies to reduce its impact.

Figures 4.8a-4.8c show the BER under the frequency selective channel when a $\frac{1}{2}$ rate convolutional code is used for SIR = -20 dB. All of the BER curves include the convolutional code with the exception of the theoretical AWGN curve. The TV-FRESH is able to remove a large portion of the effects from multipath channel as well as the radar interference, allowing the error correcting code

to better remove any residual impairments to the signal. The BER for all FRESH-related curves is well below the AWGN curve, similar would be seen for a convolutional code in only AWGN. The improvement on the results in Figures 4.6a-4.6c is more than two orders of magnitude, which is substantial for a slight investment in signaling overhead. The interleaving of the data bits also allows errors to be distributed more evenly, another factor in the improved BER performance.

4.5 Conclusion

The proposed method has demonstrated the ability of the proposed TV-FRESH filter to mitigate radar interference to an OFDM signal. This approach is novel in its ability to reject radar interference at the receiver, rather than avoid interference through exclusion zones or through a centralized spectrum access scheme. The ability to mitigate the impact of the interference can therefore be used to reduce the size of exclusion zones and aid in the transition of spectrum from legacy radar users into co-existence bands. The TV-FRESH filter can also be employed ad-hoc as the spectral environment changes, such as when a user is mobile and operating around the boundary of the exclusion zone where interference can come and go. The resistance to interference power was also demonstrated, showing that the BER is largely independent of the SIR value.

The TV-FRESH filter is able to exploit the spectral redundancies within a received signal, containing an OFDM signal and a chirped radar signal. By partitioning the frequency domain filter in time, and jointly filtering over segments of time domain samples, the spectral redundancy of these signals can be exploited better than the ACS FRESH filter. The new filtering structure is better suited to pulsed signals as its time-varying weights can be applied in correspondence with the radar's duty cycle. Simulation results demonstrate that increasing the number of time segments of the TV-FRESH can produce a better BER and SINR than the ACS FRESH and Wiener filter.

Chapter 5

Exploiting Spectral Redundancy in Whitening Filters for Blind Signal Detection

5.1   Introduction

This paper presents a novel signal detector for detecting two signals overlapping in frequency as can be seen in the case of the hidden node problem. The hidden node is a difficult problem in which a high power transmitter and low power transmitter are using the same channel, but the low power transmitter cannot be seen. This is most common in a decentralized or non-cooperative networks such as WiFi in the industrial, scientific and medical (ISM) bands as well as in dynamic spectrum access and spectrum sharing systems [110].

The paper makes the following contributions:

- Implements a blind signal detector based on only the cyclostationary properties of the masking signal.

- Improves detection of the hidden signal by 20% over a time-invariant whitening filter in a

simulated scenario.

- Produces a deflection that is more than 30 times larger than a time-invariant-based whitener in one simulation scenario.

- Produces a better probability of detection than the time-invariant whitening filter for any probability of false alarm in two simulated scenarios.

- A computationally efficient detection method due to the frequency domain implementation.

The proposed signal detector measures the output of a time-varying whitener (TVW) and compares against a detection threshold in order to determine if a signal is new to the environment. A whitening filter is used to flatten the spectrum of the output, in effect "white-listing" any existing signals, and then the filter weights are fixed such that any new signals will be visible in the spectrum.

Where a time-invariant whitener (TIW) is only able to flatten the output spectrum based on attenuation and amplification of a filter, a TVW does so by exploiting the cyclostationarity of the masking signal. The TIW rejects signals which have similar power levels near the same frequencies due to the whitening filter, making the detection of such signals difficult. By whitening the output spectrum according to the spectral correlation of the masking signal, the TVW is able to pass the otherwise hidden signal which overlaps in frequency, enabling its detection.

5.1.1 Outline

The remainder of the paper is outlined as follows. Section 5.2 proposes a novel method for detecting signals overlapping in frequency by filtering based on their cyclostationary properties. Section 5.3 presents simulation results for the probability of detection and false alarm for the proposed method, and Section 5.4 concludes the paper.

5.2 Signal Detection with Cyclic Whitener

The proposed method uses an adaptive FRESH filter trained as a time-varying whitening filter as a way to reject known signals in the environment, and pass any others which do not spectrally

correlate in the same fashion. The output of the TVW is then used for detection, comparing the power levels of the frequency bins in aggregate against a threshold level.

5.2.1 Signal Model

The proposed detection algorithm will be used for hypothesis testing to determine the ability to detect the presence of the hidden signal while also measuring its false alarm rate in its absence. The terms masking signal and hidden signal will be used to be more clear about their roles in the hidden node problem. As such there will be two received signals, $x_{H_0}(t)$ and $x_{H_1}(t)$, corresponding to the two hypotheses, H_0 and H_1 respectively. The received signals are:

$$x_{H_0}(t) = d(t) + n(t), \tag{5.1}$$

$$x_{H_1}(t) = d(t) + i(t) + n(t), \tag{5.2}$$

where $d(t)$ is the desired signal or masking signal, $i(t)$ is the interference or hidden signal, and $n(t)$ is additive white Gaussian noise (AWGN). For simplicity and generality, the received signal will also be described as $x(t)$ or $X(f)$, where $X(f) = \mathcal{F}\{x(t)\}$. The desired signal is a BPSK signal with symbol period T_d given by [92]:

$$d(t) = \sum_{k=-\infty}^{+\infty} d_k p_d(t - kT), \tag{5.3}$$

where d_k is the kth BPSK symbol and $p_d(t)$ is the pulse shaping filter. The hidden signal is a Quadrature Phase Shift Keying (QPSK) signal with symbol period T_i:

$$i(t) = \sum_{k=-\infty}^{+\infty} i_k p_i(t - kT) e^{j2\pi f_i t}, \tag{5.4}$$

where i_k is the kth QPSK symbol, $p_i(t)$ is the pulse shaping filter and f_i is the carrier frequency.

5.2.2 Non-Maximally Decimated Filter Bank as Channelizer

A non-maximally decimated filter bank (NMDFB) is used to transform the received signal into the frequency domain [2] such that the TIW and TVW can utilize the benefits of such an implementation. Implementing a discrete-time filter in the frequency domain offers two benefits: it is often more computationally efficient than doing so in the time domain and can improve the convergence properties of an adaptive filter [94].

The NMDFB is chosen for its ability to channelize wideband signals with minimal distortion. A maximally decimated filterbank with N_{FFT} channels provides them with a bandwidth of f_s/N_{FFT}, where f_s is the sampling rate. A NMDFB, when oversampled by 2, produces the same number of channels but with twice the output bandwidth, $2f_s/N_{FFT}$. The additional bandwidth gives the channelizing filter additional transition bandwidth which allows it to reject the neighboring channels with minimal distortion. The sidelobe levels can be designed to a certain level, for example -60 dB or -96 dB worth of Spurious Free Dynamic Range (SFDR).

A polyphase implementation of the NMDFB reduces the computational complexity by efficiently and intelligently avoiding unnecessary computation through partitioning of the filter coefficients. The polyphase representation in the Z-domain is given by [2]:

$$H_M(Z) = \sum_{k=0}^{M-1} Z^{-k} W_M^{-km} E_k(Z^{M/D}), \tag{5.5}$$

where M is the number of channels, the phase rotator for each channel is defined as $W = e^{-j2\pi/M}$, and $E_k(Z^{D/M})$ is the kth polyphase partition of the prototype filter. Figure 5.1 gives the graphical representation of (5.5).

5.2.3 Time-Varying Whitening Filter

Prior work for the adaptive FRESH filter has included filtering to enhance the output signal to interference and noise ratio (SINR) of the desired signal [34], however it will be modified to operate as a time-varying whitener. The ability to reject interference by exploiting the spectral correlation
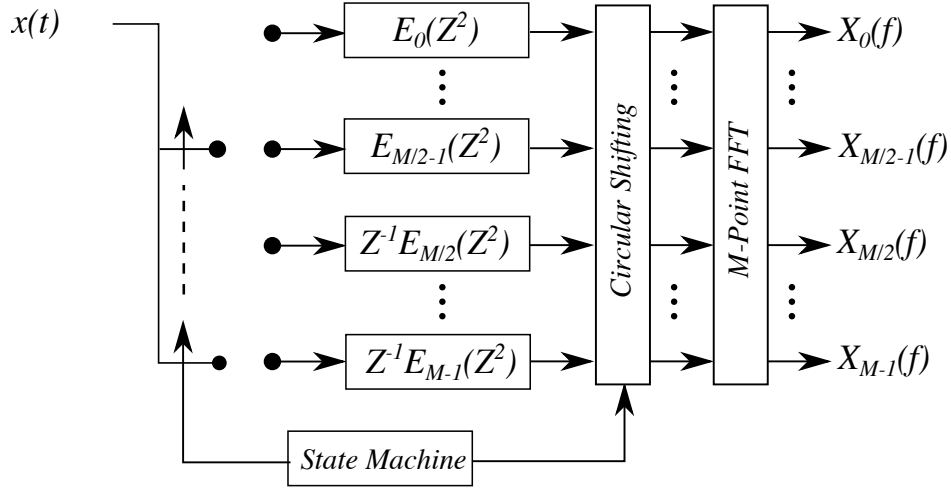
Figure 5.1: A polyphase implementation of a NMDFB [2].

of cyclostationary signals will be used to detect interfering signals when overlapping in frequency.

The TVW will operate in a similar fashion as the TIW in Section 2.2.5, but will exploit the spectral redundancies of the known signals using a FRESH filter. The filter weights of the TVW will be adapted with $d[k] = \delta[k]$, therefore the left-hand terms from the design equations (2.44) and (2.45) can then be reduced to the following:

$$\mathbf{S}_{\delta x}^{\alpha_p}\left(f - \frac{\alpha_p}{2}\right) = \mathbf{X}_0^{\alpha_p}\left(f - \frac{\alpha_p}{2}\right), \tag{5.6}$$

$$\mathbf{S}_{\delta x^*}^{\beta_q}\left(f - \frac{\beta_q}{2}\right) = \mathbf{X}_0^{\beta_q}\left(-f + \frac{\beta_q}{2}\right)^*. \tag{5.7}$$

The output of the TVW will be represented by:

$$\begin{aligned}
Y(f) &= \sum_{m=0}^{M-1} A_m(f) X\left(f - \alpha_m\right) \\
&+ \sum_{n=0}^{N-1} B_n(f) X^*\left(-f + \beta_n\right),
\end{aligned} \tag{5.8}$$
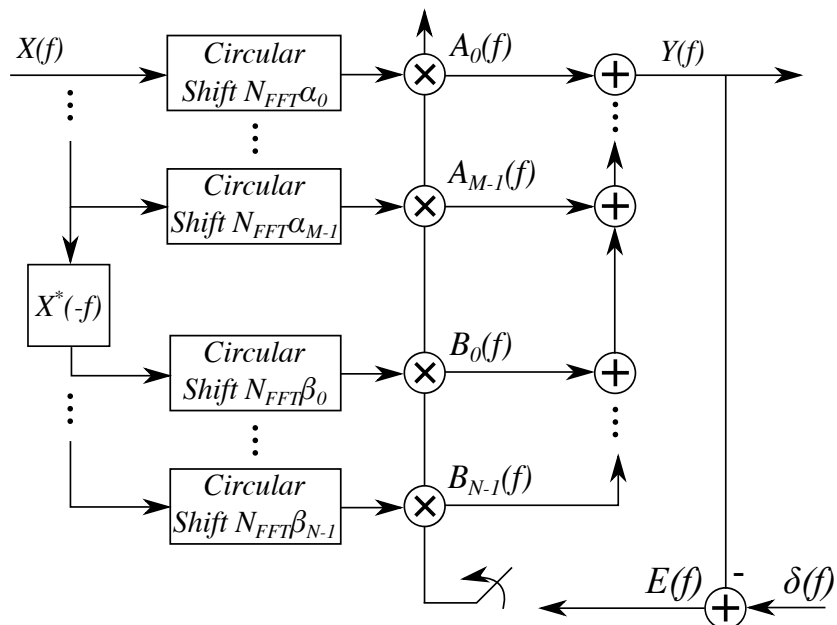
Figure 5.2: The frequency domain implementation of the TVW, where N_{FFT} is the number of channels.

which produces an example whitened spectrum as in Figure 5.2.

It is important that the windowed time-domain samples are properly spectrally portioned, and *not* overlapped or averaged, since the FRESH filter exploits the spectrally redundant information in the received signal. Such modifications to the input signal would destroy the cyclostationary properties [47], dramatically limiting the performance of the TVW.

The TIW is able to whiten a spectrum by adapting the filter weights but it has difficulty when two signals are overlapping in frequency because it is a brute force approach, simply attenuating or amplifying various parts of the spectrum to make it flat. A FRESH filter can be used which can improve the ability to see when signals are overlapping by exploiting the cyclostationarity of such signals in order to mitigate the interference. Only the cycle frequencies of the reference signal will be implemented in the TVW, as they can be estimated from the known signal for the purpose of cancellation. Figure 5.3a displays the whitened spectrum when only the masking signal is received in order to train them filter weights, and Figure 5.3b when the TVW with fixed filter weights is applied to both the masking signal and the hidden signal. Multiple peaks can be seen in Figure 5.3b due to the multiple frequency shifted and added branches in the TVW, as compared to the
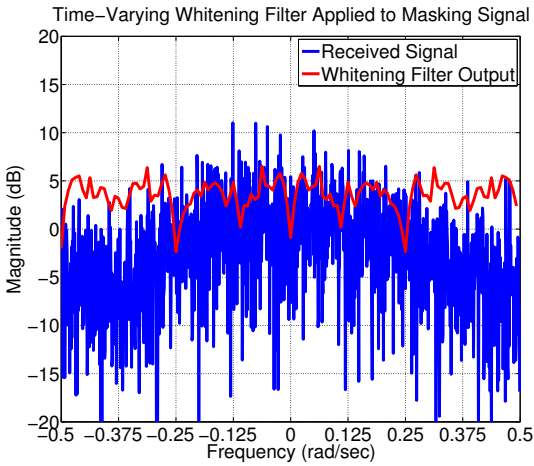
(a) The TVW adapts to the masking signal by whitening the output spectrum.
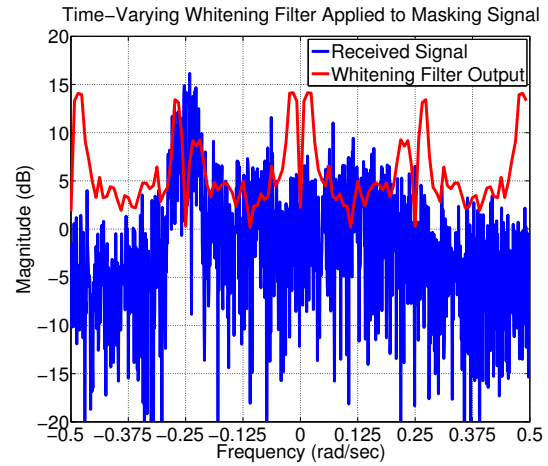
(b) Multiple peaks of the hidden signal can be seen in the whitened output.

Figure 5.3: The input and output spectra to the TVW when two signals are overlapping, SNR = 5 dB and SIR = 0 dB. The SNR and SIR is with respect to the masking signal. The output of the TVW has multiple peaks which correspond to the frequency shifts in the filter, and as such the peaks are predictable.

TIW which only has a single peak in Figure 5.3b.

The output of the whitening filter is fed into a signal detection algorithm which determines if a signal is detected through hypothesis testing. The two hypotheses are when the hidden signal is not present, $x_{H_0}(t)$, and when the hidden signal is present, $x_{H_1}(t)$. The energy output of the whitening filters, ψ, is compared against a threshold according to:

$$\psi = \sum_f |Y(f)|^2 \underset{H_0}{\overset{H_1}{\gtrless}} \lambda. \tag{5.9}$$

When $\psi > \lambda$, then it is determined that the H_1 hypothesis applies. When the decision is made correctly it is a valid detection, otherwise when a detection is made but the hidden signal is not present it is a false alarm. Increasing the Probability of Detection (P_oD) while maintaining or reducing the Probability of False Alarm (P_{fa}) is an indication of an improved detection algorithm.

5.2.4 Deflection

In addition to characterizing a detector using the probability of detection and false alarm the deflection can also be used, which is defined as [45]:

$$z(t) = \frac{|\mathbb{E}\{g(t)|H_1\} - \mathbb{E}\{g(t)|H_0\}|}{\sqrt{Var\{g(t)|H_0\})}}, \tag{5.10}$$

where $g(t)$ is the decision statistic and $Var()$ is the variance. The deflection is a measure of confidence in the detector, where a detector whose variance is small with respect to the two mean values will be more reliable and therefore produce a large deflection value. The proposed frequency domain deflection is defined as:

$$Z(f) = \frac{|\mathbb{E}\{\psi|H_1\} - \mathbb{E}\{\psi|H_0\}|}{\sqrt{Var\{\psi|H_0\})}}, \tag{5.11}$$

where the mean of the detector can then be found from (5.9) as:

$$
\begin{aligned}
\mathbb{E}\{\psi\} = \mathbb{E}\Bigg\{ & \sum_{m_1,m_2} S_y^{\alpha_{m_2}-\alpha_{m_1}}\left(f - \frac{\alpha_{m_2}+\alpha_{m_1}}{2}\right) A_{m_1}(f)A_{m_2}^*(f) \\
& + \sum_{m,n} S_{yy^*}^{\beta_n-\alpha_m}\left(f - \frac{\alpha_m+\beta_n}{2}\right) A_m(f)B_n^*(f) \\
& + \sum_{m,n} S_{yy^*}^{\beta_n-\alpha_m}\left(f - \frac{\alpha_m+\beta_n}{2}\right)^* A_m^*(f)Bn(f) \\
& + \sum_{n_1,n_2} S_y^{\beta_{n_2}-\beta_{n_1}}\left(-f + \frac{\beta_{n_2}+\beta_{n_1}}{2}\right) B_{n_1}(f)B_{n_2}^*(f)\Bigg\}.
\end{aligned}
\tag{5.12}
$$

The variance of the detector is therefore:

$$Var\{\psi\} = \mathbb{E}\{\psi\psi^*\} - \mathbb{E}\{\psi\}\mathbb{E}\{\psi^*\}. \tag{5.13}$$

The deflection is also used to validate the simulation results, as a closed form solution for the

probability of detection and probability of false alarm under colored and non-stationary noise and interference is outside the scope of this paper.

5.3 Simulation Results

Simulation is used to estimate the Probability Distribution Function (PDF) of ψ under H_0 and H_1, P_oD and P_{fa} for both the TIW and TVW, as well as the deflection as a function of SNR of the masking signal. The scenario is detecting a narrowband hidden signal in the presence of a wideband signal of interest. The signal of interest is a BPSK signal at 2 samples per symbol, and the hidden signal is a QPSK signal with 16 samples per symbol. The results are demonstrated for different combinations of cycle frequencies in the TVW. The number of channels is constant over all results, $N_{FFT} = 128$. The TIW is simulated when $\alpha = 0$ and $\beta = \varnothing$, and the TVW is simulated for all other combinations of the cycle frequencies.

5.3.1 Simulated Probability Distributions for the Whitening Filters

The simulated PDFs for the detector ψ under H_0 and H_1 for SIR = 0 dB and SNR = 5 dB are given in Figures 5.4a and 5.4b. The histograms both show that increasing the number of frequency shifts both increases the mean, which will produce more reliable detections on average, but at the cost of increasing the variance of the detector. Figures 5.5a and Figures 5.5b show a detailed plot of the simulated PDF for the TIW and the TVW, respectively, under both H_0 and H_1. A comparison of the plots shows the TIW is estimated to have a false alarm probability of 15% and a missed detection probability of 23%, while the TVW is estimated to have a false alarm probability of 9% and a missed detection probability of 15% for the given PDFs. The P_oD and P_{fa} curves in Section 5.3.2 show a similar result, where the TVW improves the probability of detection over the TIW for the same false alarm rate.

(a) The simulated PDFs under H_0.

(b) The simulated PDFs under H_1.
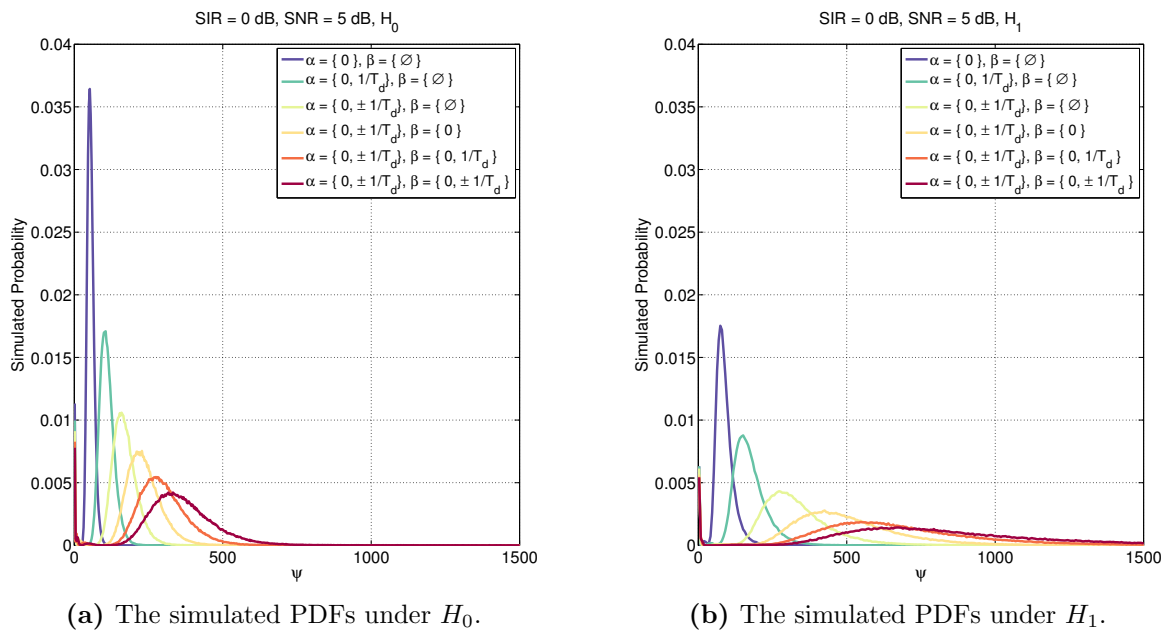
Figure 5.4: The simulated PDFs for the whitening filters when the hidden signal is not present, H_0, and when it is present, H_1. The SIR = 0 dB, and SNR = 5 dB. The SNR and SIR is with respect to the masking signal.
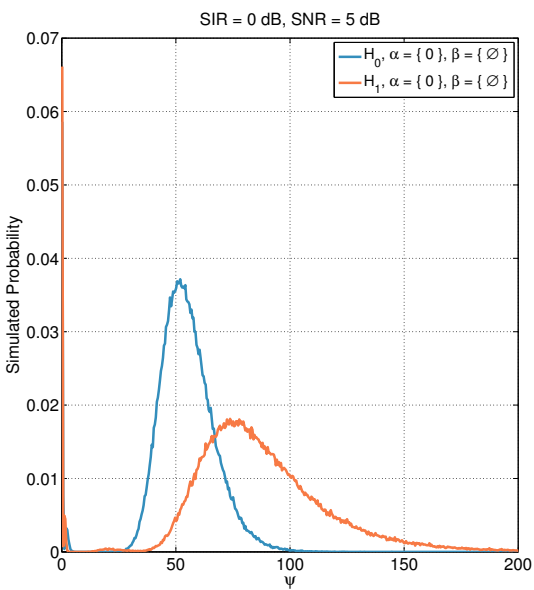
(a) The simulated PDFs for the TIW under both H_0 and H_1.
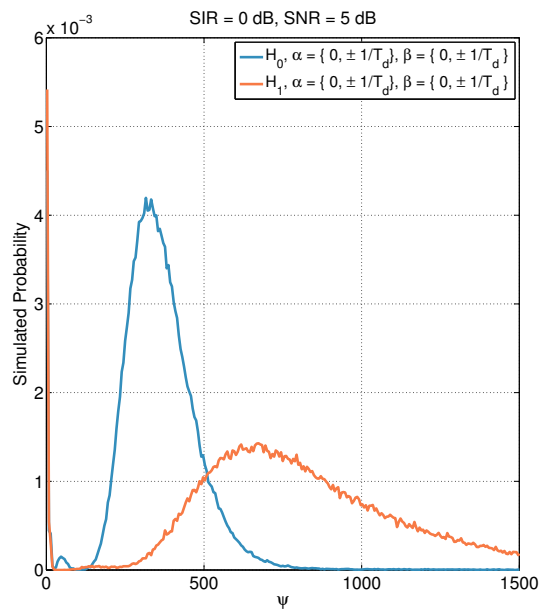
(b) The simulated PDFs for the TVW with all frequency shifts under both H_0 and H_1.

Figure 5.5: A comparison of the simulated PDFs for the TIW and TVW under both H_0 and H_1, for SIR = 0 dB, and SNR = 5 dB. The SNR and SIR is with respect to the masking signal.
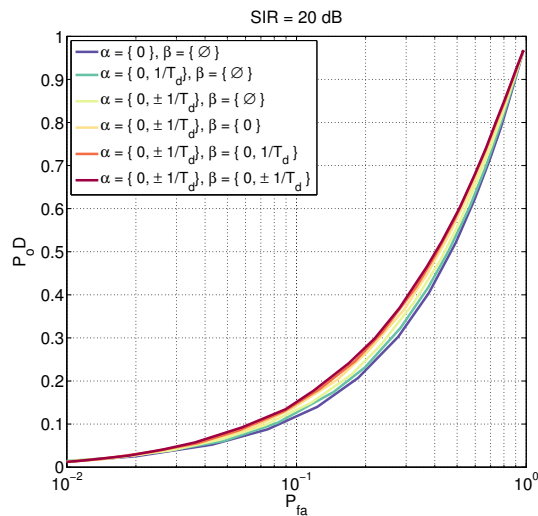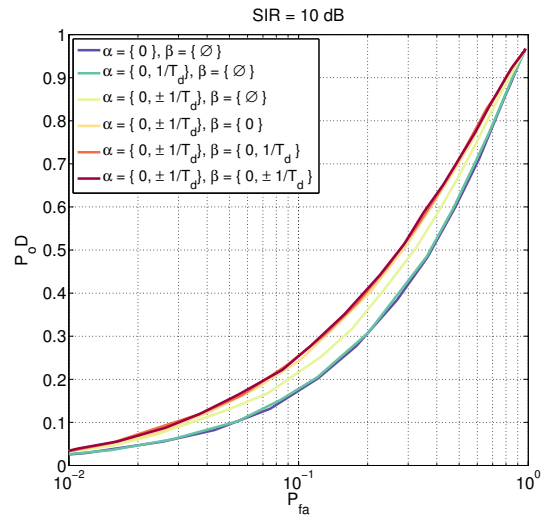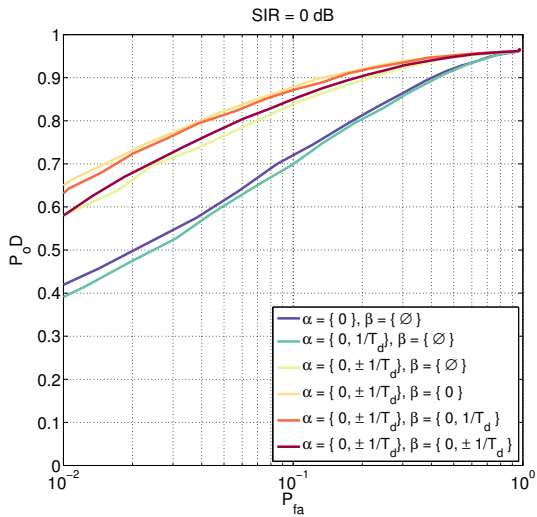
Figure 5.6: The probability of detection is plotted against probability of false alarm for the TIW and TVW for SNR = 5 dB, displaying the increase in performance as the number of cycle frequencies are increased. The SNR and SIR are with respect to the masking signal.

5.3.2 Probability of Detection and False Alarm

The simulated P_oD and P_{fa} for the TIW and TVW is given in Figures 5.6a - 5.6c. The threshold λ is swept logarithmically from 10 to 10,000 over 120 values to compute each of the data points. A large spread of thresholds is needed to cover the space for all of the different cycle frequency combinations of the TVW. Multiple branches summed within TVW result in more power at the output, and as such a larger threshold is required to avoid an abnormally high false alarm rate. The input time sequence to the whitening filters is 256,000 samples long, and each point on the P_oD and P_{fa} curves is the average of 193,920 iterations.

The best performance for both the TIW and TVW maximizing P_oD with respect to P_{fa} is found for SIR = 0 dB, when the hidden signal is the strongest as the larger power results in more reliable detections. Increasing the number of frequency shifts tends to improve the performance of the detector, but not in all cases. When a FRESH filter's weights are set according to the MMSE condition and applied against the same signal, the contributions of cycle frequencies which do not help to minimize the filter error are severely reduced. However, under these circumstances the TVW applies the MMSE weights to a different received signal and therefore the addition of cycle frequencies can increase the filtering error. For example, for SIR = 0 dB, the TIW marginally outperforms the TVW with two cycle frequencies 0 and $1/T_d$ by improving the P_oD by less than 3% for the same P_{fa}. The best result, the TVW with $\alpha = \{0 \pm 1/T_d\}$ and $\beta = \{0\}$, improves the P_oD by more than 20% for $P_{fa} = 10^{-2}$ as compared to the TIW.

The relative improvement of the TVW as compared to the TIW is reduced with the SIR, as the lower power makes it more difficult to detect. For SIR = 10 dB, using additional cycle frequencies always results in a better P_oD for the same P_{fa}. The TVW is able to exploit the spectral redundancy of the masking waveform, reducing its impact on the output signal to increase the SINR of the hidden signal and allow for better detection. The gains mostly disappear as P_{fa} approaches both 0 and 1 due to the nature of thresholding detection. When the threshold is too low, any perturbation will set off the detector which means that the hidden signal will always be detected, but many false alarms will also be raised. Similarly when the threshold is too high, no detection is ever made and thus no false alarms are set either. The important points for characterizing the detector are
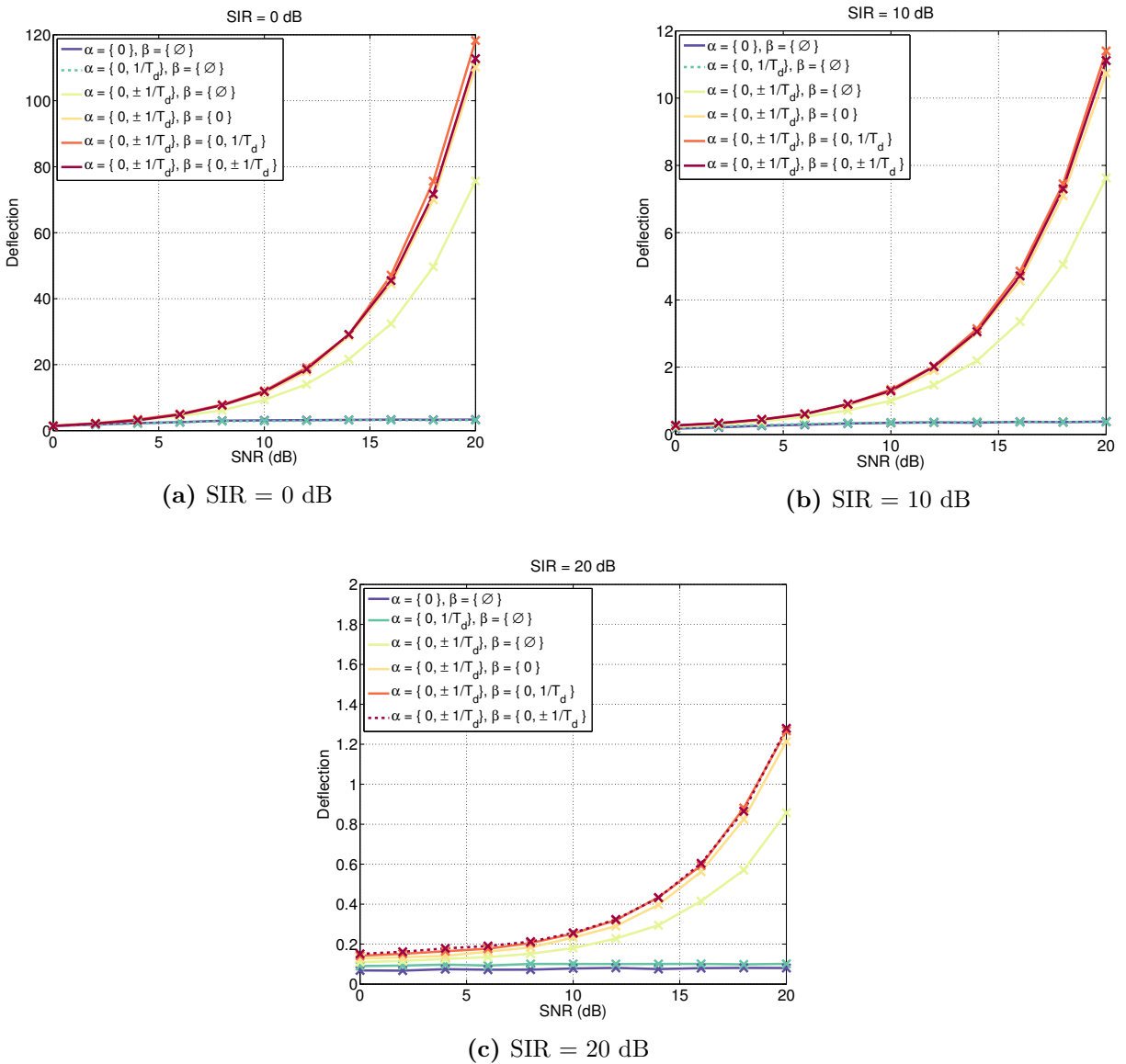
Figure 5.7: The frequency domain deflection plotted against the SNR for the TIW and TVW for various combinations of cycle frequencies. The theoretical results from (5.11) are marked by x.

between these two extremes. For $P_{fa} = 10^{-1}$ the TVW with all cycle frequencies improves the PoD by 8%. Similarly for SIR $= 20$ dB, the improvement in P_oD with the TVW using all cycle frequencies is 4% for $P_{fa} = 10^{-1}$.

5.3.3 Deflection Simulation Results

The simulated results for deflection versus SNR are plotted in Figures 5.7a - 5.7c, along with the theoretical results from (5.11) and (5.12). The deflection results show a similar effect to the P_oD versus P_{fa} curves, in that using more cycle frequencies results in a better detection algorithm. The largest gain is seen when SIR $= 0$ dB and SNR $= 20$ dB, when the TVW includes all of the cycle frequencies α and conjugate cycle frequencies β. The deflection is 118, much larger than for the other SIR values, while the deflection is 11 for SIR $= 10$ dB and 1.28 for SIR $= 20$ dB. A trend can be seen that as the SIR is increased the overall deflection is decreased, which is to be expected given that the power of the hidden signal is decreasing, making it much harder to detect. Another trend can be seen, which is that increasing the number of cycle frequencies typically results in a larger deflection. While the addition of specific cycle frequencies can improve the deflection more than others, it can be seen that generally speaking adding more of them improves the performance of the detector. The best performance of the detector comes when the SNR is increased and many of the cycle frequencies are included in the TVW, since they can mitigate the impact of the masking signal and increase the probability of detection for the hidden signal.

5.4 Conclusion

A blind signal detection algorithm is proposed which is based on exploiting the spectral redundancy of a masking signal to better whiten the received spectrum. The FRESH filter is trained on an impulse signal to whiten the received spectrum and then the adaptation is stopped. Signals in the environment which do not have the same spectral correlation properties as the masking signal then come through the TVW and can be detected with thresholding.

Simulation results are computed for various combinations of cycle frequencies in the TVW, and it is demonstrated under the given scenario that the TVW always produces a higher P_oD for the

same P_{fa} with respect to the TIW. The largest improvement is an increased in P_oD by 20% over the TIW for $P_{fa} = 10^{-2}$.

The TVW can be used for signal detection in the hidden node problem as well as other scenarios where non-cooperative wireless networks are transmitting on top of one another, such as in the ISM bands. The number of peaks of the hidden signal at the output of the TVW is predictable and related to the number of frequency shifts in the filter. More sophisticated methods other than energy detection might be used to detect and classify the hidden signal, including the application of a neural net-based classifier. New waveforms might also be created for the TVW such that their spectral correlation enables better detection of hidden signals.

Chapter 6

Conclusion

The contributions within this dissertation propose novel ways to use spectral redundancy as a design parameter for communicating in interference limited environments, develop the optimal filter for exploiting the spectral redundancy, apply the filter and its periodically time-varying filter weights to mitigate the effects of radar signals on OFDM communications and for improving the detection of interference by using a time-varying whitening filter.

The first contribution, Chapter 3, establishes the method for repeating data symbols across an OFDM symbol in both time and frequency, creating a paramorphic multicarrier waveform. This forms a new type of spectral redundancy, and thus a new type of filter to exploit it, the TV-FRESH. The structure of the frequency domain TV-FRESH filter is presented and the MMSE filter weights are found.

The paramorphic method introduces symbol-level redundancies, analogous to bit-level redundancies created using an ECC. The important distinction is the paramorphic waveform is designed to operate within cyclostationary interference, where the compared ECCs are not, and accordingly the simulations show large gains over ECCs for the same overhead rates.

A simulated annealing optimization is used to select the best signaling parameters under a specific interference scenario, and the results show that a balance between ECCs and symbol repetition maximize the spectral efficiency while minimizing the BER. The effect is that the paramorphic

FRESH demodulator is able to exploit the symbol-level redundancies and therefore mitigates a large portion of the interference. The residual signal is effectively noise limited, a situation in which ECCs excel, producing a net effect of a smaller BER than either approach could have achieved alone.

Prior work with FRESH filtering has focused on communication signals which are constantly interfering with the desired signal. The novelty of the second contribution, Chapter 4, is that it applies the TV-FRESH filter to mitigate a pulsed chirp radar interfering with an OFDM signal. The TV-FRESH filter segments the received signal into multiple time slots and jointly filters them, exploiting spectral redundancies across time. Since the radar signal is deterministic, each sample is a spectral redundancy that can be exploited with respect to all of the other samples in the pulse.

A method for blindly detecting signals in the frequency domain is proposed, which improves upon prior work by exploiting the spectral redundancy in the desired signal. An adaptive FRESH filter is used to whiten the received spectrum by training against the frequency response of an impulse when only the desired signal is present. The adaptation of the TVW filter weights is stopped, and then applied to the received signal when the interference is present. This creates the ability to allow signals that overlap in frequency with the desired signal but do not share the same spectral correlation properties to pass through the TVW.

Simulation results show that using a TV-FRESH filter with more time segments can improve the BER and SINR with respect to the traditional FRESH filter under the specific interference scenario. The BER and SINR comparisons are done by filtering the same number of input data samples. The cost of the increase in performance is the additional filtering complexity of the TV-FRESH filter.

Future work for the first contribution could include developing waveforms with more general or irregular repetition patterns, as well as the amount of repetition per symbol, and determining what performance gains can be achieved. The redundancies could also be transmitted over multiple antennas, and the corresponding TV-FRESH filter could be adapted into an array processor. The design of a multicarrier waveform from the ground up to include the benefits of symbol repetition could also yield interesting results. A cognitive engine could also be applied to adapt and optimize the waveform in real time.

Additional study of the TV-FRESH on other types of radar signals is warranted and could yield

interesting results. The performance of the TV-FRESH to rejecting OFDM from the radar receiver could also produce insight into better ways to coordinate and plan for radar and communication systems co-existence. The structure of the TV-FRESH filter could also be adapted, such as the number of time segments, based on the characteristics of the interference.

Future work for the TVW might include studying the improvement in detection performance for multicarrier signals, such as OFDM in the ISM bands. A follow on neural network might also be used to classify the type and location of interference based on the frequency domain output of the TVW.

Bibliography

[1] W. A. Gardner, "Cyclic wiener filtering: theory and method," *IEEE Transactions on Communications*, vol. 41, no. 1, pp. 151–163, Jan 1993.

[2] X. Chen, F. J. Harris, E. Venosa, and B. D. Rao, "Non-maximally decimated analysis/synthesis filter banks: Applications in wideband digital filtering," *IEEE Transactions on Signal Processing*, vol. 62, no. 4, pp. 852–867, Feb 2014.

[3] N. Wiener, *Extrapolation, interpolation, and smoothing of stationary time series*. Cambridge, MA: Technology Press of the Massachusetts Institute of Technology, 1949.

[4] W. Gardner and L. Franks, "Characterization of cyclostationary random signal processes," *IEEE Transactions on Information Theory*, vol. 21, no. 1, pp. 4–14, Jan 1975.

[5] X. Zhang, L. Chen, J. Qiu, and J. Abdoli, "On the waveform for 5g," *IEEE Communications Magazine*, vol. 54, no. 11, pp. 74–80, November 2016.

[6] M. Lichtman, J. H. Reed, T. C. Clancy, and M. Norton, "Vulnerability of LTE to hostile interference," in *2013 IEEE Global Conference on Signal and Information Processing*, Dec 2013, pp. 285–288.

[7] M. Lichtman, R. P. Jover, M. Labib, R. Rao, V. Marojevic, and J. H. Reed, "Lte/lte-a jamming, spoofing, and sniffing: threat assessment and mitigation," *IEEE Communications Magazine*, vol. 54, no. 4, pp. 54–61, April 2016.

[8] Z. Xue, J. Wang, Q. Shi, G. Ding, and Q. Wu, "Time-frequency scheduling and power optimization for reliable multiple uav communications," *IEEE Access*, vol. 6, pp. 3992–4005, 2018.

[9] J. I. Choi, M. Jain, K. Srinivasan, P. Levis, and S. Katti, "Achieving single channel, full duplex wireless communication," in *Proceedings of the Sixteenth Annual International Conference on Mobile Computing and Networking*, ser. MobiCom '10. New York, NY, USA: ACM, 2010, pp. 1–12. [Online]. Available: http://doi.acm.org/10.1145/1859995.1859997

[10] L. Verma, M. Fakharzadeh, and S. Choi, "Wifi on steroids: 802.11ac and 802.11ad," *IEEE Wireless Communications*, vol. 20, no. 6, pp. 30–35, December 2013.

[11] J. H. Reed, A. W. Clegg, A. V. Padaki, T. Yang, R. Nealy, C. Dietrich, C. R. Anderson, and D. M. Mearns, "On the co-existence of td-lte and radar over 3.5 ghz band: An experimental study," *IEEE Wireless Communications Letters*, vol. 5, no. 4, pp. 368–371, Aug 2016.

[12] S. Gao, X. Dai, Y. Hang, Y. Guo, and Q. Ji, "Airborne wireless sensor networks for airplane monitoring system," *Wireless Communications and Mobile Computing*, vol. 2018, pp. 1–18, May 2018.

[13] J. Kakar, K. McDermott, V. Garg, M. Lichtman, V. Marojevic, and J. H. Reed, "Analysis and mitigation of interference to the LTE physical control format indicator channel," in *2014 IEEE Military Communications Conference*, Oct 2014, pp. 228–234.

[14] M. J. L. Pan, M. Lichtman, T. C. Clancy, and R. W. McGwier, "Protecting physical layer synchronization: mitigating attacks against ofdm acquisition," in *2013 16th International Symposium on Wireless Personal Multimedia Communications (WPMC)*, June 2013, pp. 1–6.

[15] M. Carrick, J. Reed, and C. Spooner, "Paramorphic multicarrier communications for interference mitigation," *EURASIP Journal on Advances in Signal Processing*, vol. 2018, no. 1, pp. 1–18, January 2018.

[16] M. Carrick, J. H. Reed, and fred harris, "An optimal filter for signals with time-varying cyclostationary statistics," in *2017 IEEE International Conference on Digital Signal Processing (DSP)*, 2017, pp. 1–5.

[17] M. Carrick and J. H. Reed, "Improved gfdm equalization in severe frequency selective fading," in *2017 IEEE 38th Sarnoff Symposium*, 2017, pp. 1–6.

[18] ——, "Exploiting the cyclostationarity of radar chirp signals with time-varying filters," in *2017 IEEE Global Conference on Signal and Information Processing (GlobalSIP)*, 2017, pp. 1–4.

[19] M. Carrick, V. Marojevic, and J. Reed, "Method for jointly adapting an ofdm waveform and the demodulator for interference mitigation and harsh channels," U.S. Patent PCT/US16/25 609, April, 2017.

[20] ——, "Method for jointly adapting an ofdm waveform and the demodulator for interference mitigation and harsh channels," U.S. Patent 62 144 039, April, 2015.

[21] W. A. Gardner, A. Napolitano, and L. Paura, "Cyclostationarity: Half a century of research," *Signal Processing*, vol. 86, no. 4, pp. 639–697, April 2006.

[22] A. Napolitano, "Cyclostationarity: New trends and applications," *Signal Processing*, vol. 120, pp. 385–408, March 2016.

[23] R. Meyer and C. Burrus, "A unified analysis of multirate and periodically time-varying digital filters," *IEEE Transactions on Circuits and Systems*, vol. 22, no. 3, pp. 162–168, Mar 1975.

[24] S. Vaseghi, *Advanced digital signal processing and noise reduction.* Chichester, West Sussex: John Wiley and Sons Ltd., 2000.

[25] W. Gardner, "Representation and estimation of cyclostationary processes," Ph.D. dissertation, University of Massachusetts Amherst, August 1972.

[26] W. A. Gardner, "Non-parametric signal detection and identification of modulation type for signals hidden in noise: an application of the new theory of cyclic spectral analysis," in *Colloque sur le traitement du signal et des images*, 1983, pp. 119–124.

[27] W. Gardner, "The spectral correlation theory of cyclostationary time-series," *Signal Processing*, vol. 11, no. 1, pp. 13–36, July 1986.

[28] ——, "Spectral correlation of modulated signals: Part I - analog modulation," *IEEE Transactions on Communications*, vol. 35, no. 6, pp. 584–594, June 1987.

[29] W. Gardner, W. Brown, and C.-K. Chen, "Spectral correlation of modulated signals: Part II - digital modulation," *IEEE Transactions on Communications*, vol. 35, no. 6, pp. 595–601, June 1987.

[30] W. Gardner, *Statistical Spectral Analysis*. Englewood Cliffs, N.J.: Prentice Hall, 1988.

[31] W. Brown and R. Crane, "Conjugate linear filtering," *IEEE Transactions on Information Theory*, vol. 15, no. 4, pp. 462–465, Jul 1969.

[32] W. A. Gardner and W. A. Brown, "Frequency-shift filtering theory for adaptive co-channel interference removal," in *Twenty-Third Asilomar Conference on Signals, Systems and Computers, 1989.*, vol. 2, Oct 1989, pp. 562–567.

[33] E. Ferrara, "Frequency-domain implementations of periodically time-varying filters," *IEEE Transactions on Acoustics, Speech, and Signal Processing*, vol. 33, no. 4, pp. 883–892, Aug 1985.

[34] J. H. Reed and T. C. Hsia, "The performance of time-dependent adaptive filters for interference rejection," *IEEE Transactions on Acoustics, Speech, and Signal Processing*, vol. 38, no. 8, pp. 1373–1385, Aug 1990.

[35] J. H. Reed, N. M. Yuen, and T. C. Hsia, "An optimal receiver using a time-dependent adaptive filter," *IEEE Transactions on Communications*, vol. 43, no. 2/3/4, pp. 187–190, Feb 1995.

[36] O. A. Y. Ojeda and J. Grajal, "Adaptive-fresh filters for compensation of cycle-frequency errors," *IEEE Transactions on Signal Processing*, vol. 58, no. 1, pp. 1–10, Jan 2010.

[37] B. G. Agee, S. V. Schell, and W. A. Gardner, "Spectral self-coherence restoral: a new approach to blind adaptive signal extraction using antenna arrays," *Proceedings of the IEEE*, vol. 78, no. 4, pp. 753–767, Apr 1990.

[38] J.-H. Lee and Y.-T. Lee, "Robust adaptive array beamforming for cyclostationary signals under cycle frequency error," *IEEE Transactions on Antennas and Propagation*, vol. 47, no. 2, pp. 233–241, Feb 1999.

[39] J.-H. Lee, Y.-T. Lee, and W.-H. Shih, "Efficient robust adaptive beamforming for cyclostationary signals," *IEEE Transactions on Signal Processing*, vol. 48, no. 7, pp. 1893–1901, Jul 2000.

[40] J. Zhang, K. M. Wong, Z. Q. Luo, and P. C. Ching, "Blind adaptive fresh filtering for signal extraction," *IEEE Transactions on Signal Processing*, vol. 47, no. 5, pp. 1397–1402, May 1999.

[41] P. Petrus and J. H. Reed, "Time dependent adaptive arrays," *IEEE Signal Processing Letters*, vol. 2, no. 12, pp. 219–222, Dec 1995.

[42] W. Gardner and C. Spooner, "The cumulant theory of cyclostationary time-series. i. foundation," *IEEE Transactions on Signal Processing*, vol. 42, no. 12, pp. 3387–3408, Dec 1994.

[43] C. Spooner and W. Gardner, "The cumulant theory of cyclostationary time-series. ii. development and applications," *IEEE Transactions on Signal Processing*, vol. 42, no. 12, pp. 3409–3429, Dec 1994.

[44] A. V. Dandawate and G. B. Giannakis, "Statistical tests for presence of cyclostationarity," *IEEE Transactions on Signal Processing*, vol. 42, no. 9, pp. 2355–2369, Sep 1994.

[45] W. A. Gardner, "Signal interception: a unifying theoretical framework for feature detection," *IEEE Transactions on Communications*, vol. 36, no. 8, pp. 897–906, Aug 1988.

[46] K. Kim, I. A. Akbar, K. K. Bae, J. S. Um, C. M. Spooner, and J. H. Reed, "Cyclostationary approaches to signal detection and classification in cognitive radio," in *2nd IEEE international symposium on new frontiers in dynamic spectrum access networks, 2007*, April 2007, pp. 212–215.

[47] J. H. Reed and B. G. Agee, "A technique for instantaneous tracking of frequency agile signals in the presence of spectrally correlated interference," in *1992 Conference Record of the*

Twenty-Sixth Asilomar Conference on Signals, Systems Computers, Oct 1992, pp. 1065–1071 vol.2.

[48] J. Tian, H. Guo, H. Hu, and H. H. Chen, "Frequency-shift filtering for OFDM systems and its performance analysis," *IEEE Systems Journal*, vol. 5, no. 3, pp. 314–320, Sept 2011.

[49] D. Darsena, G. Gelli, F. Verde, and I. Iudice, "Blind ltv shortening of doubly selective OFDM channels for uas applications," in *2015 IEEE Metrology for Aerospace (MetroAeroSpace)*, June 2015, pp. 557–561.

[50] N. Shlezinger and R. Dabora, "Frequency-shift filtering for OFDM signal recovery in narrowband power line communications," *IEEE Transactions on Communications*, vol. 62, no. 4, pp. 1283–1295, April 2014.

[51] D. Darsena, L. D. Virgilio, G. Gelli, and F. Verde, "Widely-linear frequency-shift compensation of cfo and i/q imbalance in OFDMA/SC-FDMA systems," in *2015 IEEE International Conference on Communications (ICC)*, June 2015, pp. 2686–2691.

[52] R. W. Heath and G. B. Giannakis, "Exploiting input cyclostationarity for blind channel identification in OFDM systems," *IEEE Transactions on Signal Processing*, vol. 47, no. 3, pp. 848–856, Mar 1999.

[53] A. Tani and R. Fantacci, "A low-complexity cyclostationary-based spectrum sensing for uwb and wimax coexistence with noise uncertainty," *IEEE Transactions on Vehicular Technology*, vol. 59, no. 6, pp. 2940–2950, July 2010.

[54] J. Lunden, V. Koivunen, A. Huttunen, and H. V. Poor, "Collaborative cyclostationary spectrum sensing for cognitive radio systems," *IEEE Transactions on Signal Processing*, vol. 57, no. 11, pp. 4182–4195, Nov 2009.

[55] S. Bokharaiee, H. H. Nguyen, and E. Shwedyk, "Blind spectrum sensing for OFDM-based cognitive radio systems," *IEEE Transactions on Vehicular Technology*, vol. 60, no. 3, pp. 858–871, March 2011.

[56] H. Bolcskei, "Blind estimation of symbol timing and carrier frequency offset in wireless OFDM systems," *IEEE Transactions on Communications*, vol. 49, no. 6, pp. 988–999, Jun 2001.

[57] A. Benjebbour, T. Asai, and H. Yoshino, "Nonparametric interference suppression using cyclic wiener filtering: pulse shape design and performance evaluation," *EURASIP Journal on Wireless Communications and Networking - Cognitive Radio and Dynamic Spectrum Sharing Systems*, vol. 2008, no. 26, pp. 1–14, Jan 2008.

[58] K. Maeda, A. Benjebbour, T. Asai, T. Furuno, and T. Ohya, "Cyclostationarity-inducing transmission methods for recognition among OFDM-based systems," *EURASIP Journal on Wireless Communications and Networking - Cognitive Radio and Dynamic Spectrum Sharing Systems*, vol. 2008, no. 23, pp. 1–14, Jan 2008.

[59] P. D. Sutton, K. E. Nolan, and L. E. Doyle, "Cyclostationary signatures in practical cognitive radio applications," *IEEE Journal on Selected Areas in Communications*, vol. 26, no. 1, pp. 13–24, Jan 2008.

[60] H. Guo, H. Hu, and Y. Yang, "Cyclostationary signatures in ofdm-based cognitive radios with cyclic delay diversity," in *2009 IEEE International Conference on Communications*, June 2009, pp. 1–6.

[61] J. Sun, D. Qu, T. Jiang, G. Zhong, and J. Guo, "Low overhead cyclostationary signatures based on hopping subcarrier in ofdm-based dynamic spectrum access networks," in *2011 IEEE Vehicular Technology Conference (VTC Fall)*, Sept 2011, pp. 1–5.

[62] P. Sutton, "Rendezvous and coordination in ofdm-based dynamic spectrum access networks," Ph.D. dissertation, University of Dublin, September 2008.

[63] W. Choi, Q. Sun, and J. Gilbert, "Repetition coding for a wireless system," U.S. Patent US 2012/0 121 046, May, 2012.

[64] R. Porat and A. Monk, "Method of bit allocation in a multicarrier symbol to achieve non-periodic frequency diversity," U.S. Patent 7 724 639, May, 2010.

[65] R. Susitaival and M. Meyer, "LTE coverage improvement by tti bundling," in *VTC Spring 2009 - IEEE 69th Vehicular Technology Conference*, April 2009, pp. 1–5.

[66] E. Drocella, J. Richards, R. Sole, F. Najmy, A. Lundy, and P. McKenna, "3.5 GHz exclusion zone analyses and methodology," in *NTIA Report 15-517*, June 2015.

[67] U. D. of Commerce, "An assessment of the near-term viability of accommodating wireless broadband systems in the 1675-1710 MHz, 1755-1780 MHz, 3500-3650 MHz, and 4200-4220 MHz, 4380-4400 MHz bands," Oct 2010.

[68] M. Ghorbanzadeh, E. Visotsky, P. Moorut, W. Yang, and C. Clancy, "Radar inband and out-of-band interference into LTE macro and small cell uplinks in the 3.5 GHz band," in *2015 IEEE Wireless Communications and Networking Conference (WCNC)*, March 2015, pp. 1–6.

[69] F. Paisana, J. Miranda, N. Marchetti, and L. DaSilva, "Database-aided sensing for radar bands," in *2014 IEEE International Symposium on Dynamic Spectrum Access Networks (DYSPAN)*, April 2014, pp. 1–6.

[70] M. Sohul, M. Yao, T. Yang, and J. Reed, "Spectrum access system for the citizen broadband radio service," *IEEE Communications Magazine*, vol. 53, no. 7, pp. 18–23, July 2015.

[71] A. Khawar, A. Abdel-Hadi, and T. C. Clancy, "Spectrum sharing between S-band radar and LTE cellular system: A spatial approach," in *2014 IEEE International Symposium on Dynamic Spectrum Access Networks (DYSPAN)*, April 2014, pp. 7–14.

[72] H. Shajaiah, A. Khawar, A. Abdel-Hadi, and T. C. Clancy, "Resource allocation with carrier aggregation in LTE advanced cellular system sharing spectrum with s-band radar," in *2014 IEEE International Symposium on Dynamic Spectrum Access Networks (DYSPAN)*, April 2014, pp. 34–37.

[73] A. Mukherjee, J. F. Cheng, S. Falahati, L. Falconetti, A. Furuskr, B. Godana, D. H. Kang, H. Koorapaty, D. Larsson, and Y. Yang, "System architecture and coexistence evaluation of licensed-assisted access LTE with ieee 802.11," in *2015 IEEE International Conference on Communication Workshop (ICCW)*, June 2015, pp. 2350–2355.

[74] D. W. Bliss, "Cooperative radar and communications signaling: The estimation and information theory odd couple," in *2014 IEEE Radar Conference*, May 2014, pp. 0050–0055.

[75] A. Turlapaty and Y. Jin, "A joint design of transmit waveforms for radar and communications systems in coexistence," in *2014 IEEE Radar Conference*, May 2014, pp. 0315–0319.

[76] W. A. Gardner, "Exploitation of spectral redundancy in cyclostationary signals," *IEEE Signal Processing Magazine*, vol. 8, no. 2, pp. 14–36, April 1991.

[77] W. A. Gardner and C. M. Spooner, "Signal interception: performance advantages of cyclic-feature detectors," *IEEE Transactions on Communications*, vol. 40, no. 1, pp. 149–159, Jan 1992.

[78] U. Mengali and A. D'Andrea, *Synchronization Techniques for Digital Receivers*. New York: Plenum Press, 1997.

[79] B. Muquet, Z. Wang, G. B. Giannakis, M. de Courville, and P. Duhamel, "Cyclic prefixing or zero padding for wireless multicarrier transmissions?" *IEEE Transactions on Communications*, vol. 50, no. 12, pp. 2136–2148, Dec 2002.

[80] A. Napolitano, "Cyclostationary signal processing and its generalizations," in *IEEE Statistical Signal Processing Workshop (SSP 2014)*, 2014.

[81] L. Izzo and A. Napolitano, "The higher order theory of generalized almost-cyclostationary time series," *IEEE Transactions on Signal Processing*, vol. 46, no. 11, pp. 2975–2989, Nov 1998.

[82] A. Napolitano, "Estimation of second-order cross-moments of generalized almost-cyclostationary processes," *IEEE Transactions on Information Theory*, vol. 53, no. 6, pp. 2204–2228, June 2007.

[83] J. J. Shynk, "Frequency-domain and multirate adaptive filtering," *IEEE Signal Processing Magazine*, vol. 9, no. 1, pp. 14–37, Jan 1992.

[84] S. Kay, *Fundamentals of Statistical Signal Processing, Volume 1: Estimation Theory*. Upper Saddle River, N.J.: Prentice-Hall, Inc., 1993.

[85] R. W. Chang, "Synthesis of band-limited orthogonal signals for multichannel data transmission," *The Bell System Technical Journal*, vol. 45, no. 10, pp. 1775–1796, Dec 1966.

[86] S. Weinstein and P. Ebert, "Data transmission by frequency-division multiplexing using the discrete fourier transform," *IEEE Transactions on Communication Technology*, vol. 19, no. 5, pp. 628–634, October 1971.

[87] A. Peled and A. Ruiz, "Frequency domain data transmission using reduced computational complexity algorithms," in *Acoustics, Speech, and Signal Processing, IEEE International Conference on ICASSP '80.*, vol. 5, Apr 1980, pp. 964–967.

[88] J. G. Andrews, S. Buzzi, W. Choi, S. V. Hanly, A. Lozano, A. C. K. Soong, and J. C. Zhang, "What will 5g be?" *IEEE Journal on Selected Areas in Communications*, vol. 32, no. 6, pp. 1065–1082, June 2014.

[89] P. Vaidyanathan, *Multirate systems and filter banks.* Englewood Cliffs, N.J.: Prentice Hall, 1993.

[90] S. Kirkpatrick, C. Gelatt, and M. Vecchi, "Optimization by simulated annealing," *Science*, vol. 220, no. 4598, pp. 671–680, May 1983.

[91] A. He, K. K. Bae, T. R. Newman, J. Gaeddert, K. Kim, R. Menon, L. Morales-Tirado, J. . Neel, Y. Zhao, J. H. Reed, and W. H. Tranter, "A survey of artificial intelligence for cognitive radios," *IEEE Transactions on Vehicular Technology*, vol. 59, no. 4, pp. 1578–1592, May 2010.

[92] J. Proakis, *Digital Communications, 5th Edition.* New York, N.Y.: McGraw Hill, 2007.

[93] E. Serpedin and G. B. Giannakis, "Blind channel identification and equalization with modulation-induced cyclostationarity," *IEEE Transactions on Signal Processing*, vol. 46, no. 7, pp. 1930–1944, Jul 1998.

[94] S. Haykin, *Adaptive Filter Theory.* Englewood Cliffs, N.J.: Prentice-Hall, Inc., 2001.

[95] W. A. Gardner, *Statistical Spectral Analysis, A Nonprobabilistic theory.* Englewood Cliffs, N.J.: Prentice-Hall, Inc., 1988.

[96] T. C. Clancy, M. Norton, and M. Lichtman, "Security challenges with LTE-advanced systems and military spectrum," in *MILCOM 2013 - 2013 IEEE Military Communications Conference*, Nov 2013, pp. 375–381.

[97] T. Newman, "Multiple objective fitness functions for cognitive radio adaptation," Ph.D. dissertation, University of Kansas, 2008.

[98] F. Guidolin and M. Nekovee, "Investigating spectrum sharing between 5g millimeter wave networks and fixed satellite systems," in *2015 IEEE Globecom Workshops (GC Wkshps)*, Dec 2015, pp. 1–7.

[99] E. T. S. Institute, "Digital video broadcasting (dvb); second generation framing structure, channel coding and modulation systems for broadcasting, interactive services, news gathering and other broadband satellite applications (dvb-s2)," *ETSI Standard EN 302 307 V1.1.1*, 2005.

[100] T. Wada, "A study on performance of ldpc codes on power line communications," in *2004 IEEE International Conference on Communications (IEEE Cat. No.04CH37577)*, vol. 1, June 2004, pp. 109–113 Vol.1.

[101] D. Kolba and T. Parks, "A prime factor fft algorithm using high-speed convolution," *IEEE Transactions on Acoustics, Speech, and Signal Processing*, vol. 25, no. 4, pp. 281–294, Aug 1977.

[102] J. Proakis, *Digital Signal Processing, 4th Edition.* London, U.K.: Pearson, 2006.

[103] G. Lellouch, A. K. Mishra, and M. Inggs, "Stepped ofdm radar technique to resolve range and doppler simultaneously," *IEEE Transactions on Aerospace and Electronic Systems*, vol. 51, no. 2, pp. 937–950, April 2015.

[104] K. Kauffman, J. Raquet, Y. Morton, and D. Garmatyuk, "Real-time uwb-ofdm radar-based navigation in unknown terrain," *IEEE Transactions on Aerospace and Electronic Systems*, vol. 49, no. 3, pp. 1453–1466, July 2013.

[105] G. Vanhoy, T. Schucker, and T. Bose, "Classification of lpi radar signals using spectral correlation and support vector machines," *Analog Integr Circ Sig Process*, vol. 91, no. 2, pp. 305–313, May 2017.

[106] A. Napolitano, "Generalizations of cyclostationarity: A new paradigm for signal processing for mobile communications, radar, and sonar," *IEEE Signal Processing Magazine*, vol. 30, no. 6, pp. 53–63, Nov 2013.

[107] L. Izzo and A. Napolitano, "Sampling of generalized almost-cyclostationary signals," *IEEE Transactions on Signal Processing*, vol. 51, no. 6, pp. 1546–1556, June 2003.

[108] W. Headley, J. Reed, and C. da Silva, "Distributed cyclic spectrum feature-based modulation classification," in *2004 IEEE Wireless Communications and Networking Conference*, April 2008, pp. 1200–1204.

[109] f. harris, *Multirate signal processing for communication systems.* Upper Saddle River, N.J.: Prentice Hall PTR, 2004.

[110] R. Menon, R. M. Buehrer, and J. H. Reed, "On the impact of dynamic spectrum sharing techniques on legacy radio systems," *IEEE Transactions on Wireless Communications*, vol. 7, no. 11, pp. 4198–4207, November 2008.